NTNU

Norwegian University of
Science and Technology

Porous filters of nanofibrillated cellulose

Linn Ingunn C. Sandberg

Nanotechnology

Submission date: June 2011

Supervisor: Øyvind Weiby Gregersen, IKP
Co-supervisor: Kristin Syverud, PFI
Gary Chinga-Carrasco, PFI

Norwegian University of Science and Technology
Department of Chemical Engineering

Acknowledgements

I want to give my sincere thanks to Øyvind W. Gregersen, Gary Chinga-Carrasco and Kristin Syverud for their guidance and useful input throughout this work. A million thanks to Bartlomiej Gawel who taught me how to operate the BET surface area instrument. I am also grateful to Mirjana Filipovic and Ingebjørg Leirset at PFI for kindly assisting me in several lab procedures and to Galina Rodionova for demonstrating solvent exchange and operation of the centrifuge. Collin Tyn Ching Hii should be thanked as he unasked took a lot of interest in helping me out in finding ways of freezing cellulose suspensions in liquid nitrogen. Finally, I want to thank my beloved Kjell Tore Fossbakk for his support and patience during these 5 months.

Abstract

Filters for air purification are predominantly produced of synthetic and non-biodegradable materials. In this work, a range of various air filters have been prepared from 100% pure cellulosic material, with the goal to create alternative air filters which are completely biodegradable. The filters have been prepared by either evaporation of solvents with varying polarity or by freeze drying aqueous cellulose suspensions. The most promising results were obtained by the latter procedure, where an air permeance of $\sim$ 2000 $\frac{\mu m}{Pa \cdot s}$ and tensile strength of $\sim$ 0.20 $\frac{kN}{m}$ was obtained.

Contents

List of abbreviations

TEMPO = (2,2,6,6-Tetramethylpiperidin-1-yl)oxyl

DP = degree of polymerization

MFC = micro fibrillated cellulose

NFC = nano fibrillated cellulose

MPPS = most penetrating particle size

SEM = scanning electron microscopy

BEI = backscattered electron imaging

TEM = transmission electron microscopy

DW% = dry weight content of cellulose mass

HEPA = High Efficiency Particulate Air

ULPA = Ultra Low Penetration Air

1 Introduction

1.1 Background

An average person breathes in about 12.5 m^3, or 16 kg of air each day[1]. It is usually normal, atmospheric air that we breathe, which generally is far from clean. Contaminated air contains everything from non-toxic, but large particles to aggressive substances which may cause ill health such as lung disease. This is why we need filters, as they clean the air we breathe in addition to purify the water we drink and control the pollution level in cleanrooms, engines and other industrial devices.

The disposable filter media market across the globe has been growing at a rate of 4-5% the last years[2], where non-woven filters represent 90% of all filter media used in dry and liquid filtration[3]. Unfortunately, a large percentage of the non-woven air filters are made of polymers from non-renewable fossil sources.

Cellulose is the main component of the cell wall in wood, plants and a number of algae and by that the most abundant organic compound on earth. Between 10^{10} and 10^{13} tonnes of cellulose are synthesized in nature every year, which exceeds the total production of synthetic polymers

Figure 1: Cellulose is the main component of all plant matter. Image: private.

by far[4][5]. Environmental concerns have increased the general interest in renewable materials. As cellulose is a readily available, lightweight, biodegradable and renewable material, it is desirable to span out the volume of applications by creating new products such as air filters based on NFC (nanofibrillated cellulose). Before this is possible, a strategy on how to control the porosity and filtering characteristics of NFC filters must be established.

1.2 Applications

The main application of porous filters made of cellulose nanofibrils is as particle filters for air purification. This includes filters in air conditioning systems for homes, offices, vehicle cabins and clean rooms in addition to air intakes for engines and in respirators worn by humans, see Figure 2. The specific applications of the NFC filters will be determined by their pore size and porosity. If the pore size of the filters may be controlled down to 0.50 nm-1.5 nm, new applications might open up within the area of osmotic power production and in purification/separation of liquids by membranes.

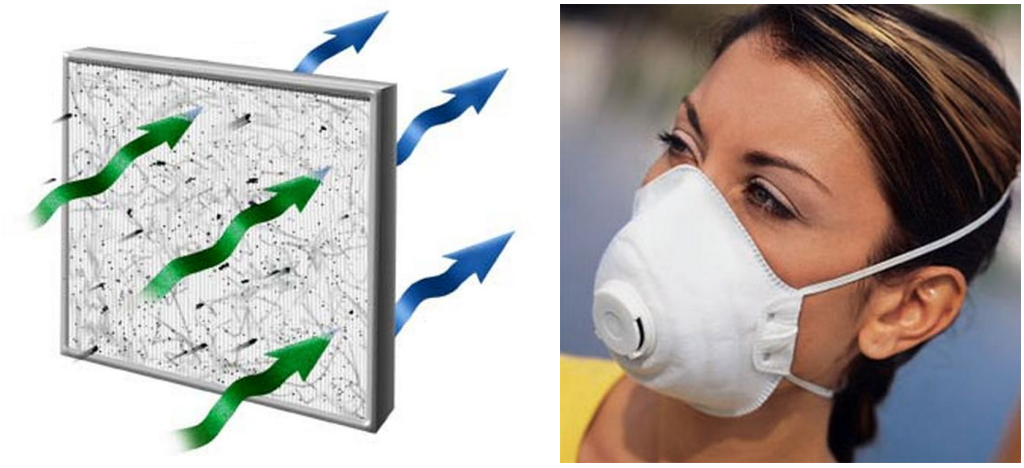

Figure 2: Left: Illustration of a typical air particulate filter, from [6]. Right: Respirator for direct air cleaning, from [7].

1.3 Aim of work

The aim of this project is to investigate whether the porosity of NFC air filters can be controlled by varying the type of cellulose mass and the general preparation method. Characterization of the filters will be performed to get an overview of the permeance and tensile strength of the resulting nanocellulose filters. The result of this screening might establish if NFC is a suitable alternative to more commonly used air filter materials which are derived from fossil resources.

2 Theory

2.1 Air pollution particles

The air we breathe can be polluted by a range of different particles such as soot from industry and wood-burning, dust due to traffic, smoke and organic debris from e.g. humans. See Figure 3 for an overview of the relative size of some common air contaminants. In Norway and many developed countries, *car traffic* is the main source of airborne solid particles which the inhabitants are exposed to[8]. As a consequence of this, several main roads in and out of e.g. Trondheim and Oslo often exceed the limit of particle concentration set by the EU.

Particles of concern to air pollution are most often measured in micrometers (i.e. 10^{-6} m), where large/coarse particles have a particle diameter larger than 10 μm, while dust and fume consist of finer particles below 1 μm[9]. Around 90% *by weight* of all airborne particulate impurities range from 0.1 to 10 μm in size[1]. Particles with size ranging between 0.7μm to 7μm are considered "lung damaging dust", as these particles manage to enter the lungs where they may cause damage.

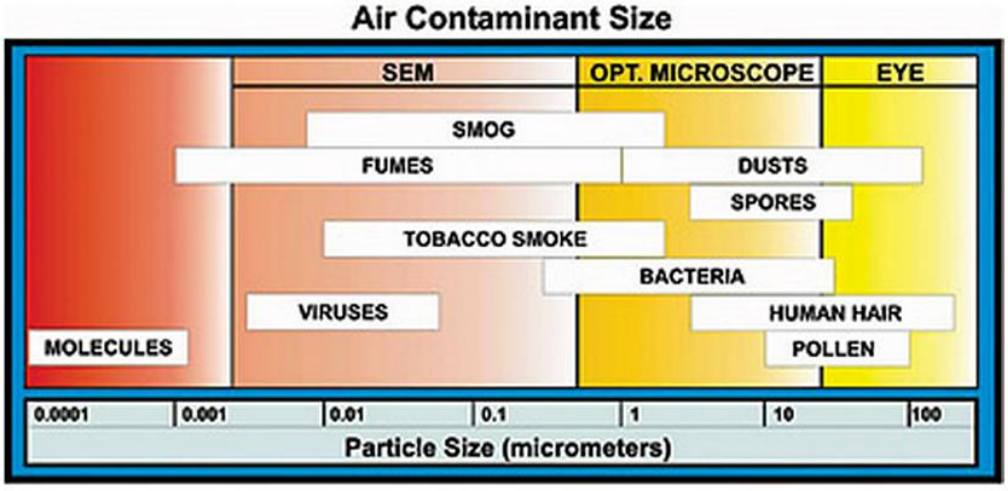

Figure 3: The most common air contaminants. Image from [10].

Particle size distribution is often given in either mass- or number distribution. As the mass of spherical particles varies with the cube of the particle diameter, small particles with a low mass% of a sample may still be the most numerous of that given sample.

2.2 Filters for air purification

2.2.1 Introduction to filters

A common definition of a general filter medium can be written as follows[3]: 'A filter medium is any material that, under the operating conditions of the filter, is permeable to one or more components of a mixture, solution or suspension, and is impermeable to the remaining components.' Filtration is almost entirely a characteristic of the *size* of the particle, droplet or molecule being separated, not the chemical properties of the particles. Hence, the separation of the particles is caused by purely mechanical means [11].

According to Eurovent and CEN (Comité Européen de Normalisation), air filters are divided into a total of 17 classes: the first nine are for coarse and fine dusts, while the five HEPA (High Efficiency Particulate Air) and three ULPA (Ultra Low Penetration Air) filters are for submicrometre particles[3] where the latter is defined as having an efficiency higher than 99.999% for particles in the 0.1 to 0.2 μ size range[1]. These filter classifications draw together standards from both Europe and the USA, which is highly convenient.

A large part of the filter market is concerned with cleaning normal atmospheric air, either as part of air condition systems in homes, vehicle cabins or office spaces[3]. Higher efficiency filters are used in cleaning the inlet air to cleanroom laboratories which are highly dust-sensitive. Respirators are a type of air filter which are worn by people exposed to dusty environments. Most filters can only be used once, followed by discarding and replacement, while others may be cleaned of their debris and have an indefinite lifetime.

2.2.2 Air filter materials and characteristics

The most commonly used material in non-woven air filters are synthetic polymers such as polyester, polyethylene, nylon, teflon and polyamides[11]. The most common materials used in air filtration devices of *woven* fabrics are presented in Figure 4.

A filter has several mechanical-, application- and filtration-specific properties. Hence, it can be characterized by everything from particle retention size and air flow efficiency to properties such as chemical/thermal stability, stiffness, rupture strength and resistance to e.g. stretch, abrasion and tearing. Small pieces of fibres and particles may be shed from the filter and contaminate the filtrate if

Material	Recommended Max Operating Temp (°F)	Recommended Max Excursion Temp (°F)	Chemical Resistance: Acid	Chemical Resistance: Base	Abrasion Resistance	Cost (per 8-ft bag)
Cotton	180	200	Poor	Good	Good	$8
Wool	200	230	Good	Poor	Fair	—
Nylon	200	250	Poor	Good	Excellent	—
Polypropylene	200	200	Excellent	Excellent	Excellent	$8
Polyester	275	300	Good	Fair	Excellent	$9
Acrylic	260	285	Good	Fair	Good	$13
Nomex®	375	400	Fair	Good	Excellent	$22
Ryton®	375	400	Excellent	Excellent	Excellent	—
Teflon®	450	500	Excellent	Excellent	Fair	$26
Fiberglass	500	550	Good	Good	Fair	$24
Coated high-purity silica	900	1050	Good	Good	Fair	$150
Ceramic candle	1650	1830	—	—	—	$1000[a]

[a] 60 mm diameter × 1.5 m.

Figure 4: Common woven filter materials and their properties. Courtesy of [9].

it is not sufficiently *dynamically* stable. This is of special concern if the filter is to filtrate clean room air or water used in the nano- and electronics industry.

The *air-to-filter ratio* is simply the gas flow rate divided by the filter area[9]. A low air-to-filter ratio provides a larger collection area. Hence, dust cake buildup and pressure drop increase at a lower rate so that a thicker dust cake can be tolerated before replacement is required. The

weight of the material used is also of importance, where more fabric increases the strength of the filter, but also the cost and pressure drop across the filter. Hence, the characteristics which are most important will depend on the intention of use and the demands which the filter is to fulfill.

The general definition of filtering efficiency can be expressed as[9]:

$$\text{Filter efficiency} = \frac{\text{Particles trapped}}{\text{Particles upstream}} \tag{1}$$

Other important characteristics of a filter include[3]:

1. Smallest particle retained
2. Retention efficiency versus particle size
3. Resistance to flow
4. Dirt-holding capacity
5. Tendency to blind
6. Cake discharge characteristics

Smallest particle retained. Considering the number of shapes a particle can have, the aerodynamic equivalent

size is most commonly used to describe the size of the smallest particle that is captured by the filter.

It is often more meaningful to characterize a filter medium according to its *retention efficiency versus particle size*. It is common to present the relationship between the particle size and the retention efficiency in grade efficiency curves, see Figure 5. The absolute cut-off value is the particle size at which the number of emerging particles is zero, which gives a filter efficiency of 100% for that particle size[1]. For any particle size smaller than this cut-off value, the efficiency must necessarily be less than 100%. Even though both filters in Figure 5 have the same cut-off value of $\sim 35\ \mu m$, they have very different efficiencies against smaller particles. It should be noted that the grade efficiency curve is only valid for the test conditions under which it was generated. A different curve will result if the filtration conditions are changed, e.g. altering the size distribution of the particles and/or the filtration velocity.

Resistance to flow of a filter medium is the reciprocal of the permeability[1]. Permeability depends on both the pore size and the number of pores per unit area.

The *dirt-holding capacity* of a filter is the amount of solids (i.e.'dirt') which can be collected without exceeding a defined pressure drop. See section 2.2.3 for definitions. A high dirt-holding capacity implies that the filter can be in use for a long time before cleaning or replacement is necessary.

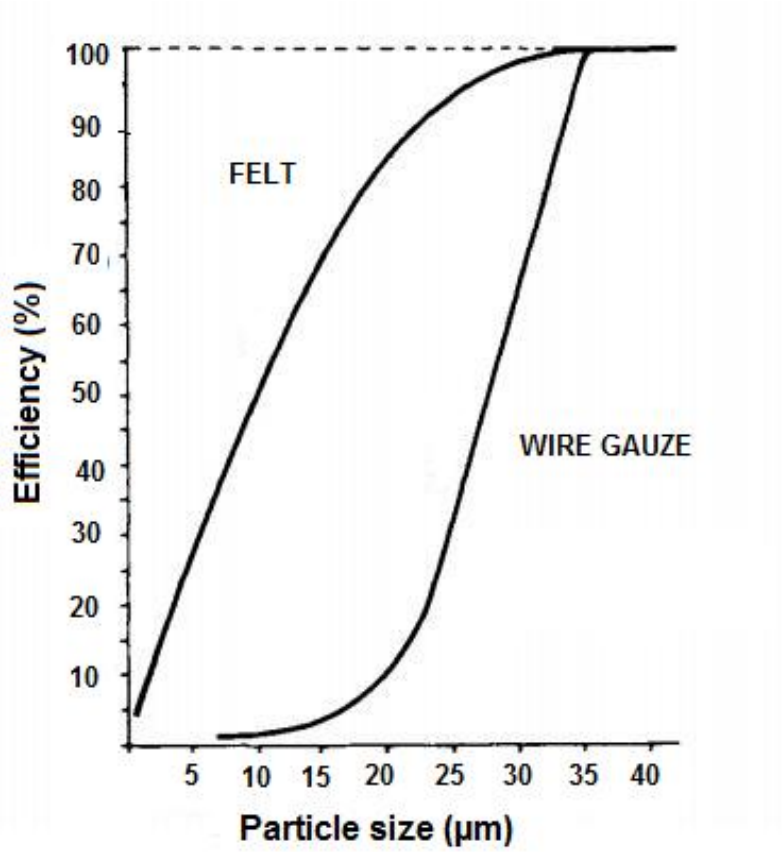

Figure 5: Grade efficiency curves for two different filter media. Courtesy of [9]

A filter medias *tendency to blind* describes how easily the dirt is removed from the filter in a cleaning process. This characteristic is therefore not of interest for dischargable filters such as those based on cellulose.

Cake discharge characteristics describes how easily it is to remove the dust cake during *continous* operation. A smooth filter surface and a low degree of fibrous material which extends from the filter surface and into the cake will make it easier to remove.

Composite filter media

Many filter media, including those produced from nanofibrillated cellulose, might need reinforcement to withstand the pressure they will be subject to. Composite structures where a part of the filter is merely for support will form gradient density media where the support itself help remove the largest particles from the gas stream. Other composite filters have embedded an additional layer to serve a specific purpose. An example is automotive cabin air filters which often combine a nonwoven particulate filter with an activated carbon layer to remove odors and fumes. The possible combinations of composite filter structures are countless, where the type of material, layer structure and stacking order may be varied.

It is worth noting that dust filtration in general may cause electrostatic charges to build up which in the worst case scenario might result in static discharge capable of causing ignition. Antistatic fabric with relatively high electrical conductivity can solve this potential problem where one solution is to weave conducting metal fibres into the filter. Fibres of the filter may also be intentionally made electrostatic to increase the collection efficiency of the medium, see Section 2.2.5.

2.2.3 Air permeance and pressure drop

Air permeance is important to filter design as it determines the type and capacity of the pump, blower or fan that should be used to force air through the filter media[11]. The definition of air permeance (P_a) is the average value of air flow ($\bar{u}$) through a filter, divided by its area A and the difference in air pressure (ΔP) across the filter[4].

$$P_a = \frac{\bar{u}}{A\Delta P} \tag{2}$$

Air permeance is given in the units of $\frac{m}{Pa\,s}$ as the air flow is given in $\frac{m^3}{s}$, the cross-sectional area of the filter is measured in m^2 and pressure difference in Pascals. It is desirable to obtain a high degree of permeance in air

filters to ensure a high through-put of air flow, but at the same time have small enough pores so that the collection efficiency is satisfactory. Generally, the goal is to maximize the permeability and to minimize the average pore size of the filter[11]. In non-woven filters such as paper filter media, fine fibers of low diameter will reduce the pore size and thereby increase the collection efficiency at the expense of the filter's permeability. The fiber diameter is inversely related to the flow resistance, that is, air filters composed of large diameter fibers have a high permeance. On the other hand, reducing the fiber diameter will boost the collection efficiency of a non-woven filter media. Obviously, filter medium design requires compromises.

The driving force that pushes the fluid through the filter is the pressure difference across the filter. The permeability of a filter medium is often expressed by this *pressure drop* which again is related to the air flow rate through it. The Kozeny-Carman equation describes the pressure drop of a fluid across a bed of particles, e.g. a filter[12].

$$\frac{\Delta P_d}{L} = \frac{150 V \mu}{\Phi_s^2 D_p^2} \frac{(1-\varepsilon)^2}{\varepsilon^3} \tag{3}$$

Where ΔP_d is the pressure drop across the filter medium thickness L. V is the superficial velocity, also known as the volumetric flow. μ represents the viscosity of the fluid, while ε is the permeable porosity of the filter, i.e. the void volume expressed as a unitless decimal fraction of the total filter medium volume. Φ_s is the sphericity of the particles which the filter is made of and D_p is the diameter of the related spherical particle. It should be noted that the relation is only valid for *laminar flow* through the filter medium.

A high pressure drop ΔP_d means that a large pressure difference ΔP across the filter is necessary to drive the flow of air through the filter, which again will give a high energy consumption during operation. The pressure drop will depend on factors such as filtration area, the air temperature and the degree of contamination of the filter medium. Pressure drop is inversely proportional to filter area, i.e. ΔP_d in Equation 3 increases if the size of filtration particles is reduced, hence, an increase in the effective filter area will reduce the pressure drop for a given flow rate. The pressure drop will also increase with time as the filter becomes clogged with particles which reduce the flow rate.

The standard air velocity in commercial and residential filtration systems is 1.52 m/s[13]. The tensile strength of the NFC filters must be a minimum of 0.032 $\frac{kN}{m}$, and preferably above 0.064 $\frac{kN}{m}$ to be able to withstand the drag force of this air velocity.

2.2.4 Filtration mechanisms of fluids

It should be noted that both gases and liquids are considered as fluids, hence, the basic principles below describes the filtration of both gaseous and liquid streams.

Four basic mechanisms are proposed on how particles are removed from a fluid, which include[3]:

1. Surface straining
2. Depth straining
3. Depth filtration
4. Cake filtration

Surface straining
Here, particles larger than the pore size deposits on the filter surface while smaller particles are allowed to pass, see Figure 6 on page 20. This is the main filtration mechanism for bar screens and plain woven monofilament mesh with uniform pore openings[11].

Depth straining

When the filters are considerably thicker than the size of their average pore size, the particles get to travel along the pores until they are trapped by a narrowing of the pore. Hence, they are deposited within the filter rather than at the filter surface. Felts and other non-woven fabrics utilize this mechanism.

Depth filtration

It is possible for a particle to get trapped even if its size is smaller than the pore size of the filter. If the particles come in close contact with the pore wall, they might stick to it due to van der Waals or other surface forces. See Figure 8 for visualization. This mechanism is affected by the humidity of the passing air and is important in all media, especially for high-efficiency air filters. Ventilation filters function primarily by depth filtration. Hence, they are difficult or even impossible to clean, and will therefore be discarded when fully loaded with particulates.

Cake filtration

In cake filtration, which is presented in Figure 9, a thick layer or cake of particles accumulates on the filter surface which define more constricted pore openings for the

next particles to arrive the filter medium. Hence, particle emission from a dirty filter will be smaller than an unused and clean filter. Cake filtration may occur after an initial period of surface straining, but smaller particles may also induce cake filtration when the particles form a bridge across the pore entrance. The bridge will then function as the foundation onto which the cake continues to grow.

A real filtration process will necessarily include more than one of the four mechanisms listed above. They also explain why smaller particles than the actual pore size are trapped by the filter medium.

It should be noted that the four mechanisms are all variants of *through-flow* filtration, where all the fluid flows through the filter medium. In *cross-flow* filtration, the fluid is directed at an angle to the filter surface so only a part of the fluid will pass the filter. In addition, material deposited on the filter surface will be swept away by the passing flow which often runs in a recycle loop.

Figure 6: Filtration by surface straining where larger particles are deposited on the filter surface.

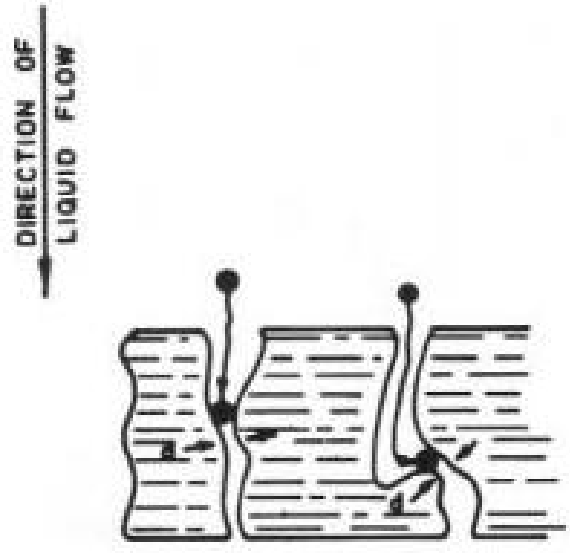

Figure 7: Filtration by depth straining where larger particles are trapped within the filter medium.

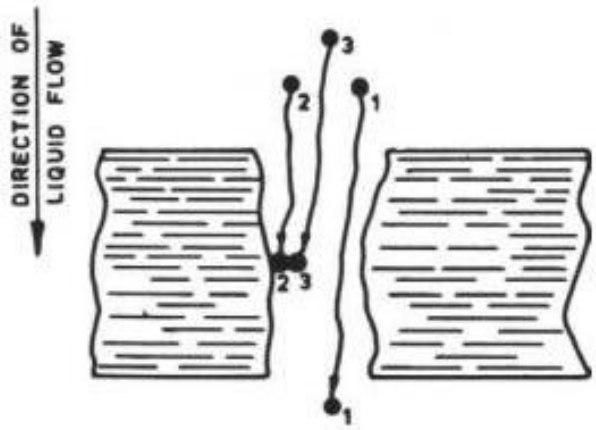

Figure 8: The depth filtration mechanism.

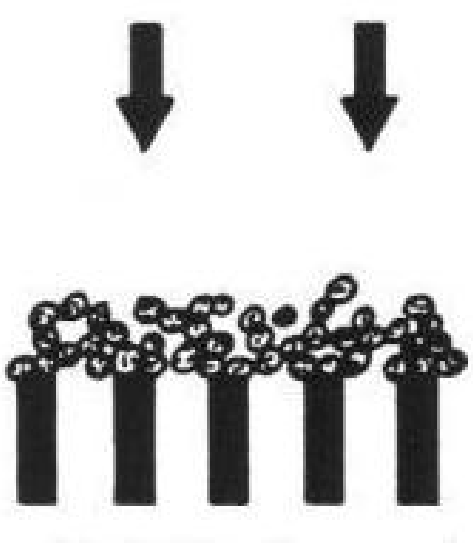

Figure 9: Cake filtration. All images from [3].

2.2.5 Mechanisms of depth filtration

Four mechanisms exist on how particles are captured internally by air filters[9]:

1. Impaction
2. Interception
3. Diffusion
4. Electrostatic attraction

See Figure 10 on how a particle in a gas stream may behave as it approaches a filtering *target*, e.g. a cellulose nanofiber in an air purification filter. If the particle comes in close contact with the target, there is a certain probability that it may stick to the target. Increasing the density or number of targets will increase the probability of particle capture, which increases collection efficiency but also the pressure drop as the filter medium porosity will decrease, cf. Equation 3 in the former section.

Impaction is characterized by larger particles with such mass and momentum that they are insignificantly affected by the diverging gas flow in close proximity to the target. Hence, they end up colliding with the target, in which they get stuck to or get buried into. The radius of curvature of the target determines the bend of the gas

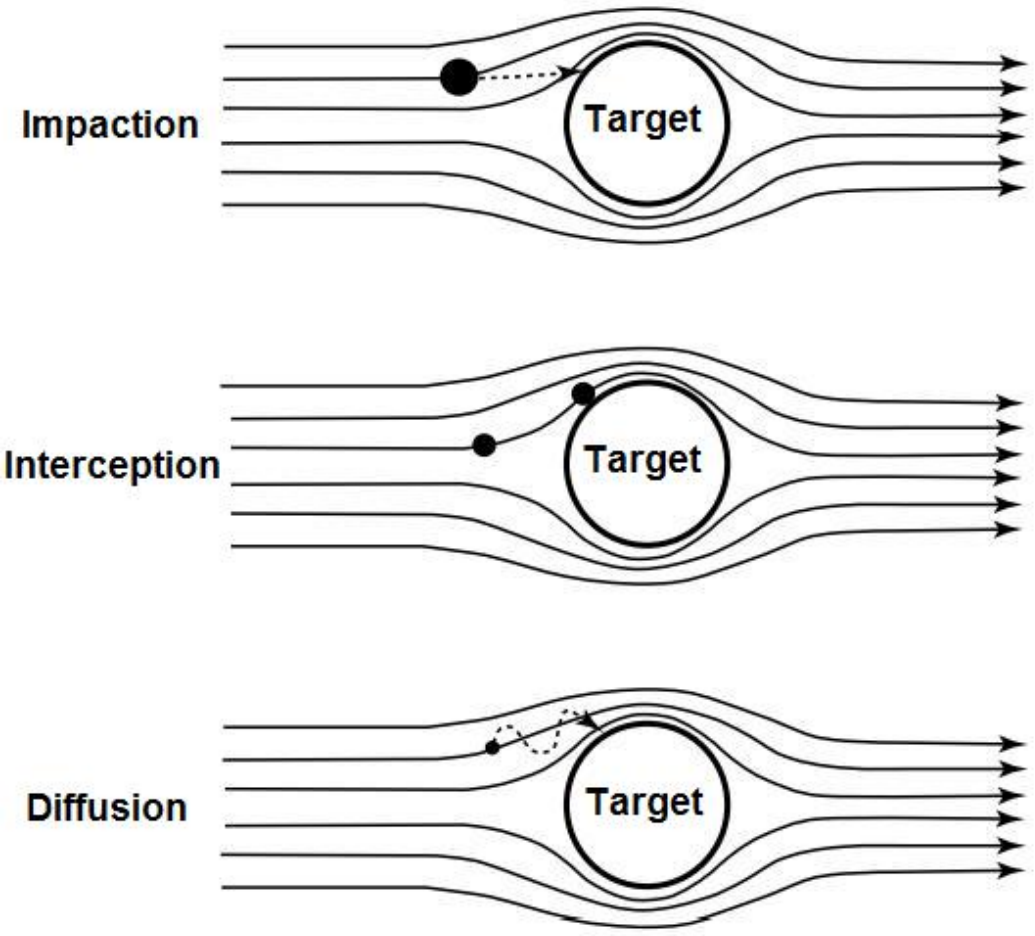

Figure 10: Basic particle collection mechanisms. Courtesy of [9].

streamlines. Smaller target particles give larger curvature of the travelling gas, which makes it more likely that the particle leaves the streamline and is collected by the target.

Interception occurs when a particle does not have enough inertia to be unaffected by the bend in the gas stream, and follows the streamline around the target. The particle is collected only if it passes close enough to the target surface and get stuck. The inertia of these particles is too big for Brownian motion (see below) to be important and too small for impaction to be the main collecting mechanism. Hence, interception explains why it is easier for both larger and smaller particles to be collected than particles in the size range $\approx 0.04\mu$m to 0.4μm[11].

Diffusion describes how nanoparticles are caught due to their constant Brownian motion which is caused by continuous collisions with gas molecules. The number of collisions with gas stream molecules is not high enough to direct their path away from the target trap, so their motion is more or less random. They may therefore be captured by a target if enough time is allowed to pass and the distance to the target is small.

Electrostatic attraction describes why particles with a charge are directed across the gas flow streamlines as they move towards an oppositely charged target. This mechanism is most efficient for small particles that can obtain a high charge/mass ratio.

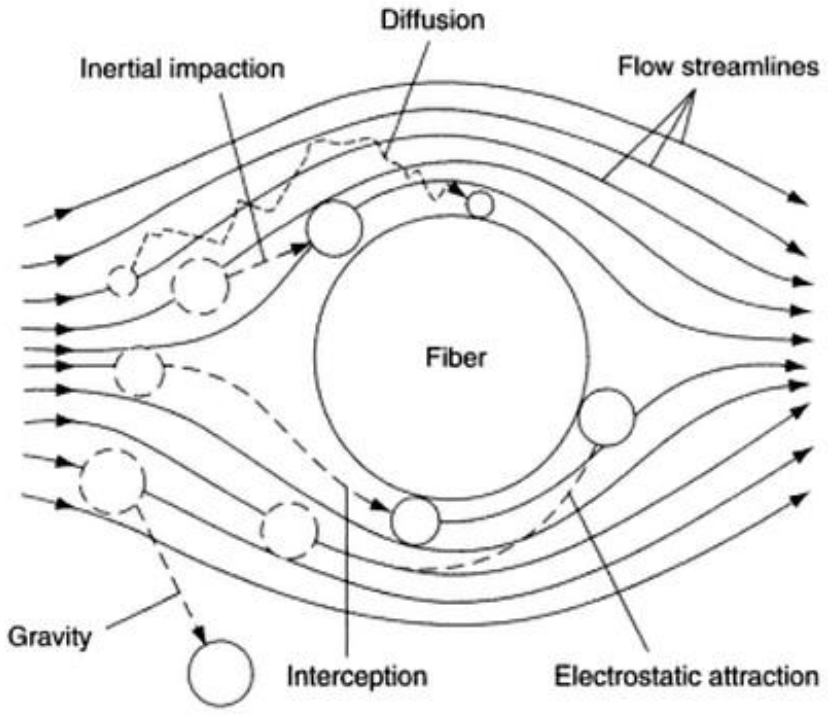

Figure 11: Summary of particle capture mechanisms. Courtesy of [11].

The four particle capture mechanisms are summarized in Figure 11. As mentioned, particles in the size range 0.04-0.4 μm are especially difficult to collect as they are too big for capture by Brownian motion and their intertia is too small to break free from the gas stream. Hence, particles of this size are the most difficult to capture by filter media and are therefore called "most penetrating particle size" (MPPS). Unfortunately, MPPS also includes "lung damaging dust" which may cause lung disease.

2.2.6 Filter testing

A large and ever increasing number of standard methods exist for testing a filter's performance. The methods are all established by either national authorities, specific industry organizations or by regional or international organizations such as CEN (Comité Européen de Normalisation) and ISO (the International Standards Organization)[3].

The filter might be tested with clean fluid to evaluate e.g. the permeability, resistance to flow per unit area of medium or the flow rate of air under a defined pressure. When the fluid contains dispersed particles, the goal is usually to determine the smallest particle retained and the relationship between particle size and retention efficiency, see section 2.1 for definitions. The most commonly used method for filtration testing is the *bead challenge test*, where spherical glass beads of various diameters are introduced to the feed flow in known concentrations[1]. The filtrate is subsequently studied for the beads that have passed through the filter. The largest bead that can be found in the filtrate represents the cut-off level of the filter medium.

2.3 Pore size control in organic materials

2.3.1 Templating

Micromolding techniques have been developed over the years, where structure directing agents such as emulsion droplets, microbeads and other colloidal templates have been used to control shape and size down to the nanometer scale. The template might or might not be removed after the templated material is in place.

An unexplored field for pore size control in nanocellulose filters is the use of hydrophobic templates. The basic idea is that the highly hydrophilic nanofibrils will avoid the hydrophobic shapes and bind less to the template than to each other. The goal is that the resulting pore size will be comparable to the repeating units of the template. No research material could be found concerning the control of pore size of filters prepared from pure NFC with the use of Ugelstad polystyrene beads (Dynabeads). Nevertheless, Dynabeads or other spherical nanoparticles have been used in controlling the pore size in other materials such as porous polyurethane films[14][15].

2.3.2 Air drying and the effect of solvent properties

Surface tension and solvent polarity

Given a system that consists of two phases separated by an interface, the surface tension is defined as[16]:

$$\gamma_{12} = \left(\frac{\partial G}{\partial A}\right)_{constant\, T,\, p} \tag{4}$$

where G is the Gibbs free energy of the entire system (phase 1 plus phase 2 plus interface) and A is the area of the interface. The SI unit for surface tension is therefore joules per square meter (J/m^2) or Newtons per meter (N/m)[17]. Surface tension is thus a measure of the additional energy associated with the interface. The term *surface free energy* is also used, and implies that *work* is required to bring e.g. water molecules from the interior of the phase to the surface (phase 1 = water and phase 2 = air). A water molecule is surrounded by a larger number of neighboring molecules within the water phase "bulk" relative to at the water surface. It will therefore cohere/bond more strongly to the water molecules directly associated with them at the surface, see Figure 12 for visualization.

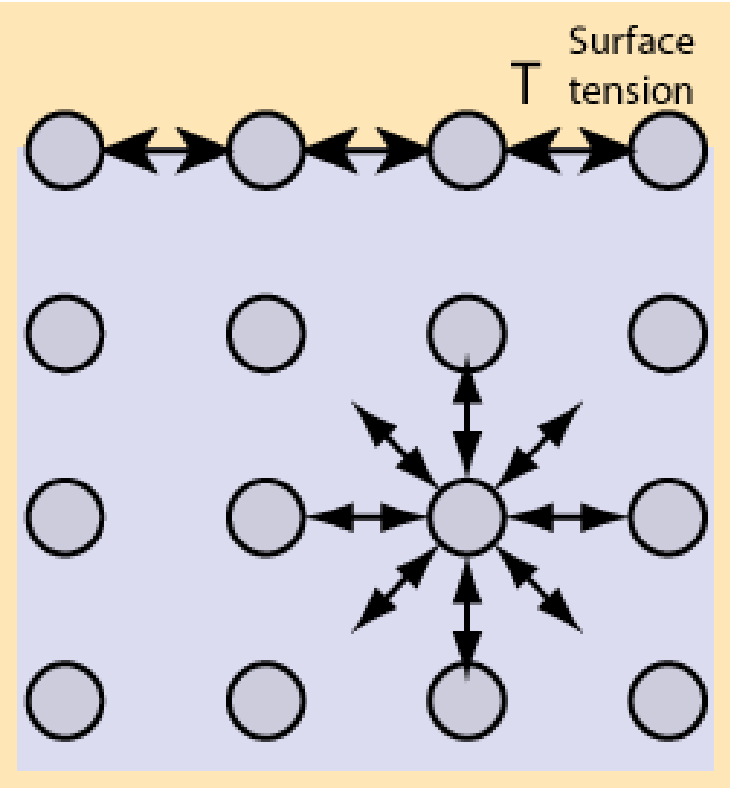

Figure 12: Molecules at the water-air interface cohere more strongly to each other as they have fewer neighboring molecules. Figure taken from [18].

The *polarity* of organic and inorganic solvents can be stated by their polarity index, which is a relative measure of the degree of interaction of the solvent with various polar test solutes. The polarity index of water, ethanol and isopropanol is 9, 5.2 and 3.9, respectively[19]. The three solvents will thus have varying surface tensions with unequal capillary pull on neighboring cellulose nanofibrils during evaporation.

Air drying and the effect of solvent on cellulose filter porosity

The driving force for water evaporation from a cellulose suspension is the difference in vapor pressure of the water in the suspension and water in the ambient air[4]. If the surrounding air is sufficiently dry, the filter will dry at room temperature, even though the drying time will be long. An increase in the temperature will boost the drying rate due to increased vapor pressure at the suspension surface. Another method to increase the evaporation rate is to use a more volatile solvent than water. For instance, pure ethanol has a vapor pressure of 5.95 kPa at 20° C, while pure water has 2.3 kPa.

When suspensions containing cellulose fibres and nanofibrils are left to air dry, solvent menisci are created between adjacent fibres/fibrils due to capillary forces. The solvent evaporation decreases the radius of curvature of the water meniscus, which again increases the capillary attraction between the fibres/fibrils[4]. The attractive force between the fibres is proportional to the surface tension of the evaporating solvent, and inversely proportional to the radius of curvature of the solvent meniscus[16]. Hence, the influence of surface tension increases as length scales decrease. Since the diameter of the smallest nanofibrils is

$\sim$ 4 nm, while fibre diameters are in the μm range, suspensions with a small average fibril dimension will form denser structures during solvent evaporation. Wood mass with various fibril diameters and solvents with different polarity and surface tension may therefore be combined to create cellulose filters with varying density and therefore filtering characteristics.

Cellulose filters prepared by different solvents No studies could be found on controlling the porosity of NFC air filters by experimenting with air drying from different types of solvents. Thus, production of pure cellulose air filters is an unexplored field. The studies mentioned here are therefore the most relevant, but it should be noted that the type of cellulose material, grammage, pretreatments and general procedures differ from the work presented in this report.

Henriksson et al[20] treated cellulose mass with enzymes to obtain a degree of polymerization (DP) of 410, 580 and 820, where the fibrils also contained carboxylic acid groups due to a second pretreatment. Here, solvent exchange was performed on wet films *after* the cellulose mass had been filtered through a glass filter funnel. The porosity of NFC films dried from pure water was shown to

reach 28%, while films dried from less polar solvents such as methanol, ethanol and acetone obtained had porosities up to 40%. The average pore size of the resulting filters was estimated to be 10-50 nm.

Porous structures from cellulose derivatives

At present, pure cellulose is not the most used material in membrane- and filtertechnology, but *derivatives* of cellulose such as cellulose acetate, cellulose triacetate and cellulose nitrate are extensively used in gas separation, reverse osmosis, microfiltration and ultrafiltration[21]. Khare et al[21] have used pure cellulose in preparation of such membranes, but the cellulose mass has been *dissolved* in e.g. N-methylmorpholine N-oxide (NMMO), dimethylacetamide (DMAc)/lithium chloride (LiCl) or NaOH with a low degree of DP. Coagulated films of NMMO-cellulose have also been studied by Zhang et al[22], who showed that the resulting films could possess pores down to 15-40 nm in size.

2.3.3 Freeze drying

Freeze drying, also known as *lyophilization*, has been used since World War II for preservation of biological matter and a wide range of products without the need for refrigeration[23]. In freeze drying, the material is frozen

below its triple point (the lowest temperature and pressure at which the solid and liquid phases of the material can coexist), with subsequent sublimation, see Figure 13. The solvent is thus transferred directly from solid to gaseous state by reducing the surrounding pressure to avoid the liquid-gas transition. In materials sciences, freeze drying is often used when a fragile, porous structure will collaps under solvent evaporation as the gentle process of freeze drying leaves the structure intact.

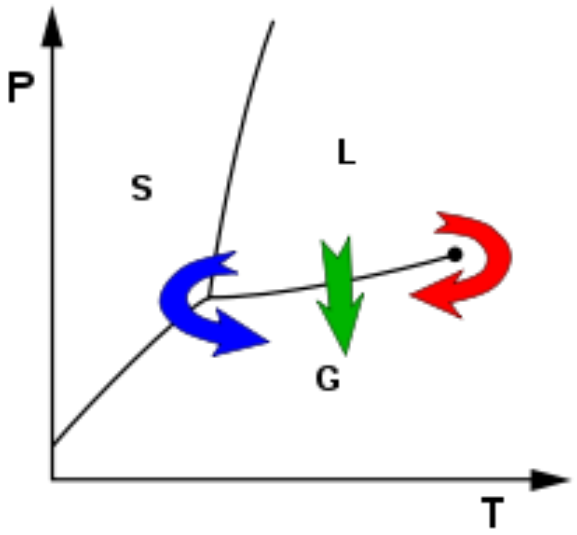

Figure 13: Freeze drying is represented by the blue arrow, avoiding the triple point, while regular air drying crosses the liquid-gas transition (green arrow). Critical point drying (red arrow) avoids this transition by circumventing the critical point at higher T and p. Figure from [24].

Porous cellulose filters obtained by freeze drying

As studies on porous filters obtained from high DP nanocellulose in different solvents are scarce, the same apply for cellulose filters prepared by freeze drying. The studies mentioned below give an overview of what is done so far in the field of freeze drying of cellulose derivatives or other biological materials.

Nanofibrillar cellulose aerogels have been prepared from dissolving cellulose powder or fibres in calcium thiocyanate tetrahydrate ($Ca(SCN)_2 \cdot 4H_2O$)[25][26].
The ($Ca(SCN)_2 \cdot 4H_2O$)-cellulose solution formed a gel that was subsequently freeze dried, supercritically dried or dried by solvent exchange to avoid pore collaps. The resulting aerogels had a density between 10 and 60 kg/m^3 and a maximum surface area of $160 m^2/g$ due to highly porous networks composed of nanosized cellulose fibrils. Such aerogels are fragile, so a support layer is necessary if they are to withstand high pressures if used in particle separation processes.

Nge et al[27] have created bio-nanocomposites by freeze drying mixtures of bacterial cellulose (BC) and chitosan with various weight ratios. The resulting porous com-

posite scaffolds had pores in the size range 120 - 280 μm and the compressive modulus and strength increased with increase of NFC content. Freeze drying has also been used to create porous scaffolds of other biological material such as collagen[28][29][30] where the main application is within tissue engineering.

Freeze drying and supercritical drying of cellulose aerogels have been compared[26]. Conventional freeze drying made the aerogels crack and more brittle compared to utilizing critical point drying. As supercritical drying is a more gentle method for removing solvents that exhibit a volume change on freezing, this method has been preferred when used in producing cellulose aerogels.

Ice crystal formation

When the ice crystals in a frozen cellulose-water suspension are removed by sublimation, gas-filled pores are left behind. The pore structure of the freeze-dried filter is therefore a direct reflection of the original distribution of ice crystals. The ice crystal size in the frozen NFC suspension is highly dependent on how the water in the suspension is frozen. It has been shown that a high *freezing rate*, (the velocity of the ice front), will result in a smaller mean size of the ice crystals, and therefore smaller

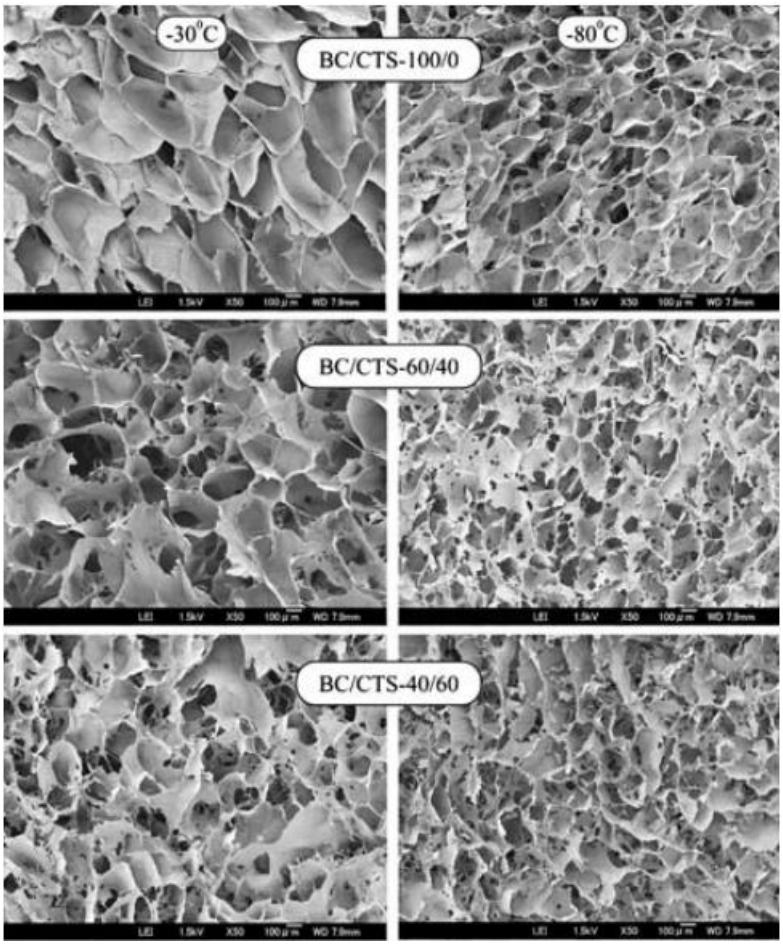

Figure 14: Difference in resulting pore size as a result of freezing of bacterial cellulose/chitosan solutions at two different temperatures, $-30°C$ and $-80°C$. The lower freezing temperature of $-80°C$ gives smaller mean pore size in the resulting porous scaffolds. SEM image from [27].

mean pore size of the freeze dried filters[27]. An example of this is shown in Figure 14. If the suspension is allowed to freeze over a longer time period with a low temper-

ature gradient (e.g. in a normal deepfreezer), larger ice crystals are allowed to form. During the freezing process, the nanocellulose fibrils are separated from the growing ice crystals and are confined to the interstitial regions between them. Typically, the contact point where two ice crystals merge will be characterised by a pit, which can be seen as a crack or fissure in the vacuum-dried sample. Loss of fibrillar morphology has been reported to be due to such merging of microcrystals caused by ice crystal formation[31], which results in a flake-like mass.

Water expands by $\sim 10\%$ when frozen due to an ordering of the water molecules. However, it is possible for water to be frozen so rapidly that it does not have time to form crystals, and remain amorphous. If there exist thermal gradients across the freezing suspension, size variations of the resulting ice crystals will exist. Above $-121°C$, amorphous ice gradually restructures as cubic ice (as vitreous ice is an unstable state), and expansion will occur. Above $-80°C$, cubic ice restructures as hexagonal ice, and expands again[32].

Liquid nitrogen is one of the coldest liquids that are readily available. Even so, N_2(liq) has the disadvantage that it boils eagerly at a warmer contact point, which results

in a vapor barrier (i.e. a layer of nitrogen gas) that hinders cold penetration into the sample which again slows down the rate of freezing in an unpredictable manner. This often results in slower freezing of the inner parts of the sample compared to freezing of outer layers that first are in contact with liquid nitrogen. The inner parts will therefore experience crystal formation in a larger degree, which makes the sample expand, followed by cracking of the outer shells due to tensile stresses[33].

2.3.4 BET surface area analysis

The BET theory (developed by Brunauer, Emmet and Teller) aims to describe molecular adsorption of gas molecules onto a solid surface. It is an extension of the *Langmuir theory* which assumes that[34]:

1. Only a monolayer of gas is adsorbed.
2. The enthalpy of adsorption is constant, i.e. the first and last molecule to arrive adsorbs equally strongly to the surface.
3. Immobile adsorption; the gas molecules do not move around when first adsorbed to the surface.
4. Dynamic equilibrium between the gaseous and adsorbed species (reversible adsorption).

The Langmuir adsorption isotherm can be written as:

$$\Theta = \frac{KP}{1 + KP} \tag{5}$$

where Θ is the fraction of all active sites on the surface that is occupied by gas molecules, P is the gas pressure and K is the ratio between the adsorption and desorption reaction constants. See Figure 15 for a visualization of the adsorption/desorption processes that takes place at the solid surface. More than one monolayer of gas might be adsorbed onto a solid surface if the pressure is sufficiently high. BET theory is distinguished from the Langmuir

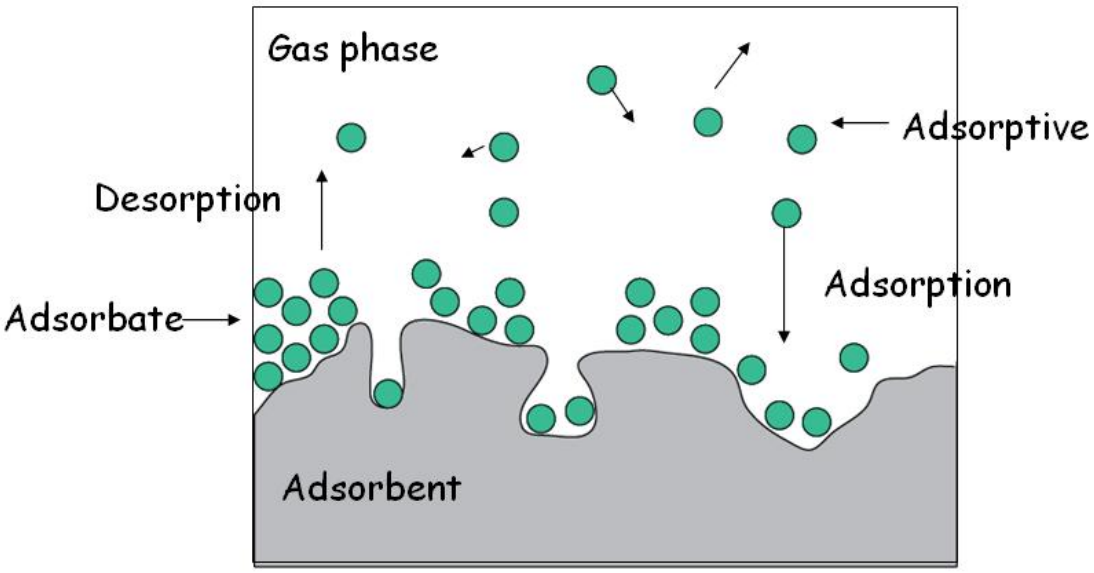

Figure 15: Adsorption of a gas on a solid porous structure. The adsorptive becomes the adsorbate on the adsorbent when adsorbed. Image from [35].

theory as it takes this into account. The BET equation is therefore slightly more complex[35]:

$$\frac{\frac{P}{P_\circ}}{v_a\left(1-\frac{P}{P_\circ}\right)} = \frac{C-1}{v_m C}\frac{P}{P_\circ} + \frac{1}{v_m C} \tag{6}$$

where v_a is the adsorbed gas volume at equilibrium pressure and v_m is the necessary volume to obtain a monolayer. P and $P_\circ$ is the equilibrium and saturation pressure of nitrogen at the temperature of adsorption. C is the BET constant, which is expressed by:

$$C = exp\left(\frac{H_1 - H_L}{RT}\right) \tag{7}$$

where H_1 is the heat of adsorption for the first layer and H_L is that for the second and higher layers, i.e. the heat of liquefaction.

As the value $\frac{\frac{P}{P_\circ}}{v_a\left(1-\frac{P}{P_\circ}\right)}$ is plotted against $P/P_\circ$, a linear BET plot of the type shown in Figure 16 is obtained. The "y"-values, the slope and the line's intercept with the y axis defines the unknown values v_m, v_a and C.

When v_m and C have been determined by the BET plot, a nitrogen adsorption isotherm that describes the amount of N_2 gas adsorbed to the porous sample as a function of the applied nitrogen pressure ($P/P_\circ$) is obtained[36]. In the surface area calculations a value of 0.162 nm^2 is used for the area of an adsorbed nitrogen molecule[37]. Physical properties such as average pore size, pore size distribution and surface area are valuable information that may be extracted from such adsorption isotherms[5].

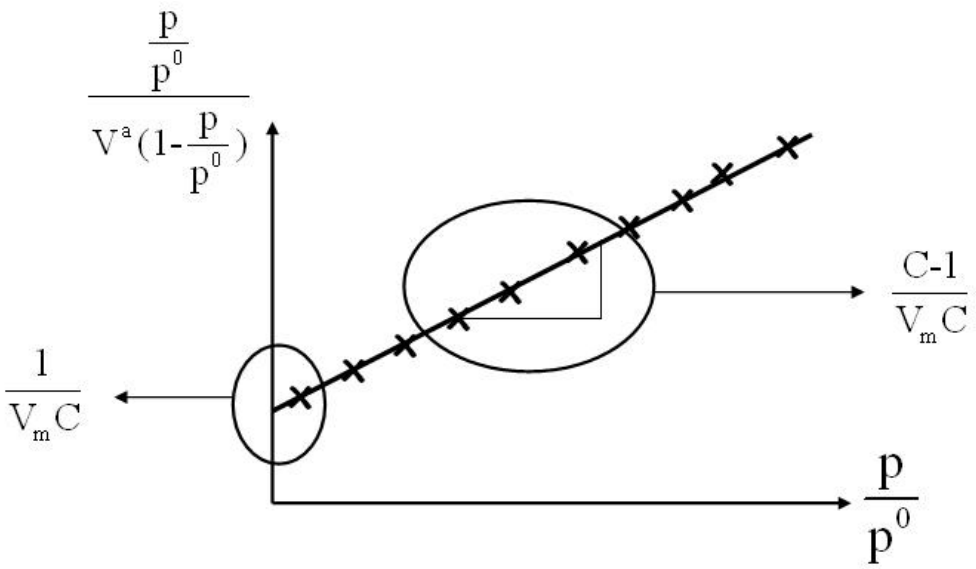

Figure 16: A BET plot which describes the linear relationship between the indirect measurement of the amount of gas adsorbed vs increasing values of P/P° (at constant T). Image from [35].

2.4 Cellulose and cellulose nanofibrils

2.4.1 Cellulose and the architecture of wood fibers

Cellulose is a polysaccharide consisting of $\beta(1\rightarrow4)$ linked D-glucose units in a linear chain with the chemical formula $[C_6H_{10}O_5]_n$, see Figure 17. Carbon # 2, 3 and 6 carry a hydroxyl group each. The high concentration of these polar groups is responsible for cellulose's hygroscopic nature[38]. The β-linkages promote the formation of *intramolecular* hydrogen bonds, which cause the molecules to line up in linear arrays which again cause *intermolecular* hydrogen bonds to form between adjacent glucose chains[39].

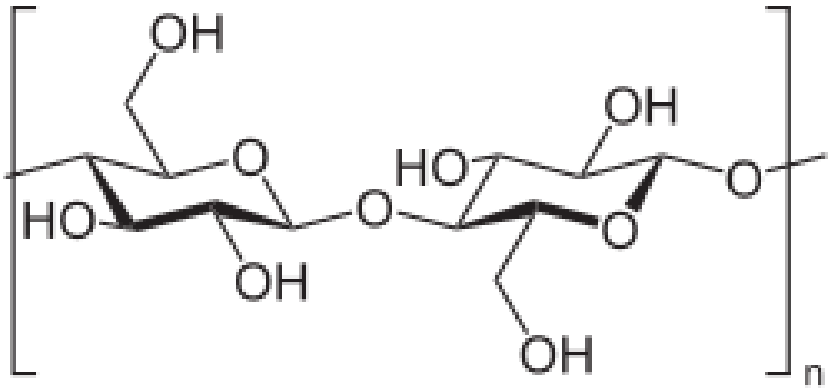

Figure 17: The repeating units in a cellulose molecule. A single cellulose molecule may consist of 9000-10 000 such double glucose units. The length of a single glucose unit is close to 0.50 nm. The degree of polymerization (DP) will correspond to 2n. Image from [40].

Cellulose is a highly crystalline and water-insoluble polymer that makes it degrade before it melts due to the strong hydrogen bonding between the hydroxyl groups[21]. When the individual cellulose chains bond strongly to neighboring chains via hydrogen bonds, they form cellulose nanofibrils which consist of ~ 6 x 6 cellulose molecules. These *elementary nanofibrils* are several micrometers long with lateral dimension of ~ 4 nm x 4 nm which consist of alternating crystalline and amorphous areas that partly blend into each other. Elementary nanofibrils tend to aggregate and form secondary nanofibril bundles with lateral size of 20-40 nm[41]. These bundles join together in larger fibrils, which are the building blocks of a wood fibre. There are approximately 1 300 000 nanofibrils per wood fibre cross-section which has a typical fiber diameter of 13 μm[42]. See Figure 18 for a visualization of the structural components of a wood fibre.

In addition to cellulose nanofibrils, wood fibers consist of hemicellulose and lignin. The degree of polymerization (DP) is typically 10 000 in cellulose, but merely 200 in hemicellulose. Further, hemicellulose is not as linear and crystalline as cellulose and contains several side groups. Cellulose is therefore responsible for the wood fiber's *mechanical strength* while hemicellulose gives *flexibility*

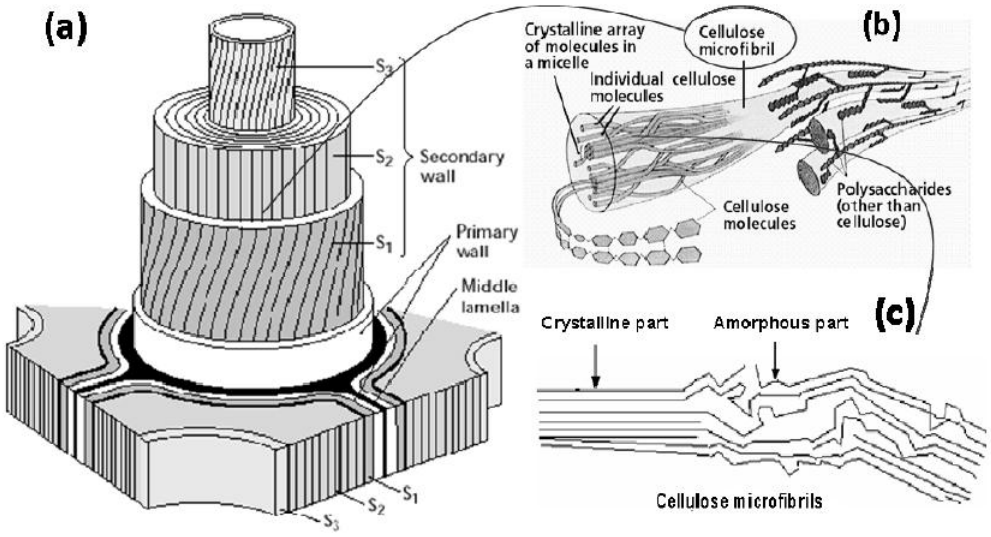

Figure 18: a) Composition of the wood cell wall. b) A schematic presentation of cellulose microfibrils. c) A microfibril with crystalline and amorphous regions. Courtesy of [43].

to the material. Hemicellulose also serves as the binding agent between cellulose and lignin, where the latter is the glue that binds the wood fibers together. Hence, the middle lamella that separates the wood fibers contains between 40-60% lignin[4], depending on the type of tree.

2.4.2 Cellulose nanofibrils and NFC film properties

The first publication on the successful isolation of cellulose nanofibrils from wood was reported in 1983 by Turbak et al[44]. Cut cellulose fibers from softwood pulp were subjected to high shear forces in a Gaulin laboratory homogenizer. The process resulted in a material in which

the wood fibers were opened into their sub-structural nanofibrils. In general, the term 'nanofibrils' is reserved fibrils with a diameter below $\sim$ 100 nm. Depending on how wood mass and how the fibres are processed, the produced nanofibrils may have diameters ranging from 4 to 100 nm and several μm in length[45].

The numerous hydroxyl groups are responsible for cellulose's high affinity for water. But even if pure cellulose is hydrophilic with a contact angle of 20°-30°[46], it is insoluble in water, i.e. the cellulose chain is not split into individual glucose units when immersed in water.

Cellulose nanofibrils have a large aspect ratio (estimated to 1000:1) which ensures a large specific surface area with reactive OH-groups. The maximum theoretical surface area a cellulose material with density of 1.5 g/m^3 and fibril diameter of 4 nm can have, is 667 m^2/g. This assumes a perfect nanofibrilliation of the material, no agglomeration of the fibrils and that the total surface area is exposed. If the average fibril diameter is 20 nm, which is typical for cellulose material that is not TEMPO pretreated[47], the maximum obtainable surface area is reduced to 133.33 m^2/g.

Films of NFC have shown to have suitable mechanical properties for e.g. packaging with tensile strength close to 150 Nm/g, elongation of 8.6% and an elastic modulus of 14 GPa at a density of $1340 kg/m^3$[48]. The downside with NFC films is the poor barrier properties against water vapor due to the hydrophilic character of the nanofibres. This causes a reduction of the tensile strength of NFC films when they are subjected to higher levels of humidity. A possible explanation of this is that water acts as a plasticizer which reduces the concentration and strength of the hydrogen bonds between the nanofibrils. This problem has been tackled by e.g. surface chemical modification of the film surface[49] or adding melamine formaldehyde which results in less water uptake of the material[20].

Characterization

Nanofibrils and nanocellulose films have been extensively characterized by the use of techniques such as transmission electron microscopy (TEM) and scanning electron microscopy (SEM) in combination with software programs[45][50].

2.4.3 Cellulose nanofibrillation

Pulping

Pulping is the first step on the way to nanofibrillation of the wood mass. During pulping of the wood, the middle lamella is almost completely removed so that the wood fibres can be separated from each other (fibrillation)[51]. As the middle lamella mainly consists of lignin, the pulping process is also called *delignification*. As no chemical is completely selective towards lignin, a certain amount of cellulose and hemicellulose is lost in this process[38]. The *kraft process* (also called the sulphate process) is by far the favored chemical pulping process where NaOH and Na_2S are used to break down the lignin molecules into smaller fragments. The pulping process may be followed by a bleaching process, which is normal when the material is to be used as filter media[11].

Homogenization

In homogenization, cellulosic wood pulp-water suspensions are passed through a mechanical homogenizer where the fibers are subjected to a large pressure drop with shearing and impact forces[52]. The fiber suspension is also forced through a gap between disks with grooves against which the fibers are subject to repeated cyclic

stresses. This combination of forces causes a delamination of the cell walls of the wood fibers, which result in a liberation of the cellulose nanofibrils. The procedure is often repeated several times (passes) in order to increase the degree of fibrillation. Homogenization leads to fibril structures with diameters between 20 and 100 nm and estimated lengths of several tens of μms[52].

The nanofibrils in cellulose are tightly bond to one another by multiple hydrogen bonds, which has proven their extraction both difficult and energy demanding. Hence, the drawback with homogenization as a method to obtain nanocellulose, is its high energy consumption where values between 20 and 30 MWh/tonne are not uncommon[52]. Despite the amount of energy required, the resulting product consists mainly of bundles of nanofibrils as it has not been possible to individualize cellulose nanofibrils using solely mechanical disruption[53]. To address these problems, enzymatic or chemical pre-treatments such as TEMPO-mediated oxidation of the fibers prior to homogenization have been developed which can reduce the energy consumption with more than 95% down to 1 MWh/tonne[54].

TEMPO-mediated oxidation

In 2006, Saito et al introduced a pre-treatment based on oxidation of cellulose by the use of TEMPO radicals[53]. TEMPO is an abbreviation for the chemical compound (2,2,6,6-Tetramethylpiperidin-1-yl)oxyl which is visualized in Figure 19. The compound is a stable nitroxyl

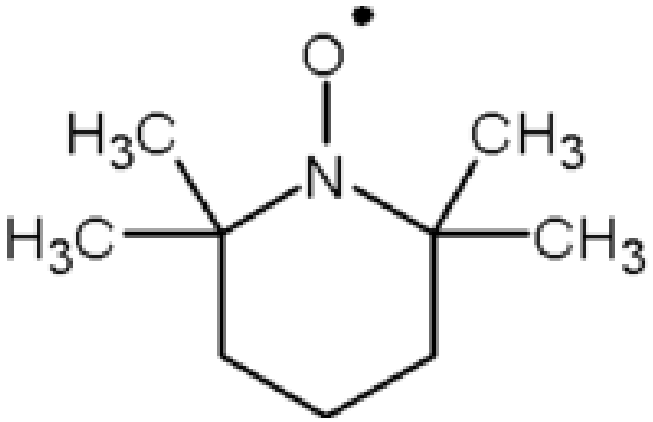

Figure 19: The chemical structure of TEMPO.

radical that is soluble in water. TEMPO-mediated oxidation introduces carboxylic acid groups in the C6 position of the glucose units, see Figure 20 for the steps in the oxidation process. The TEMPO radicals catalyze oxidation of primary hydroxyl groups at pH 9-11 by using NaBr and NaClO, which function as additional catalyst and oxidant, respectively.

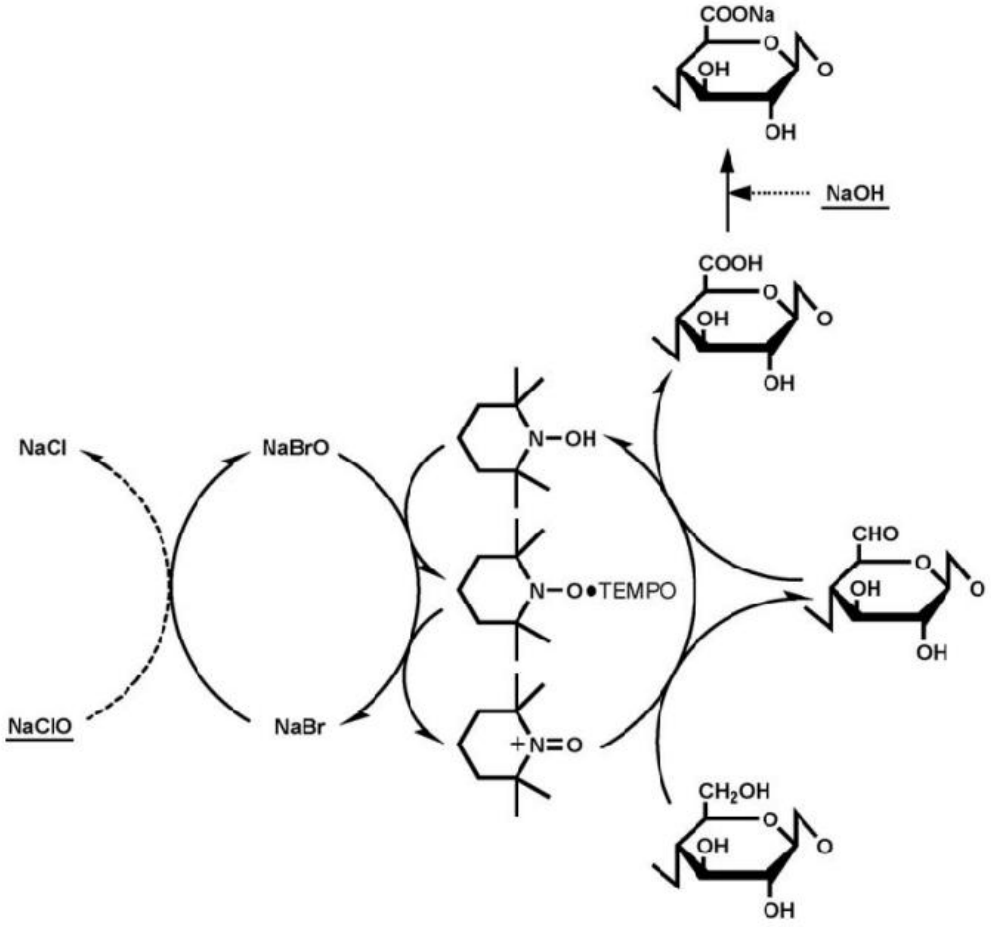

Figure 20: Scheme of TEMPO-mediated oxidation of cellulose.

The carboxylate content increases typically 150-170 times due to the pre-treatment[55]. The carboxylic acid groups facilitate the homogeneous fibrillation since the negatively charged acid groups create repulsive forces which greatly enhance the ease of separation of individual nanofibrils.

3 Experimental

3.1 Templating

Ugelstad beads with a diameter of 50 μm were mixed in either pure water, a mixture of isopropanol/water or pure isopropanol in plastic petri dishes with a diameter of 8.5 cm. The weight (= number) of beads added was calculated as to cover 90% of the petri dish bottom to avoid formation of several layers of beads. The mixing of the supensions was done both manually and by the use of an ultrasonic bath. The plastic petri dishes containing the suspensions were subsequently left in a fume hood and tilted at an angle of 2-3° with the intention to facilitate the formation of a monolayer of beads.

3.2 Filters prepared by solvent evaporation

The wood mass used in this work has solely come from Pinus Radiata which is the most widely planted pine across the globe[56]. Fibrillation of the Pinus radiata fibres has been performed either purely mechanically with 3 passes through the homogenizator at 1000 bar or chemi-mechanically by subjecting the fibres to a TEMPO-mediated oxidation prior to homogenization, see Section 2.4.3. For simplicity, the two types of processed cellulose masses have been named 3p (3 passes through the homogeniza-

tor) and T/3p (TEMPO-pretreatment combined with homogenization) throughout this work. Characterization of nanofibrils subjected to these processes has been carried out earlier[47][45].

8 NFC filters were prepared from water, ethanol or isopropanol to investigate how the type and concentration of solvent would affect the permeance, strength and general characteristics of the resulting filters:

1. 3p in 100% water
2. T/3p in 100% water
3. 3p in 50/50 weight % ethanol/water
4. T/3p in 50/50 weight % ethanol/water
5. 3p in 50/50 weight % isopropanol/water
6. T/3p in 50/50 weight % isopropanol/water
7. 3p in 100% ethanol
8. 3p in 100% isopropanol

Two filters of each type of suspension were prepared, i.e. a total of 16 filters. Solvent exchange was performed on the mechanically fibrillated mass (3 pass), where it was

centrifugated with a Heigar IEC Centra-3C 5 times at 2500 rpm for 30 minutes; first in water, then four times after washing with either ethanol or isopropanol. See Appendix A.3 for more details. Solvent exchange could not be performed on the TEMPO-pretreated mass, as it remained a homogeneous gel without NFC precipitation, even at centrifugation of 3600 rpm. Higher rotation speeds were not attempted, as this could cause the glass holders to break. Hence, the planned filters made from TEMPO-pretreated mass in 100% ethanol and isopropanol could not be prepared.

The dry weight content was established for all cellulose suspensions. This was done by recording the wet and dry weight of samples from all the cellulose suspensions before and after overnight evaporation of the solvent in an oven which held 105°C. The resulting dry weight content ranged from 0.23% for T/3p in 50% ethanol to 0.61% of 3p in 100% ethanol. Subsequently, the correct amount of each cellulose mass was carefully poured into plastic petri dishes with a diameter of 8.5 cm to produce films with a set grammage of 20 g/m^2. The time required for complete air drying of the filter cellulose mass spanned from 5 to 31 hours depending on the vapor pressure of the solvent.

3.3 Filters prepared by freeze drying

A second procedure for creating porous cellulose filters was established by freezing the cellulose suspensions with either liquid nitrogen or in a deep freezer prior to vacuum drying. Only mechanically treated wood mass in water was used here, as the TEMPO-pretreated mass had resulted in dense and brittle filters.

3.3.1 Freeze drying with liquid nitrogen

The first set of filters were to contain either 2 or 4% dry weight content (DW%) of cellulose before subjecting them to freeze drying. The suspension of 3p wood mass in 100% H_2O had a DW% of 0.44%, hence, the petri dishes containing the cellulose suspension had to air dry until they reached the wanted DW%. Test filters were therefore prepared to make it possible to estimate the necessary drying time. Here, the weight of pure NFC in every petri dish (still with diameter 8.5 cm) was always $\sim$ 0.1135 g to maintain the set grammage of $20 g/m^2$ from former experiments. The test filters were let to air dry in a fume hood, while the weight of the mass including petri dish was measured periodically.

As the last volume of solvent had evaporated during the night, a mathematical function of the form

$$\text{f(t)} = (\text{total mass}) \cdot e^{-xt}$$

was used to fit the weight data and then estimate the necessary drying time to obtain the wanted DW%.

New sets of samples were then prepared and left to air dry until either 2 or 4% dry weight content had been reached. The petri dishes containing the partly dried NFC suspension were then set to float on boiling, liquid nitrogen in a metal pan. When the samples were frozen solid, they were rapidly transferred to a vacuum chamber for freeze drying. In addition, a filter with dry weight content of 0.44% was prepared in this way, to compare the resulting filters with 0.44, 2 and 4% weight content.

3.3.2 Freeze drying with deepfreezer

The last set of cellulose filters were prepared from leaving cellulose suspensions with varying grammage and dry weight content in a deep freezer with constant temperature of $-28°$C. The frozen samples were transferred to a vacuum dryer of the type 'Heto Lyopro 6000' and left to dry over 1-3 days & nights depending on the total volume

of water to be evaporated. At this stage, only water was used as the 3 pass solvent since the suspensions with 50 and 100% ethanol and isopropanol have a lower freezing point than -28°C[57][58]. See Tables 1 and 2 below for an overview of the filters prepared:

Varying the dry weight content	
Filters with equal grammage of $20 g/m^2$	0.44 $DW\%$ 0.52 $DW\%$ 0.88 $DW\%$ 1.00 $DW\%$ 2.00 $DW\%$ 4.00 $DW\%$

Table 1: Overview of filters with equal grammage and varying dry weight content.

Varying the grammage	
Filters with equal dry weight content of 0.44%	20 g/m^2 25 g/m^2 30 g/m^2 35 g/m^2 40 g/m^2

Table 2: Overview of filters with same dry weight content, but varying grammage.

5 filters were prepared for statistical analysis on how the permeance varies as a function of grammage and wood mass height in the petri dish before freeze drying. The grammage and wood mass height of the 5 filters are presented in Figure 21.

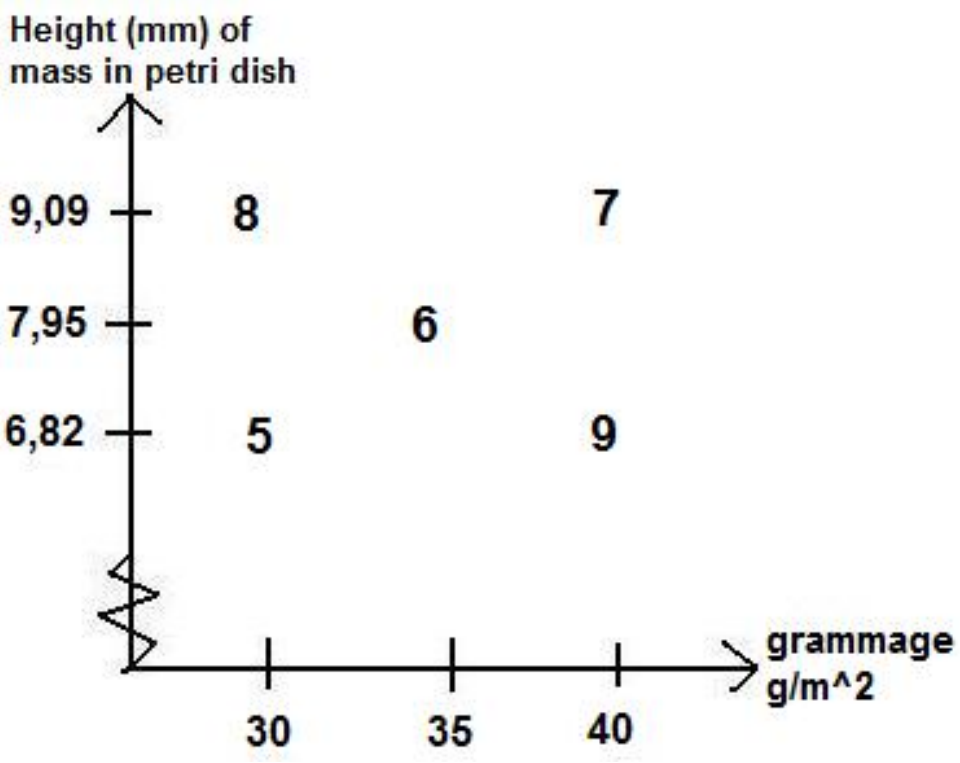

Figure 21: Filters 5, 6 and 7 have all a dry weight content of 0.44%, i.e. they were set directly in the deep freezer without evaporation. Filter 8 was diluted to have a DW% of 0.33 and filter 9 was left to air dry until a DW% of 0.59 was reached.

3.4 Instruments and methods used for characterization

3.4.1 Air permeance measurements

All filters that were not too bulky, brittle or with large cracks were tested with a Gurley apparatus which has the ability to measure air permeance in a quick and simple way. See Figure 22 for a sketch of the apparatus. A given volume of air is compressed and pushed through the filter by the weight of an inner cylinder which floats on oil. Ten measurements were done on different areas of each filter and the average number of seconds it took for the air to pass through a set area of the filter was registered and converted into permeance.

For all the filters prepared by solvent evaporation, the maximum possible test area with a diameter 2.87 cm was evaluated in combination with a minimum air volume of 50 ml. As the permeance values of filters prepared by freeze drying were $\sim$ 5000 times higher, the tested area was narrowed down to a hole of diameter 5.5 mm punched out from a plastic film which was inserted over the filter when tested. Here, a maximum air volume of 200 ml was pushed through the filters.

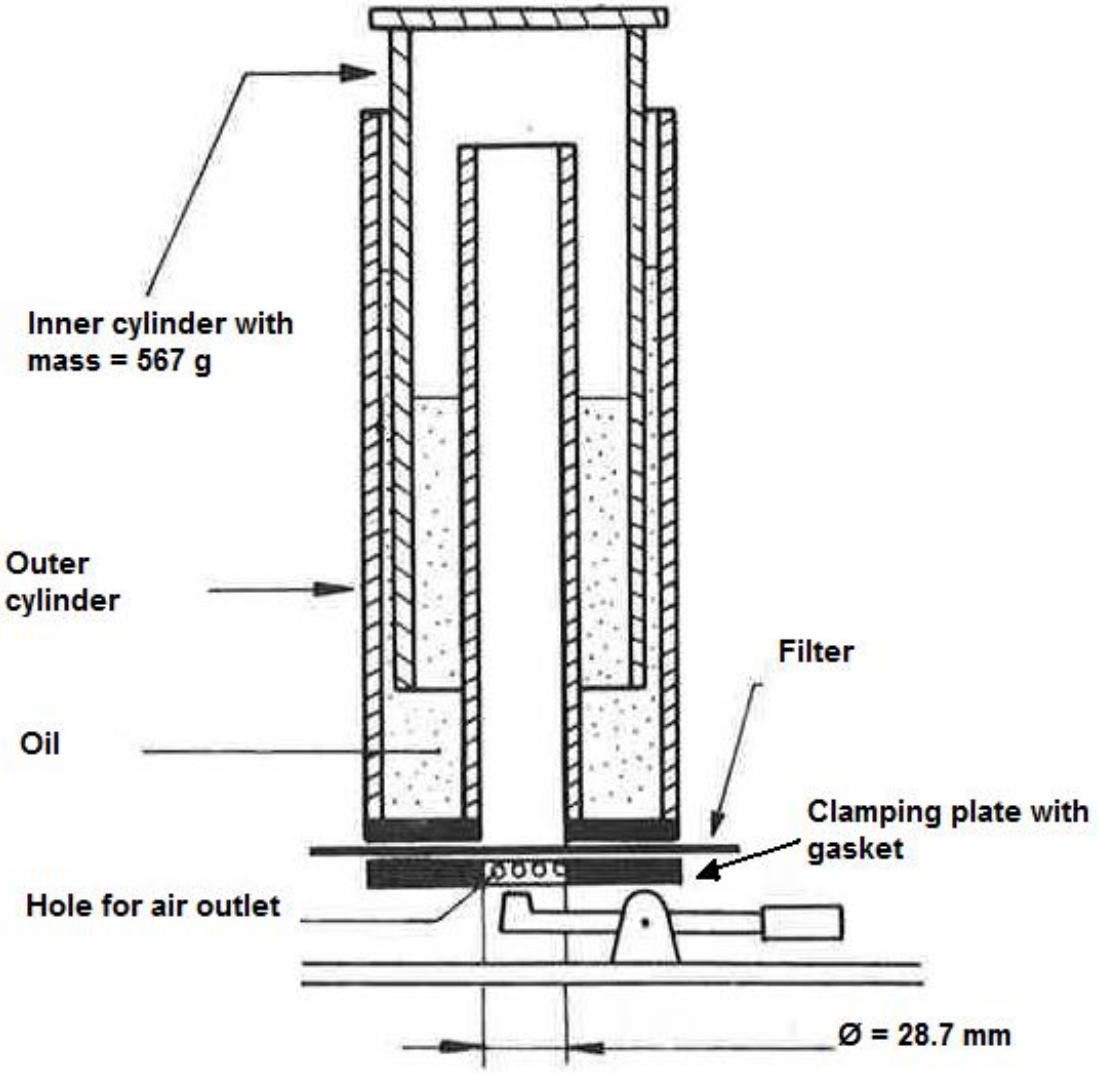

Figure 22: Sketch of a Gurley apparatus. Scanned image from [59].

3.4.2 Scanning and surface/cross section visualization

The filters prepared by solvent evaporation were scanned by an Epson Perfection 4990 Photo. As the filters prepared by freeze-drying were thicker, more sponge-like and prone to deformation, visualization of them was assessed by an IXUS digital camera with 8 Mpixels.

The surface of selected filters was assessed with a Hitachi S-5500 In-Lens ultra high resolution S(T)EM. 3 random areas for each magnification (200 X, 2000 X and 20 000 X) were imaged to get a good overview of both the macro- and microstructures of the surface morphology. A special sample holder was employed to obtain an impression of the cross section of selected filters, see Figure 23.

3.4.3 Filter thickness measurements

The filter thickness was evaluated by three different methods: a standard instrument designed for paper thickness assessment, cross-section in SEM of a sample cast in epoxy or with S(T)EM. When calculating the volume of the filters, a radius of 4.25 cm was used for all filters for simplicity, as some were quite bulky with a small degree of shrinkage.

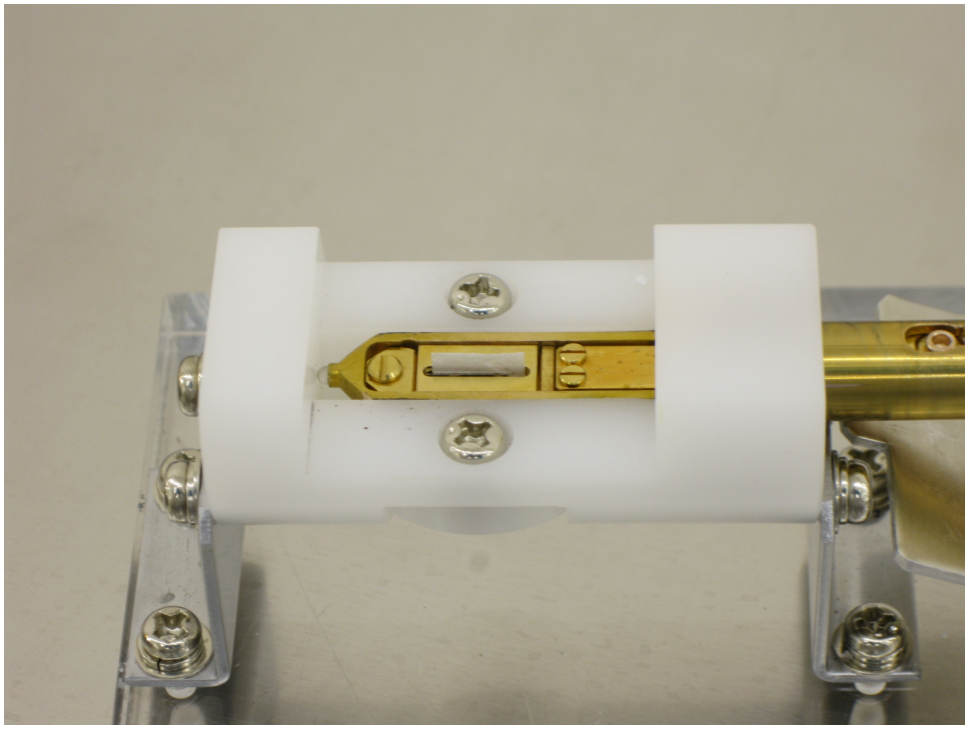

Figure 23: S(T)EM cross section sample holder with cellulose filter sample mounted.

The porosity of the filters could then be calculated by linking their density to porosity with the relation:

$$porosity = 1 - \frac{\rho_f}{\rho_c} \tag{8}$$

where ρ_f is the density of the film and ρ_c is density of cellulose, which is assumed to be $1500 kg/m^3$[20], i.e. $1.5 g/cm^3$.

Standard instrument for paper thickness measurements

The thicknesses of most filters were assessed by a standard instrument from Lorentzen & Wettre AB, Sweden, which is developed for determining paper thickness. The instrument automatically lowers a metal probe which stops when registrating a certain resistance. A small area of $< 1mm^2$ is measured at a time. When studying cellulose filters with a rough surface, one should be aware of that such standard instruments will most likely give an exaggerated value for the thickness[50]. See Figure 24 for visualization of actual and apparent thickness of a rough cellulose film.

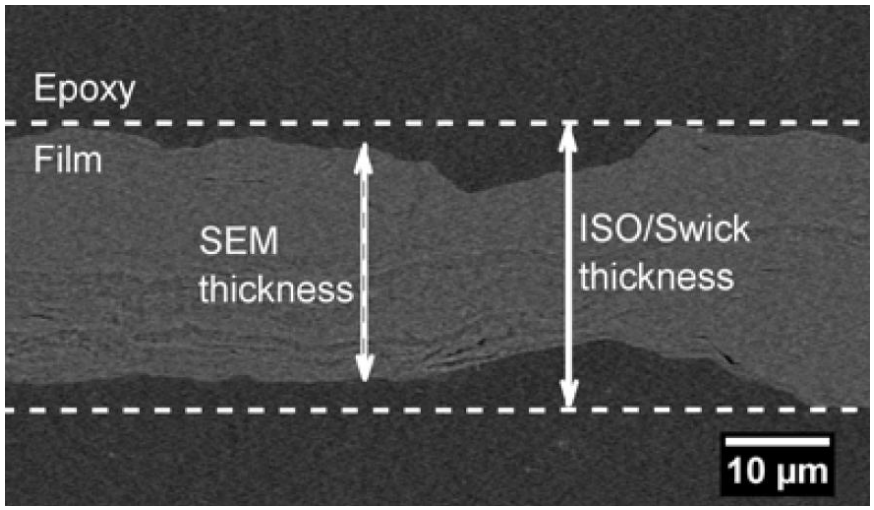

Figure 24: While the intrinsic film thickness is measured with a SEM, the exaggerated, apparent thickness is given by standard instruments. Image taken from [50].

SEM of filters cast in epoxy

As mentioned above, the instrument from Lorentzen & Wettre AB is likely to *overestimate* both the thickness and the calculated porosity of the resulting filters. A selection of filters were therefore cast in epoxy, where their cross-section could be assessed by a Hitachi S-3000N SEM in BEI mode:

First, the filter samples were cut to rectangular pieces (1 cm x 2 cm) which were aligned in a parallel fashion on two stretched spirals that function as the sample holder. The samples were subsequently oven-dried and put in a a small plastic container before a mixture of Epofix resin and Epofic hardening agent was added at 200 mBar in an Epovac vacuum chamber. Hardening of the epoxy occurs after $\sim$48 hours at room temperature. The samples were then transferred to an Accustop holder and $\approx$ 1 mm of the epoxy was grinded away so that the cross section of all filters are found at the epoxy surface. Polishing of the surface was first done on an MD-Largo grinding wheel in combination with DP-Spray P 9 μm diamant spray, and finally on an MD-NAP grinding wheel with 1 μm diamant spray. See Figure 25 to see the resulting grinded and polished epoxy blocks.

Figure 25: The three epoxy blocks which were examined by SEM in BEI-mode.

The epoxy filter blocks were coated with carbon as it is the lightest electronically conductive material, and therefore do not shadow the backscattered electron signal from the underlying filter cross sections. The average filter thickness was determined by measuring 3 x 3 cross sections for each filter in centimeters and converted from cm to μm according to the image scalebar, see Figure 26.

Cross section imaging with S(T)EM

A final attempt to measure the filter thickness was done by mounting the filter samples in the S(T)EM sample holder shown in Figure 23, and studying the filter cross section. The filter thickness was evaluated by a built-in utility function in the S(T)EM software.

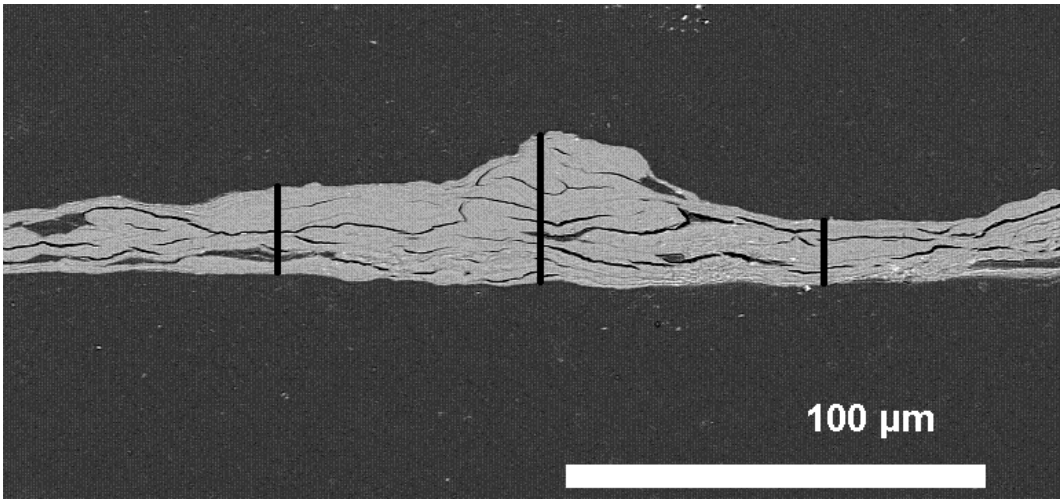

Figure 26: Cross section of a filter prepared by evapoaration of 50/50 ethanol and water. The black lines show where the thickness measurements were performed on each filter image.

3.4.4 Tensile strength

All filters that could be cut into strips were tested with a Zmart.pro apparatus from Zwick/Roell. The strips with an edge length of 15 mm were mounted vertically between two clamps that moved apart until complete tearing of the strip. The testXpert software was employed to calculate and display the resulting tensile strength. Between 3 and 8 measurements were conducted on each filter, the number depending on the possibility of multiple measurements on one single strip.

3.4.5 Surface area

The surface area of the cellulose filters was assessed with a Micromeritics Tri Star 3000 Surface Area and Porosity Analyzer. The instrument uses N_2 adsorption and the implemented BET equation to estimate the total surface area of the sample. A vacuum is combined with a test temperature of -196°C and known amounts of nitrogen gas are injected into the sample. See section 2.3 for more information on the BET theory.

The specific surface area of 3 selected filters was determined. The filters had a grammage of $20g/m^2$ and a dry weight content of either 0.44%, 0.88% or 2.00% before they were left in the deep freezer and subsequently vacuum dried. Several pretreatments were attempted to obtain satisfactory plots. The first set of test samples was degassed at $\approx$ 0.15 mBar overnight and the second set was degassed at 70°C at 0.15 mBar overnight before BET analysis. The amount of mass in each test tube was between 13 and 61 mg for these two individual experiments. As they resulted in unreliable plots, it was assumed that unsatisfactory drying of the hydrophilic cellulose samples was the underlying problem. The third set of samples was therefore left in an oven at $105°C$ for $>$ 48 hours be-

fore they were degassed at 0.15 mBar at $105°C$ overnight. Exposing the samples to ambient air was minimized by carrying them in an exsiccator and using rubber plugs on the glass test tubes containing the material. When the test tube containing the *highest sample mass* gave a usable plot, a 4th set of samples was produced. These filters were given the same pretreatment as set 3, but the sample mass in each test tube exceeded 100 mg as one entire filter was inserted into each test tube. The combination of test mass beyond 100 mg and thorough drying/degassing was therefore the chosen procedure for the three filters.

3.4.6 Regression analysis

Regression analysis deals with finding the best relationship between a dependent variable (response) and one or several independent variables. A linear relationship which describes the effect of these variables on the response is obtained, in addition to a set of estimators that describe how strongly they correlate[60]. If the relationship is exact, the relationship between the two variables is said to be *deterministic*. This is usually *not* the case, as most scientific and engineering phenomena are probabilistic in nature.

A multiple regression structure in which the response (Y) is determined by two independent variables (x_1 and x_2) might be written as:

$$Y = \alpha + \beta_1 x_1 + \beta_2 x_2 \tag{9}$$

where α and the β's are the unknown intercept and slope parameters, respectively. A quantity called *random disturbance*, η, with an expectation value of 0 and variance of σ^2 is often included in the response. Y will therefore be a random variable since η is random, while the values of the regressor variables are measured with negligible error (e.g. the grammage of the air filters). The estimates for α and the β's are calculated by using the method of least squares. Here, a value for the intercept and slope predictors of the regression line is found when the sum of all squares of the residuals (distance from actual point to regression line) is minimized. The adequacy of the fitted model is described by several parameteres such as R^2 and P-values. The quantity R^2 is called the *coefficient of determination* and is a measure of the proportion of variability explained by the fitted model[60]. If the fit is perfect, all residuals are zero, and the value for R^2 is 1.0 (or 100%). I.e., the closer R^2 is to 100%, the better fit between data points and the linear trend line. A low

P-value is good as it tells us how probable it is to obtain our regression line if there were no linear relationship between X and Y overall. I.e., the P-value is the probability of obtaining such a regression line as far from horizontal (or further) from *random data points*.

Minitab is a statistical analysis program which was employed for regression analysis to assess how the filter grammage was linked to the resulting permeance and maximum strength of the cellulose filters. The small amount of filters tested was limited to give a *trend*, but still gave useful information.

4 Results

4.1 Templating

The goal of obtaining a perfect monolayer of Ugelstad beads was not reached, see Figure 27 for a photographic image of the best result. The beads were studied in an op-

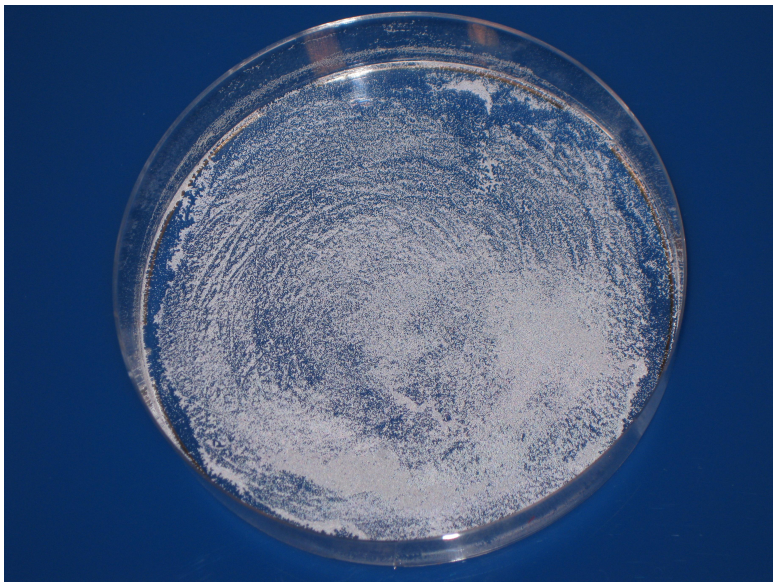

Figure 27: The attempt to create a perfect monolayer of Ugelstad beads was not successful.

tical microscope (without photo-options), where it could be seen that the petri dish bottom consisted of areas without beads and areas where several layers of beads lay on top of each other like a small mountain formation.

4.2 Filters prepared by solvent evaporation

As presented in section 3.2, 2 sets of 8 different filters from various solvents were prepared. These include:

1. 3p in 100% water
2. T/3p in 100% water
3. 3p in 50/50 weight % ethanol/water
4. T/3p in 50/50 weight % ethanol/water
5. 3p in 50/50 weight % isopropanol/water
6. T/3p in 50/50 weight % isopropanol/water
7. 3p in 100% ethanol
8. 3p in 100% isopropanol

4.2.1 Scanning of filters

7 of the 8 types of cellulose filters were scanned to give an impression of their general appearance and light transmittance, see Figures 28 - 31. Filter nr 8, i.e. 3p in 100% isopropanol could not be scanned or subjected to air permeance and thickness measurements as both the filters were completely stuck to the plastic petri dish after isopropanol evaporation. A new set of filters prepared by NFC in 100% isopropanol would have been created in

Teflon petri dishes, as this might have avoided sticking of the filters to the petri dish bottom.

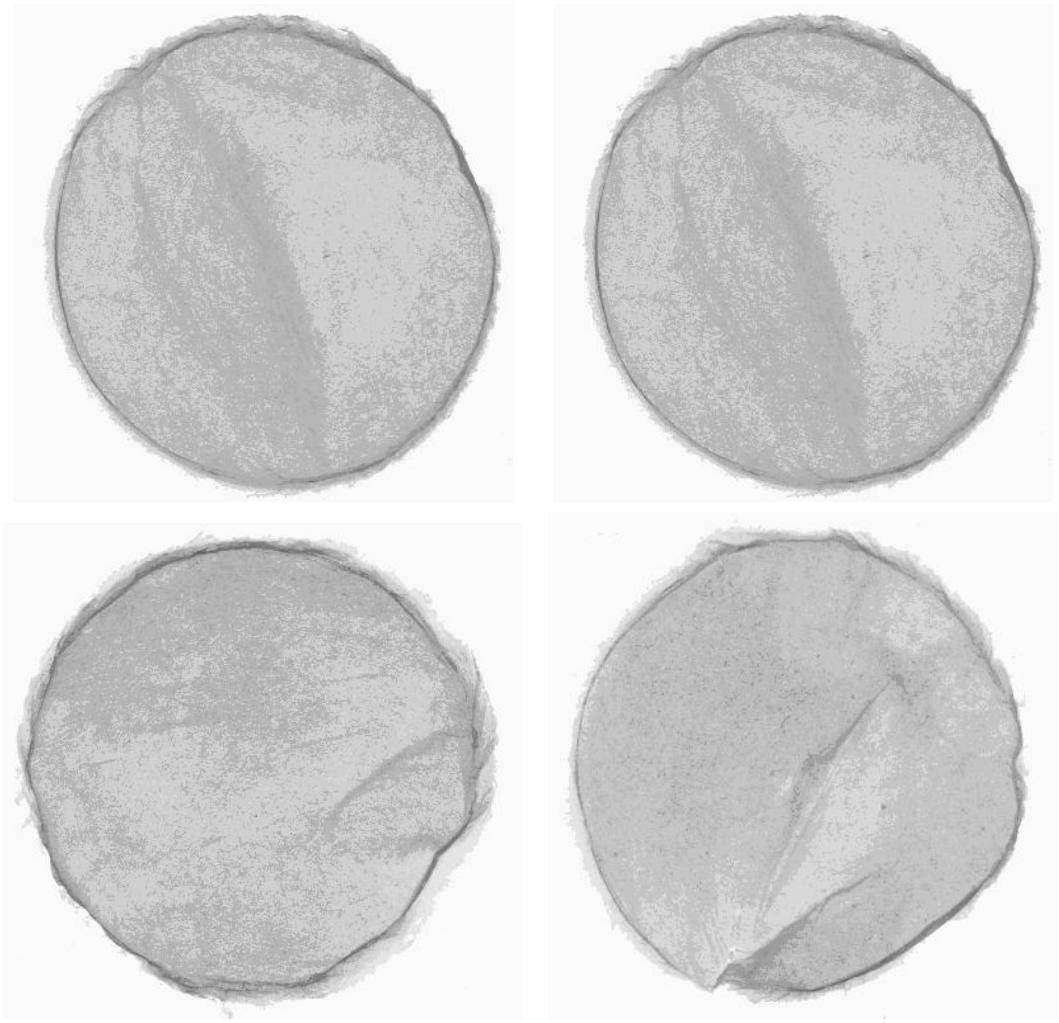

Figure 28: The two upper filters are prepared from 3 pass in 100% water while the two lower ones from NFC in 50/50 isopropanol/water. Their apperance, thickness and air permeance were comparable.

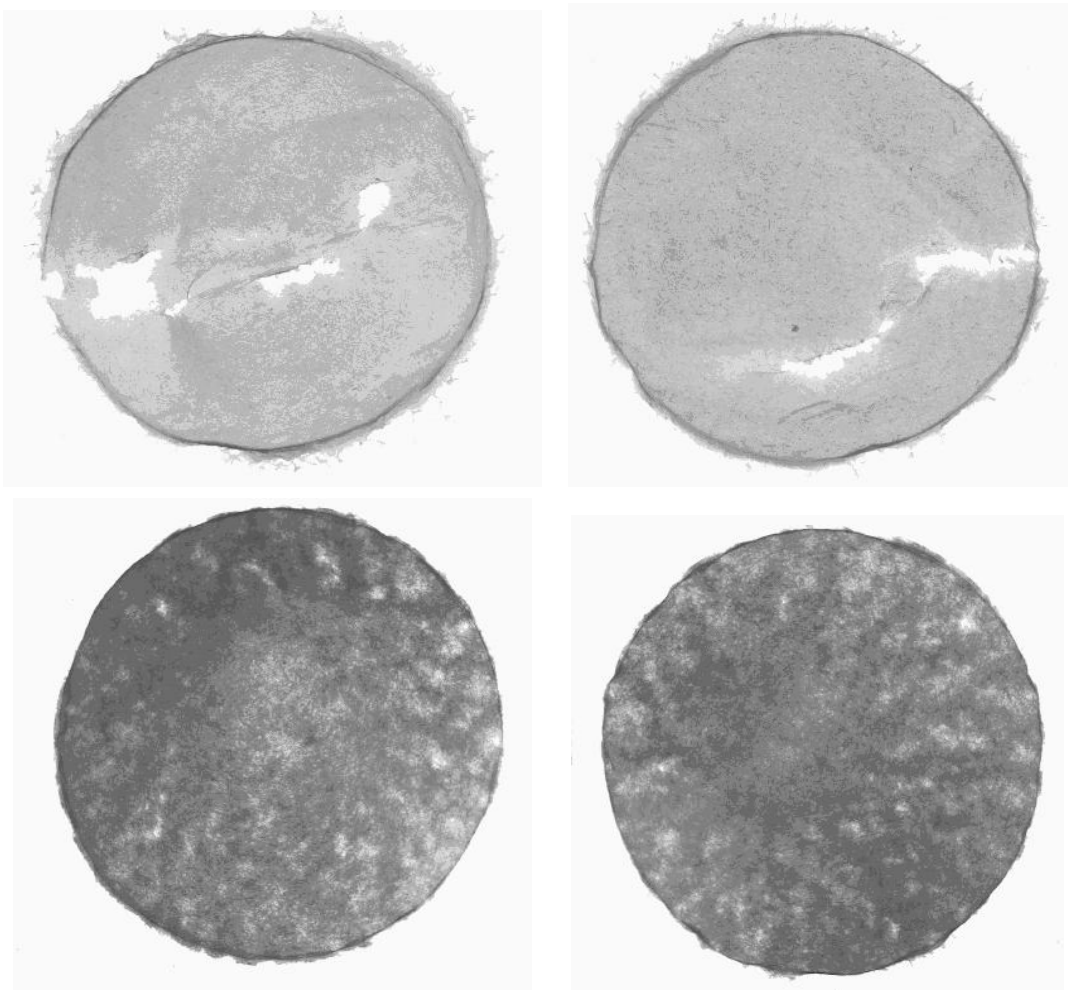

Figure 29: The two upper filters are prepared from 3 pass in 50% ethanol. Both of them contained large cracks which made permeance measurements more difficult. The two lower filters are from from 3 pass in 100% ethanol which gave the highest permeance values for filters prepared by solvent evaporation.

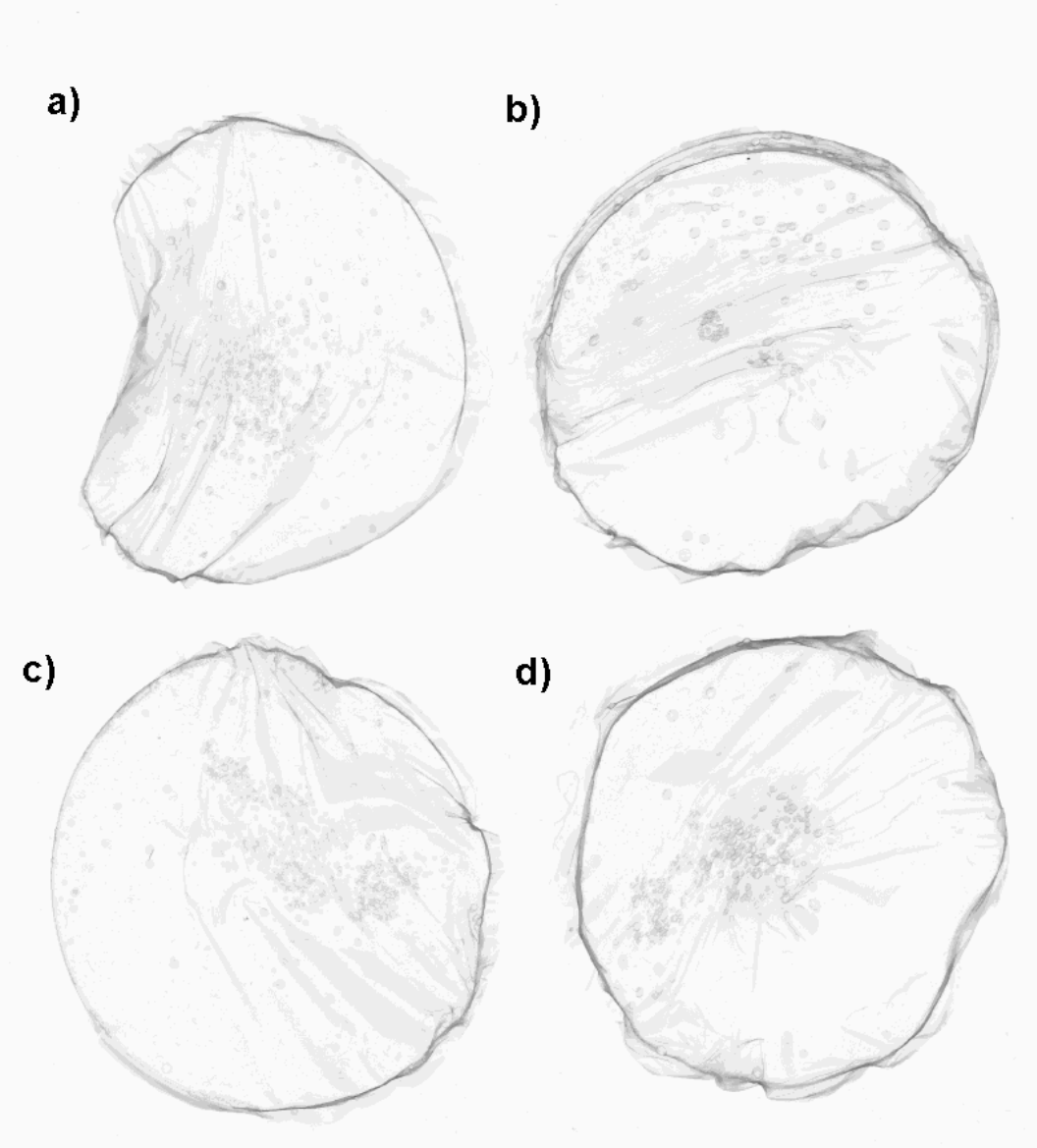

Figure 30: a) and b) are filters prepared by T/3 pass NFC in 50% isopropanol, while c) and d) are from the same mass in 50% ethanol.

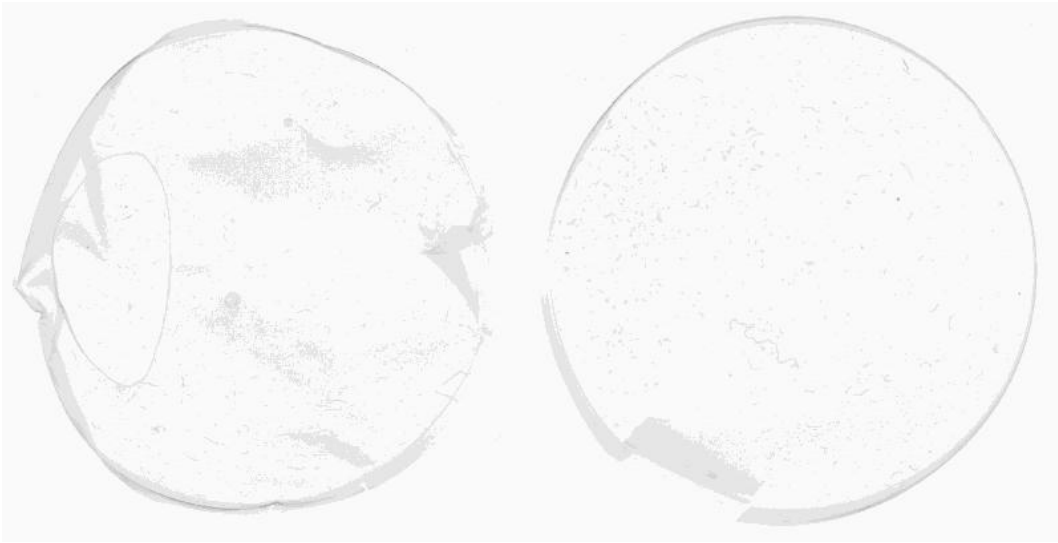

Figure 31: Filters prepared from T/3 pass in 100% water. Filters prepared from TEMPO-pretreated wood mass generally resulted in translucent, dense and brittle films.

4.2.2 S(T)EM images of surface morphology

S(T)EM images were obtained to characterize the surface morphology and apparent porosity of the filters prepared by 3 pass in various solvents. The surface of the filters prepared from the TEMPO-pretreated cellulose mass was seemingly structureless, and at increased magnification, the film just cracked and burned under the electron beam, see Figure 32.

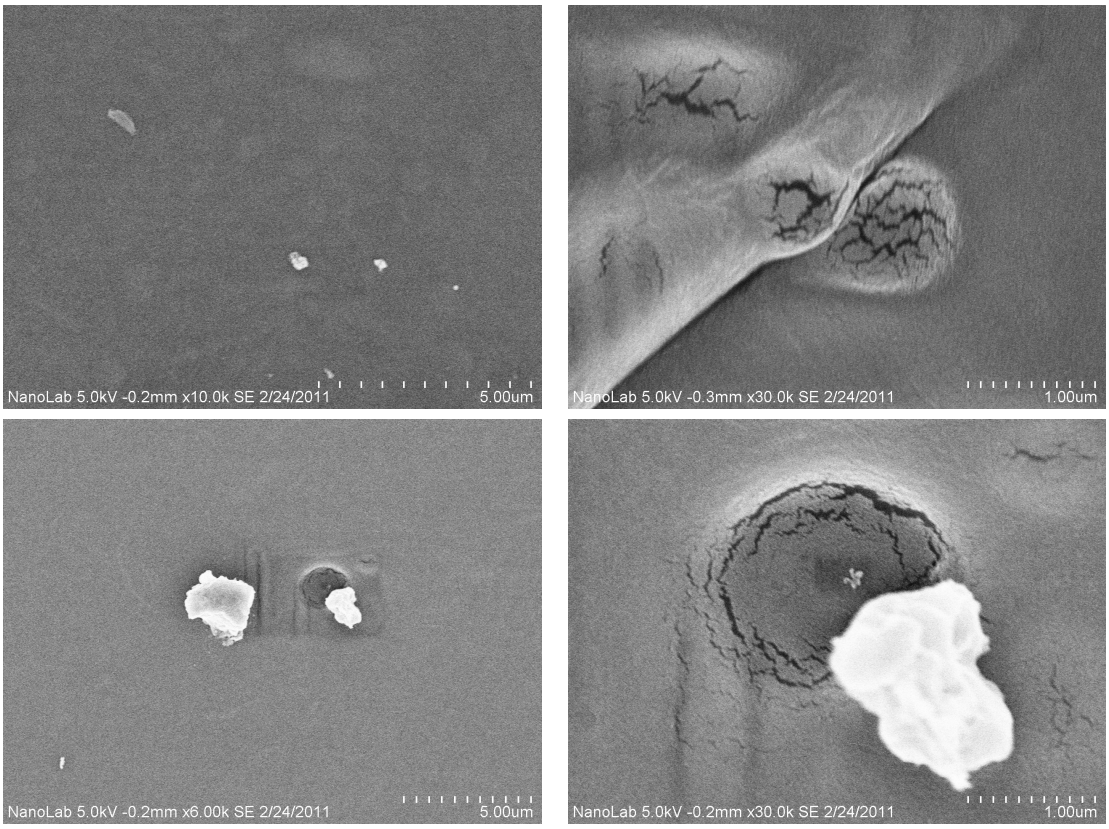

Figure 32: Up, left: T/3 pass in 50/50 water and isopropanol. A typical featureless filter surface due to the effective fibrillation caused by TEMPO-pretreatment. The fibrils are so small and densely packed that no larger structures except dust particles and some fringes are visible. Last 3 images: T/3 pass in 100% water. Burning and cracking of the filters occured when attempting to focus under high magnification.

For the remaining filters, a magnification of 200 X gave an overview of the surface, while the magnification of 2000 X and 20000 X ensured a visualization of the surface microstructures. The imaged areas were all chosen by random or by the homing point* of the instrument to ensure a non-biased presentation of the filters.

Only 2 of the 3 images taken for each magnification per filter is included here, as to limit the total number of images. In all the following image arrays, the images in the first column represent increasing magnification from the *same area**, while images in the second column are not. The first row of all arrays has a magnification of 200 x and a scale bar of 200 μm, the second row are images with 2 000 x magnification and a 20 μm scale bar and the third row: magnification of 20 000 x with a resulting scale bar of 2 μm.

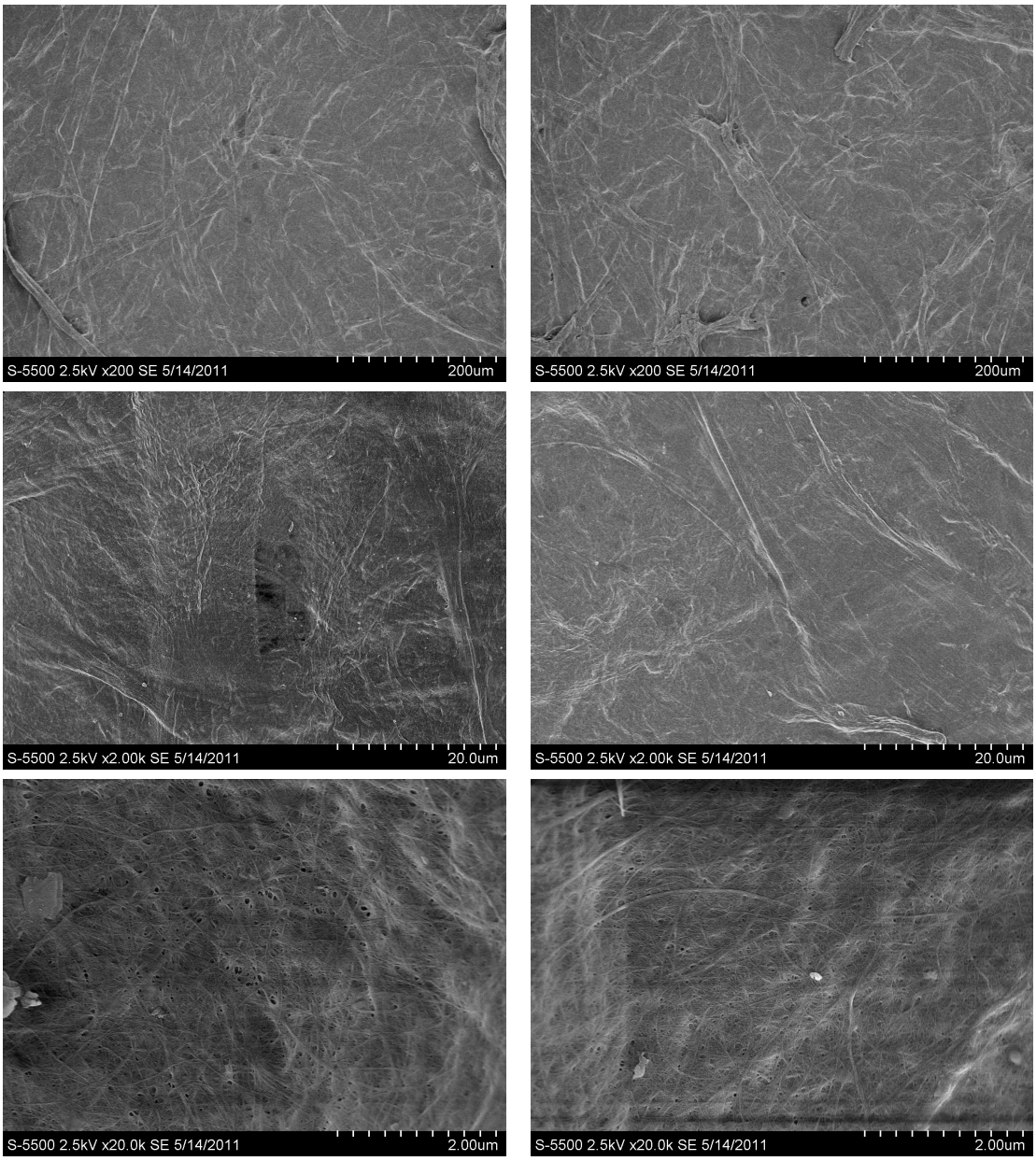

Figure 33: Surface images of filter prepared from 3 pass in 100% H_2O.

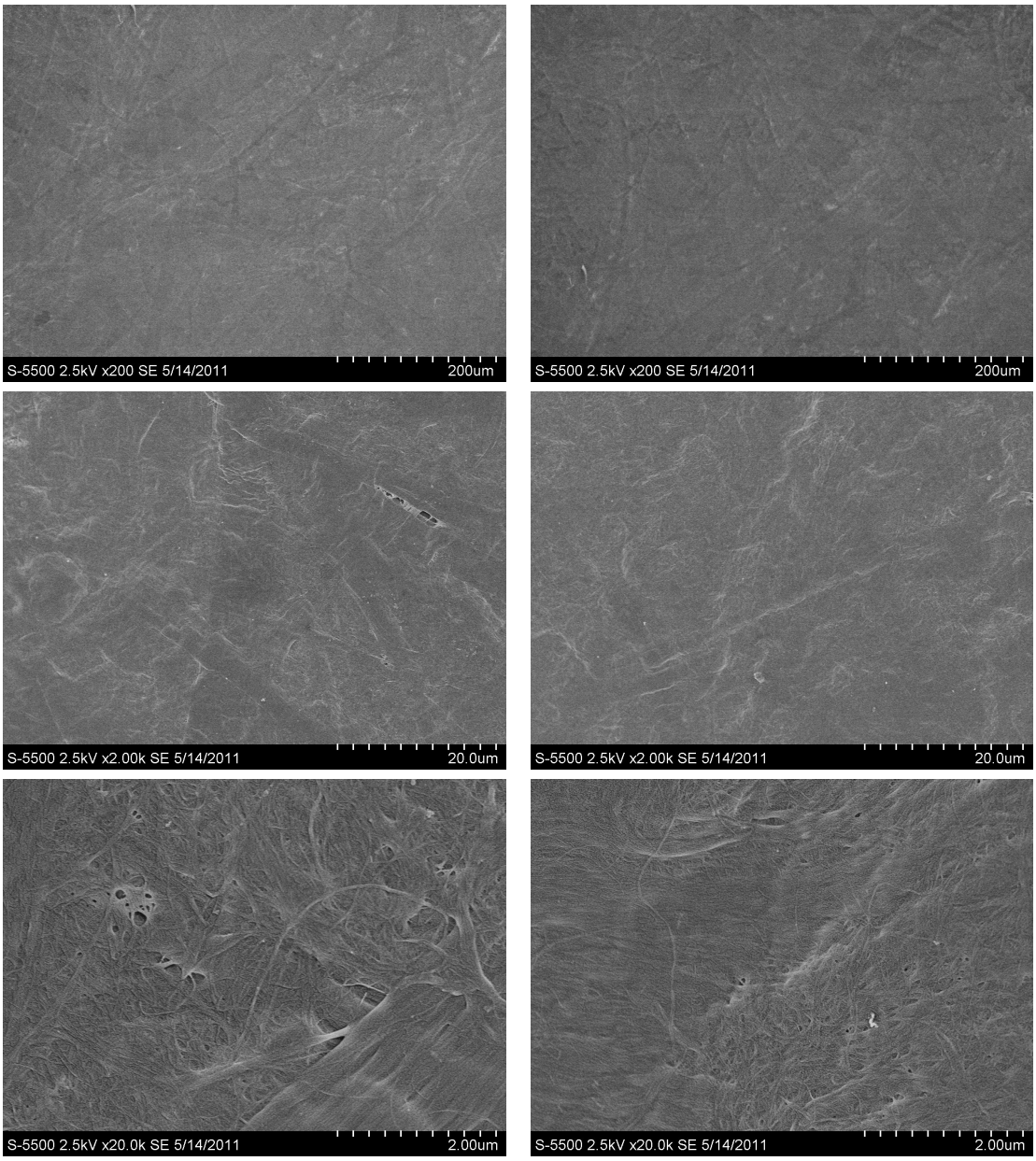

Figure 34: Surface images of filter prepared from 3 pass in 50% isopropanol.

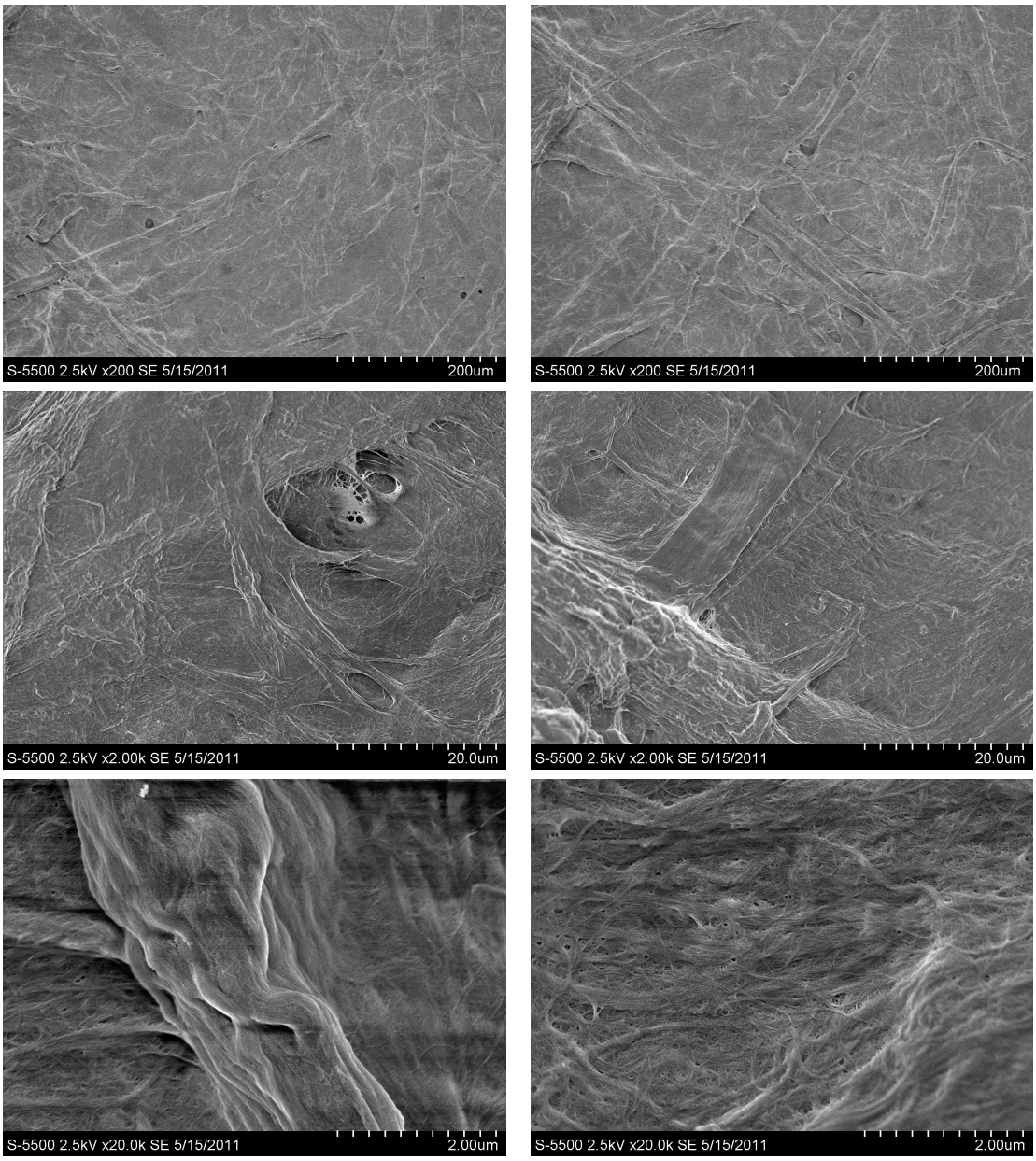

Figure 35: Surface images of filter prepared from 3 pass in 50% ethanol.

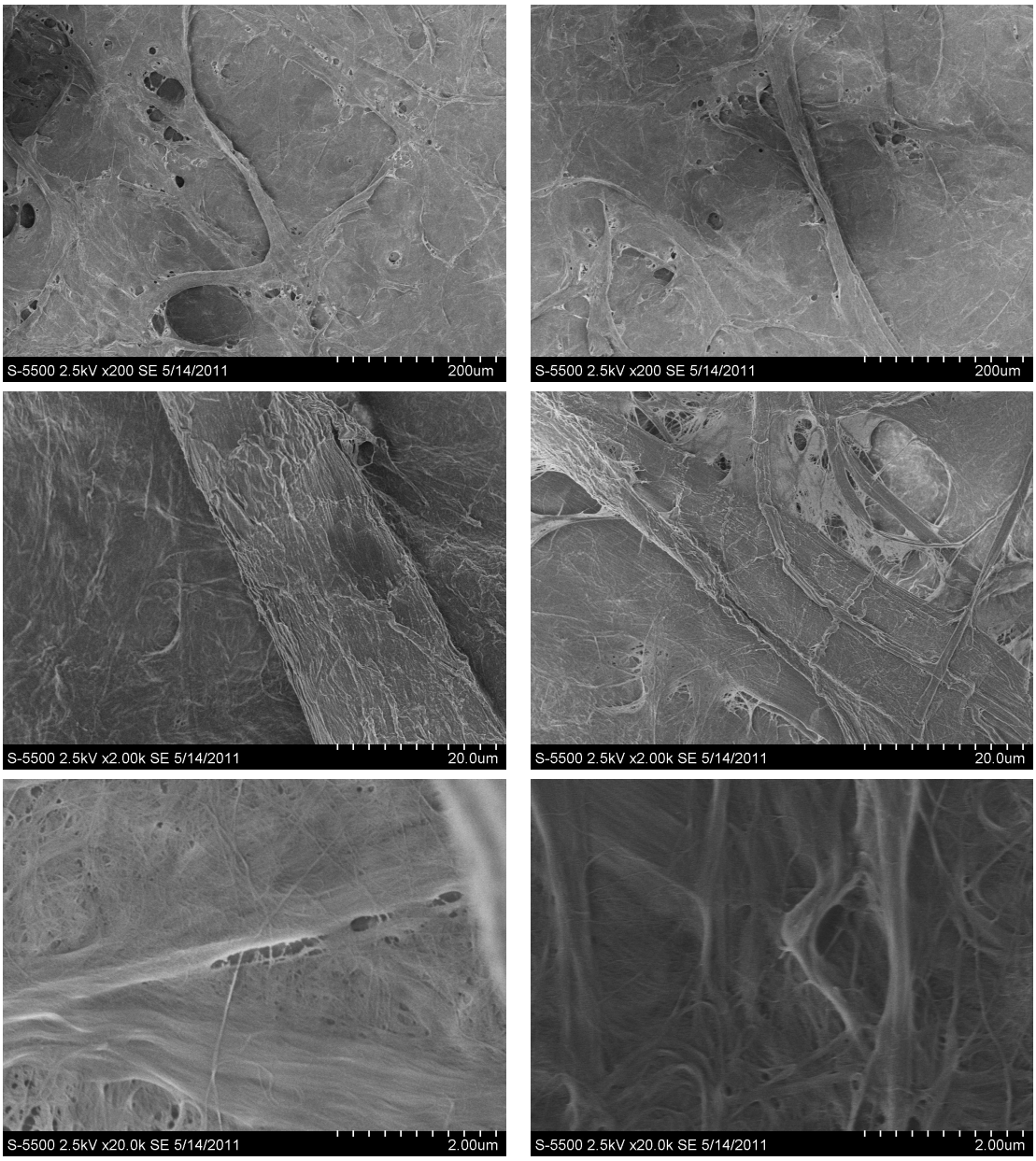

Figure 36: Surface images of a nanocellulose filter prepared from 3 pass in 100% ethanol.

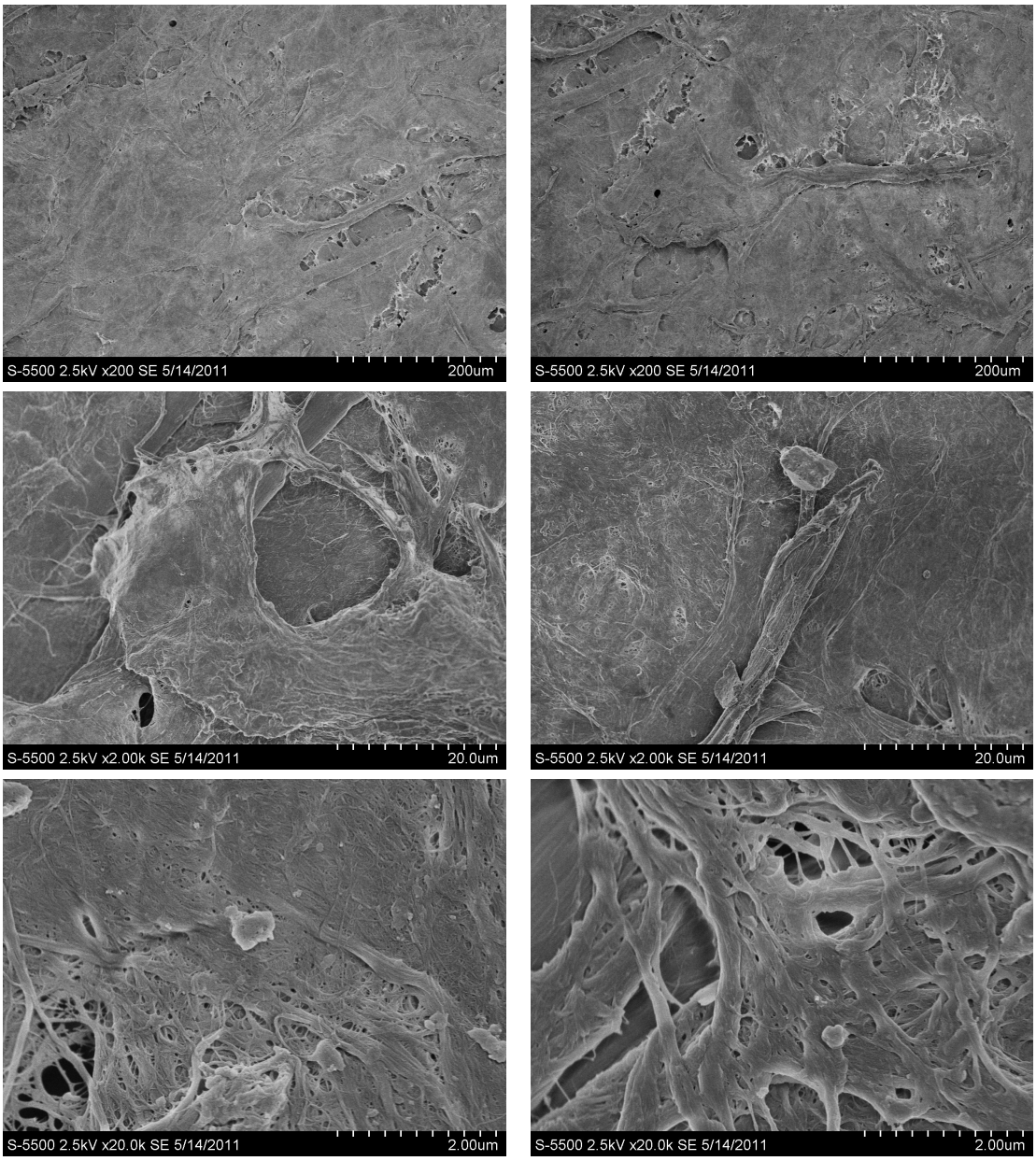

Figure 37: Surface images of filter prepared from 3 pass in 100% isopropanol.

4.2.3 Filter thickness, strength, porosity and permeance

The thickness of filters prepared by solvent evaporation was assessed with both a standard instrument and by imaging the cross section of filters cast in epoxy by SEM in BEI-mode or with a S(T)EM. The raw data can be found in Appendix A.1 while the most interesting values are presented in Table 3 below. Thickness 1 is the average measured with the standard instrument with the resulting porosity 1. Thickness 2 is the average thickness of the filters which were cast in epoxy, with resulting porosity 2. All thickness values are given in μm, porosity in % and the unit for permeance is $\frac{\mu m}{Pa \cdot s}$.

Filter	**Thickness1**	**Porosity1**	**Thickness2**	**Porosity2**	**Permeance**
3p, H_2O	35,29	57,54	15,43	2,88	0,0839
3p, 50%etOH	39,57	62,77	18,87	21,93	0,09771
3p, 50%iso	37,07	60,04	21,46	30,97	0,09464
3p, 100%etOH	63,69	77,75	23,93	40,79	0,3748

Table 3: Average thickness and resulting porosity determined by standard instrument(1) and SEM in BEI-mode(2).

The average permeance of filters prepared by solvent evaporation is presented in Figure 38 and the filters which could be tested for tensile strength are found in Figure 39. Note that the column colors do not represent the same type of filter in the two figures.

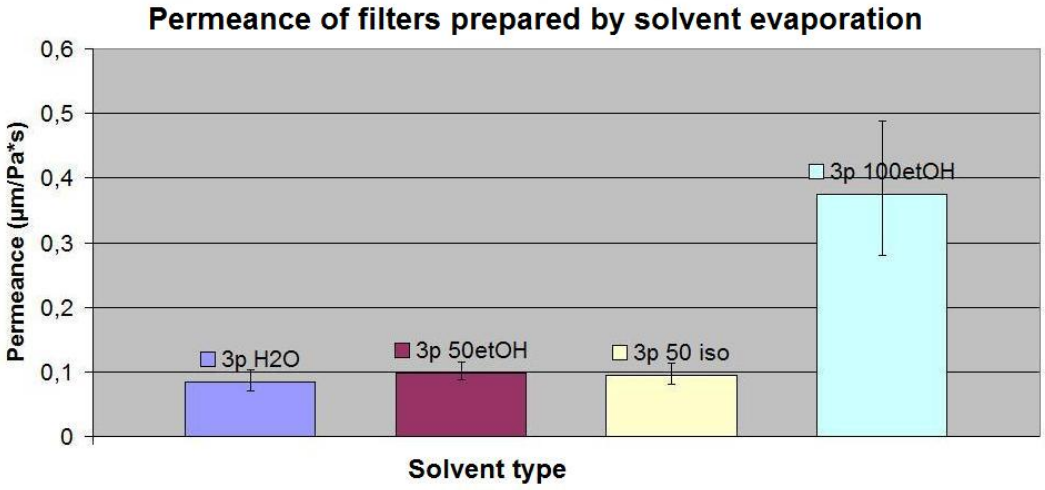

Figure 38: Average permeance of the filters that could be evaluated by the Gurley apparatus. Maximum and minimum values are included as error bars.

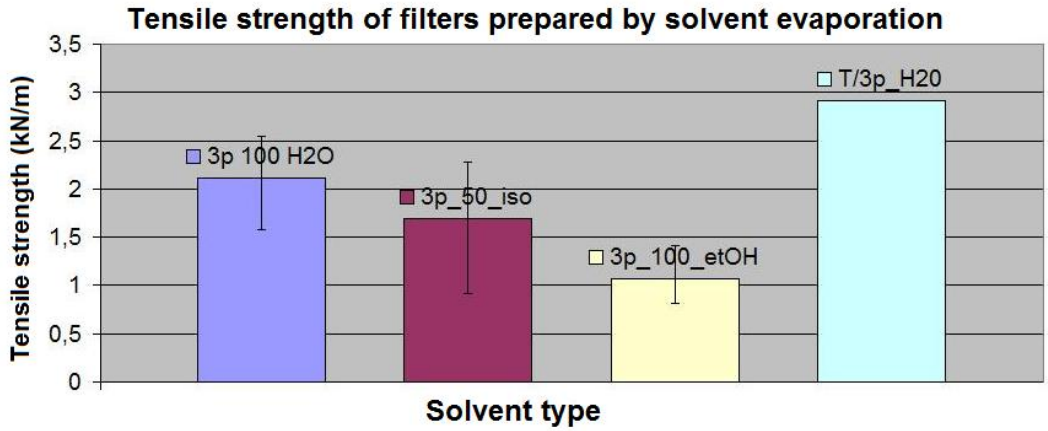

Figure 39: Average tensile strength of the filters that could be evaluated. Maximum and minimum values are included as error bars.

4.3 Filters prepared by freeze drying

The procedure which included liquid nitrogen resulted in cracked filters which were weak and deformed easily. Hence, no permeance or strength measurements were performed on these filters. Since the filters gave of fuzz easily, they were not inserted into the sensitive S(T)EM instrument, and sample preparation would also affect the images if the filters were to be squeezed onto sticky carbon tape. The only characterization done on filters prepared with liquid nitrogen was therefore photography, see pictures in Figure 40 below. The typical appearance of filters prepared by freezing in a deep freezer followed by vacuum drying is presented in Figure 41 and 42.

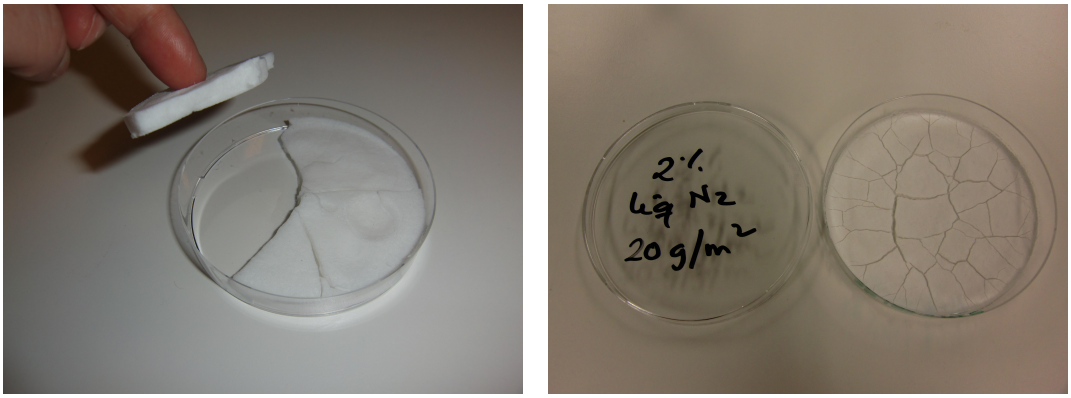

Figure 40: Sponge-like filter from 3 pass DW%=0.44 to the left and cracked filter from 3 pass DW% 2.00 to the right.

Figure 41: NFC filter which has been frozen in a deep freezer followed by vacuum drying.

Figure 42: Thickness variation of filters with grammage of 20, 30 and 40 $\frac{g}{m^2}$, respectively. All filters in the image has the same dry weight content of 0.44%.

The following results concern only *filters frozen in a deep freezer* followed by vacuum drying. The wood mass used here has only been 3 pass in water, hence, no filters from TEMPO-pretreated mass in other solvents were prepared by this process.

4.3.1 S(T)EM images of surface- and cross section morphology

4 filters were chosen to represent the span of filters produced by freeze drying: Three filters with equal grammage of 20 g/m^2 and DW% of 0.44, 0.88 and 2.00 and a fourth filter with grammage of 30 g/m^2 combined with a lower DW% of 0.33. As for Section 4.2.2, all images in the first row on all pages have a magnification of 200 x, the second row; 2 000 x and the third rows will show filter areas which are magnified 20 000 times. The left column are of the same area with increasing magnification, and the right column are randomly chosen areas.

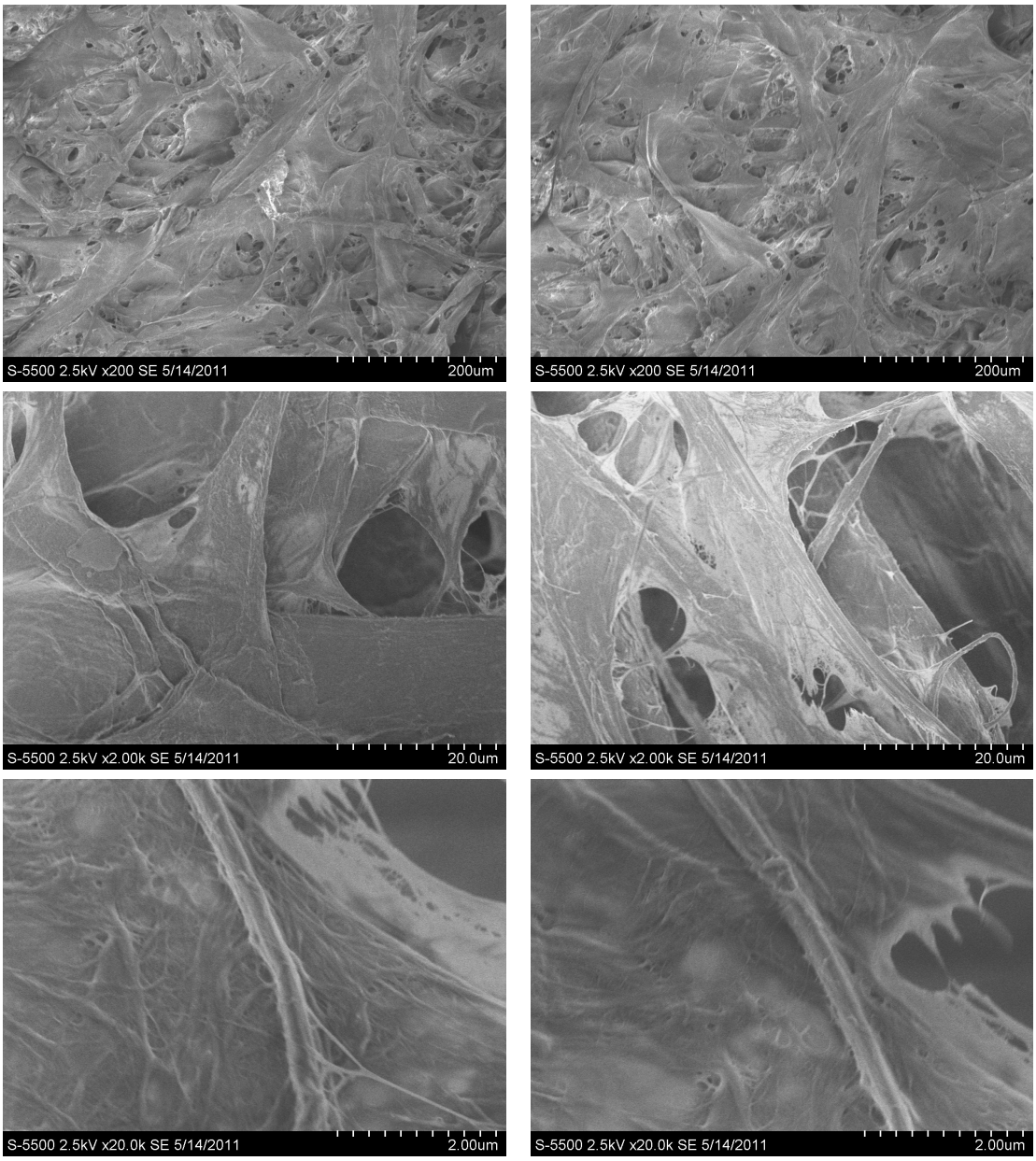

Figure 43: Surface images of filter with grammage 20 g/m^2 and dry weight content of 0.44%.

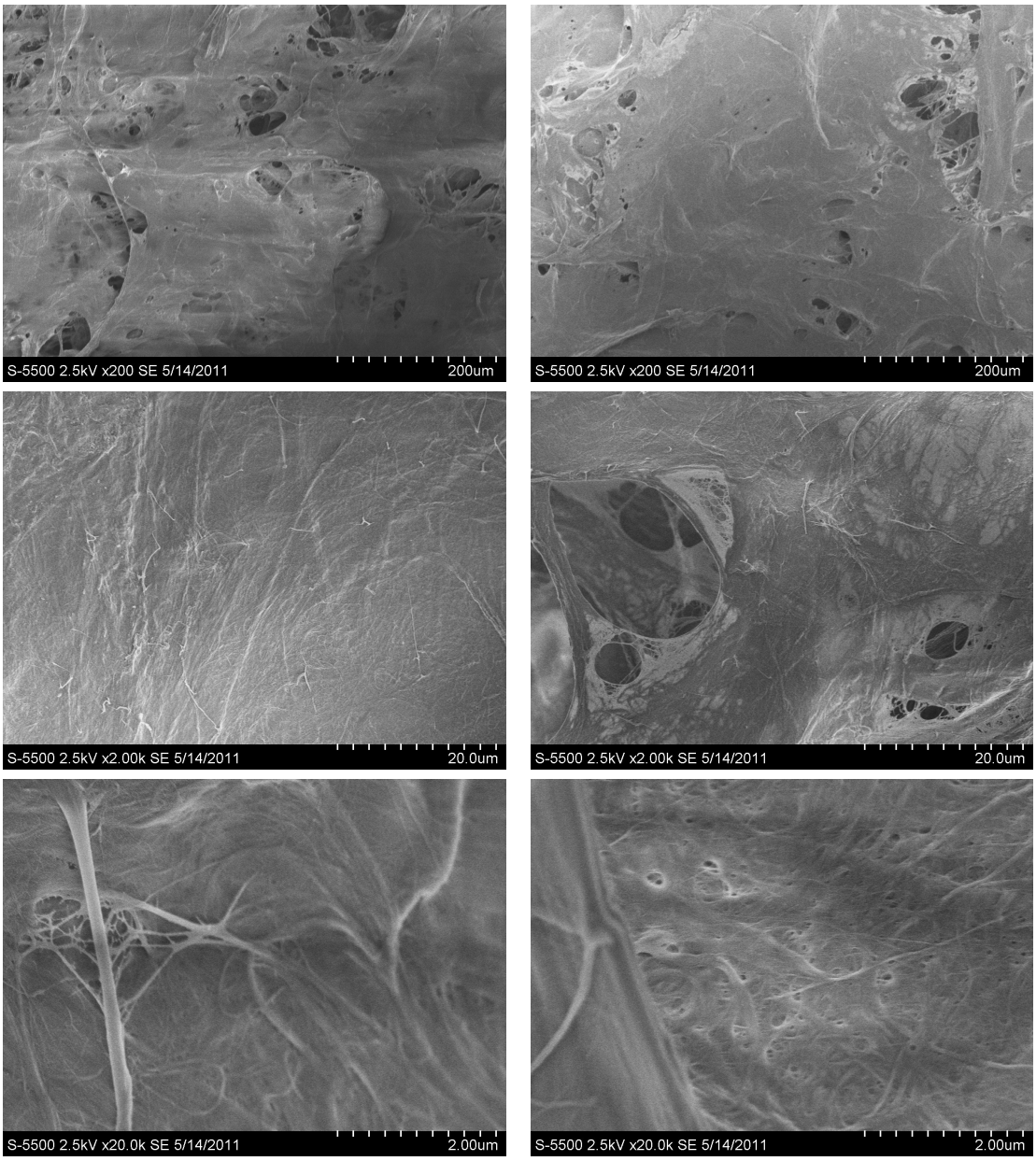

Figure 44: Surface images of filter with grammage 20 g/m^2 and dry weight content of 0.88%.

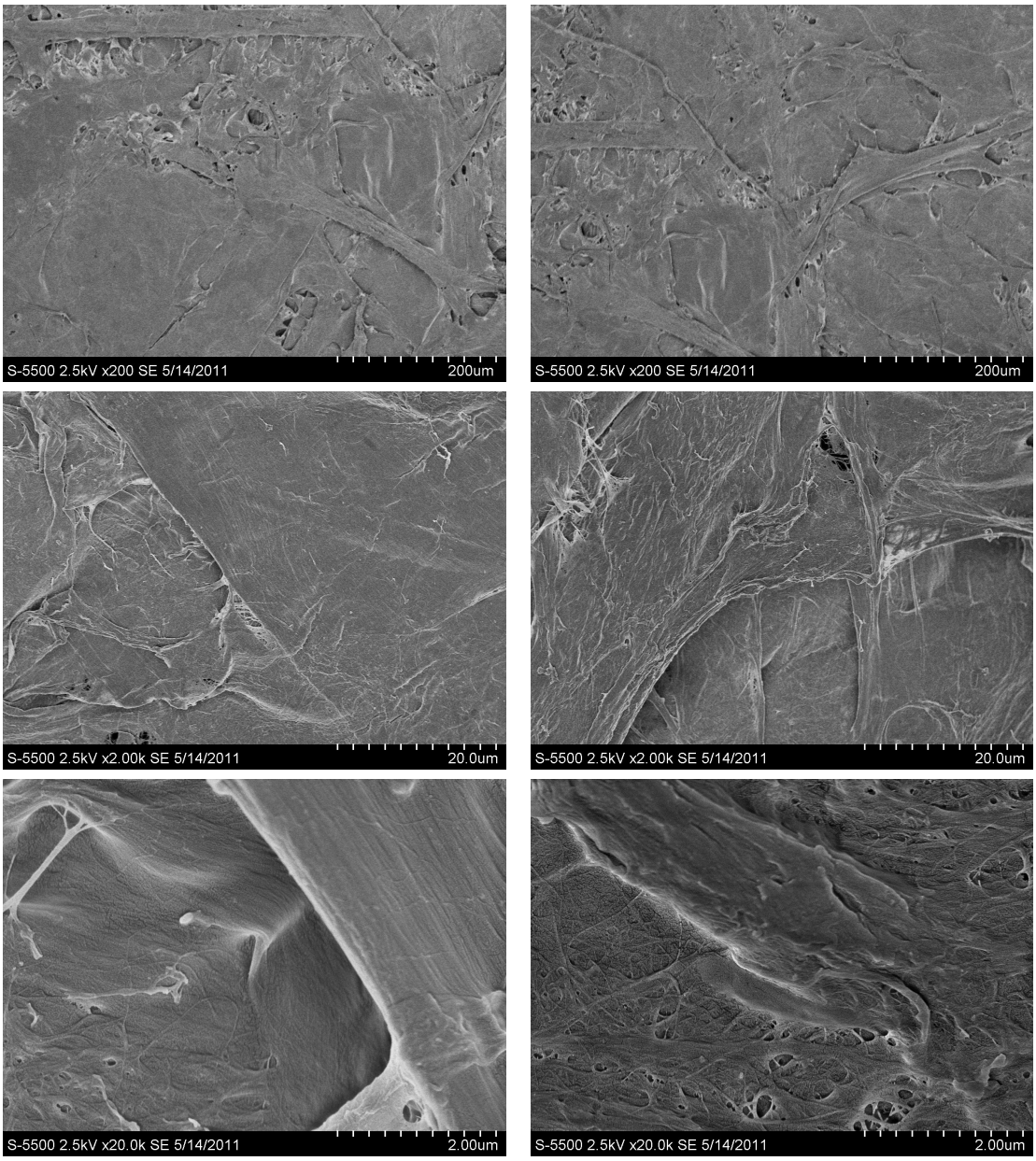

Figure 45: Surface images of filter with grammage 20 g/m^2 and dry weight content of 2.00%.

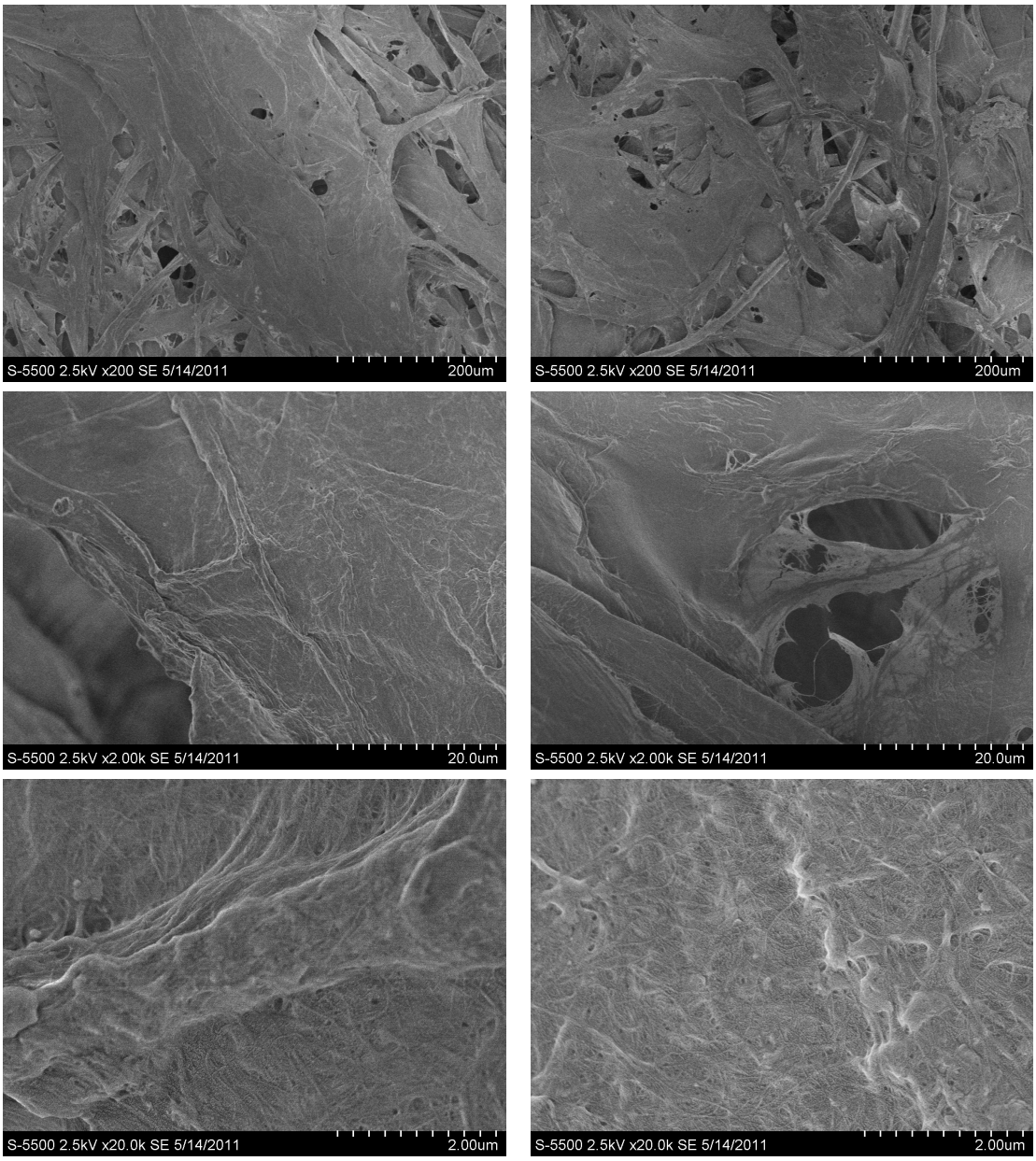

Figure 46: Surface images of filter with grammage 30 g/m^2 and dry weight content of 0.33%.

All freeze dried filters with a dry weight content of $\leq 0.44\%$ had similar cross section appearance. An example of which is presented in Figure 47.

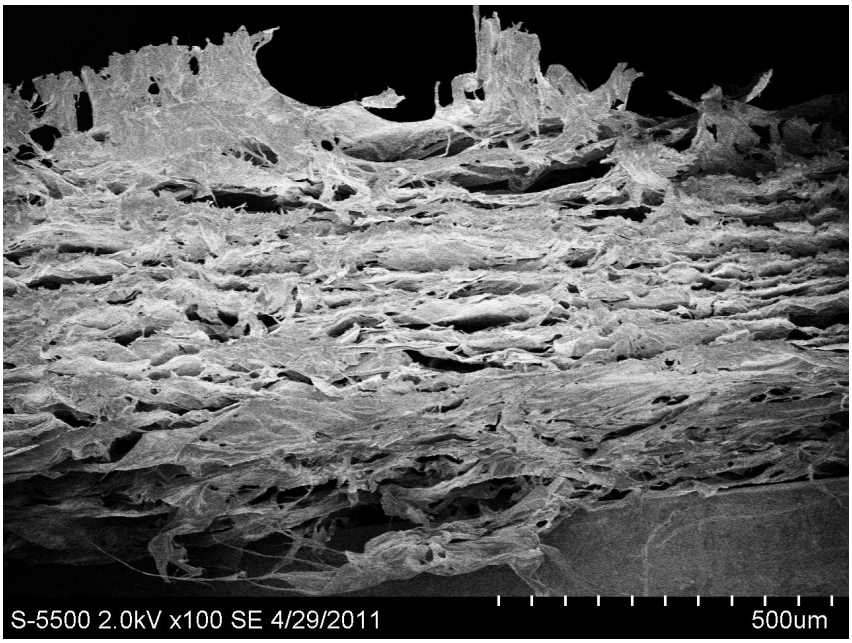

Figure 47: Cross section view of a 3 pass cellulose mass which has been subjected to freeze drying. Notice the layered structure.

4.3.2 Filter thickness, strength, porosity and permeance

As for filters prepared by solvent evaporation, the thickness of filters prepared by freeze drying was also evaluated with either the standard instrument, cross-section view in SEM-BEI mode or cross-section view in a S(T)EM.
See Appendix A.1 for all values.

Minitab was employed to determine if there was a relevant correlation between filter grammage, DW% and cellulose mass height in the petri dish before freeze drying on the average permeance and tensile strength of the resulting filters. First, the effects on filter permeance was evaluated. An overview of how the average permeance varied with filter grammage and dry weight content can be seen in Figure 48 and Figure 49, respectively.

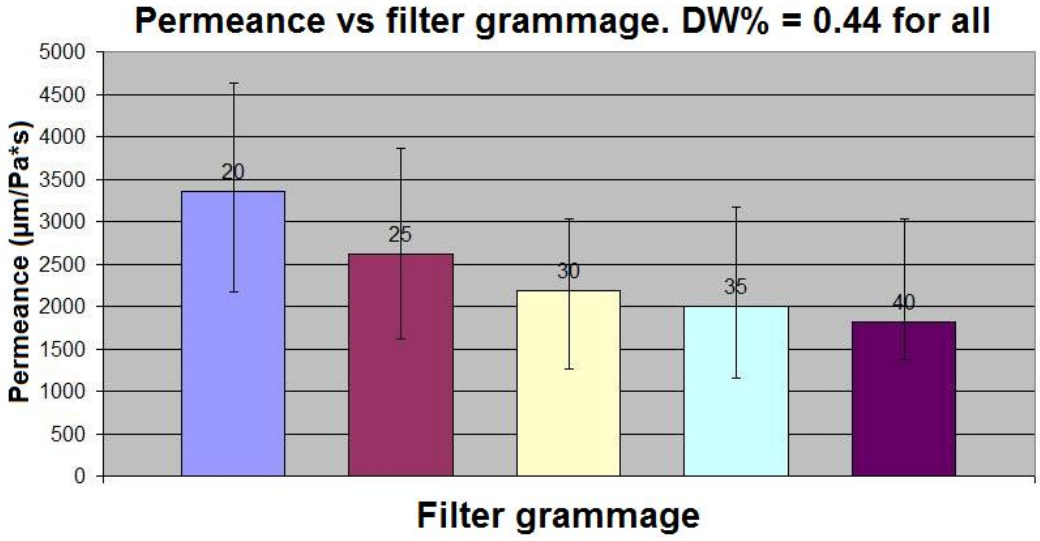

Figure 48: How the permeance varied with filter grammage that had a constant dry weight content of 0.44%. Maximum and minimum values are included as error bars.

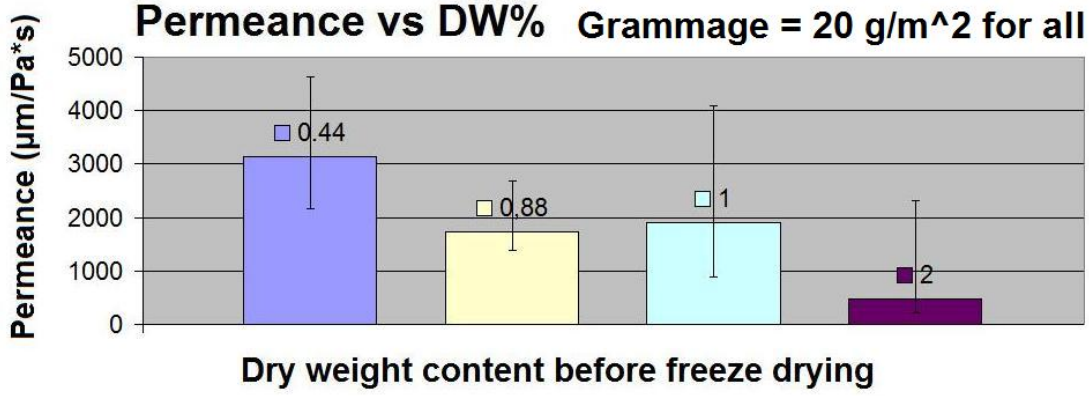

Figure 49: How the permeance varied with dry weight content. All the filters have the same grammage of 20 g/m^2. Maximum and minimum values are included as error bars.

The resulting regression line of permeance vs filter grammage and DW% can be seen in Figure 50 and Figure 51. The predictors (see Section 3.4.6) of permeance vs filter grammage are:

$R^2 = 96.2\%$
P constant = 0.001
P filter grammage = 0.003

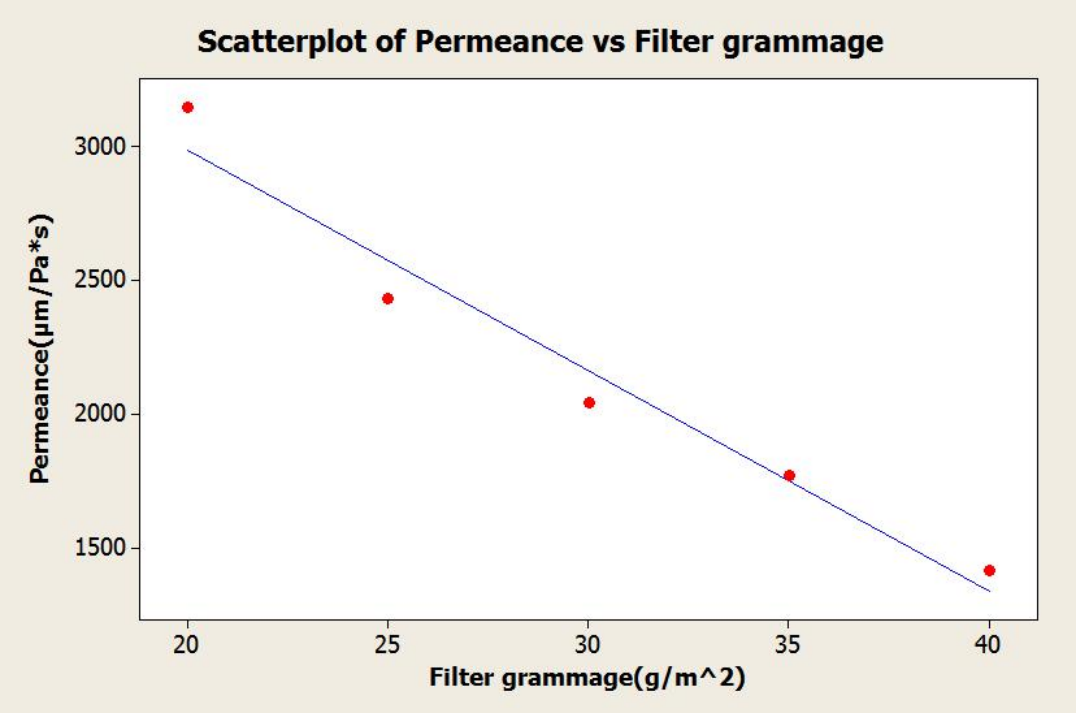

Figure 50: Linear regression line of how average permeance varies as a function of filter grammage.

The predictors of permeance vs filter dry weight content are:

$R^2 = 92.2\%$
P constant = 0.013
P DW% = 0.04

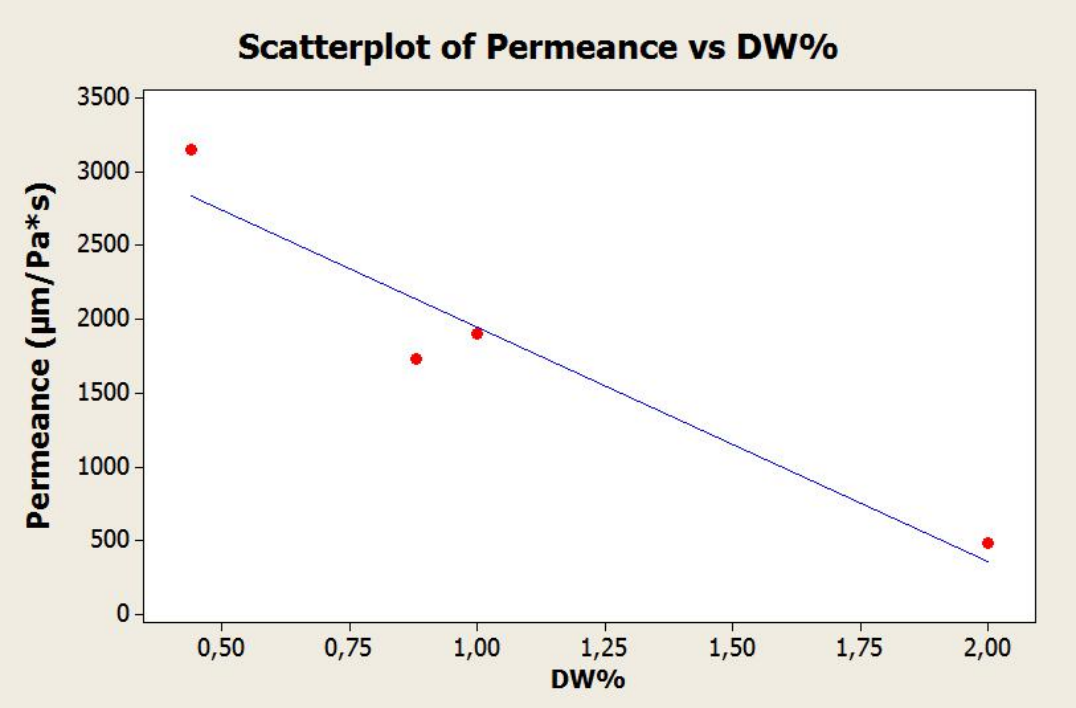

Figure 51: Linear regression line of how average permeance varies as a function of dry weight content of cellulose mass.

For the combined effect of filter grammage and cellulose mass height on the filter permeance, the predictors of the straight (3D) line (not presented in a 2D Figure) are:

$R^2 = 95.5\%$
P constant = 0.041
P mass height = 0.091
P filter grammage = 0.029

An overview of how the filter tensile strength varied with filter grammage and dry weight content can be seen in Figure 52 and Figure 53, respectively.

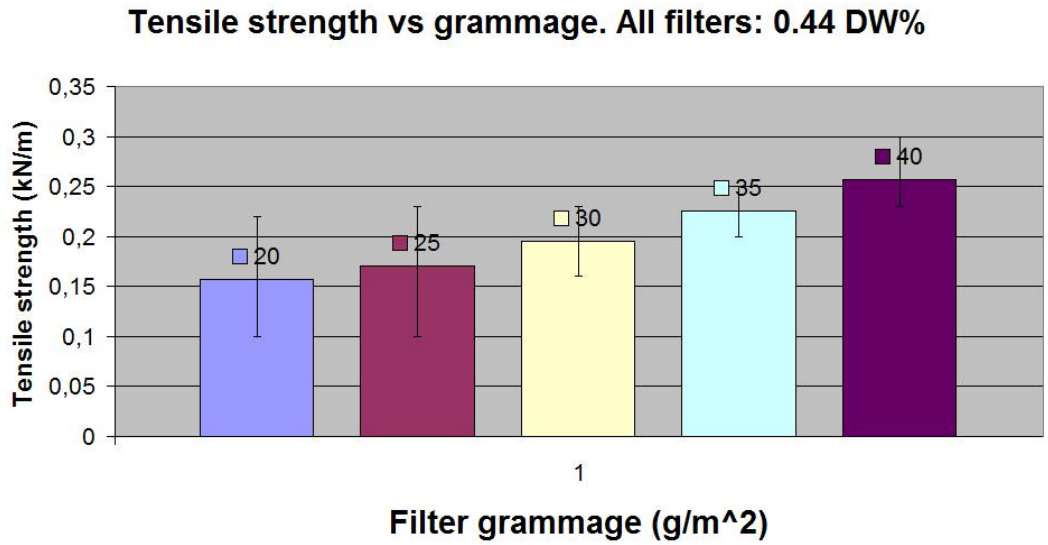

Figure 52: A presentation of how the tensile strength varied with grammage for a constant dry weight content of 0.44%. Maximum and minimum values are included as error bars.

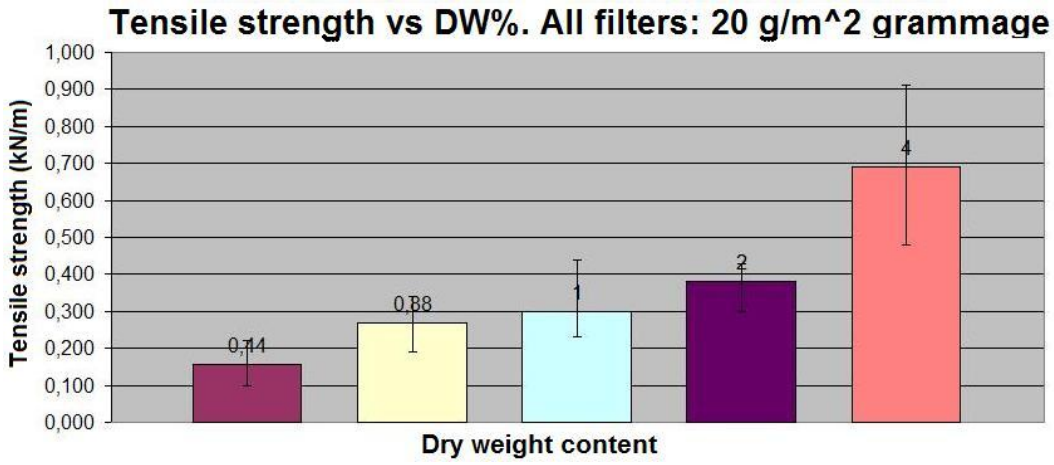

Figure 53: A presentation of how the tensile strength varied with DW% of filters with an equal grammage of 20 g/m^2. Maximum and minimum values are included as error bars.

The correlation between dry weight content, filter grammage and the resulting average filter tensile strength, was also evaluated with Minitab. See Figure 54 and 55 for the resulting regression lines.

The predictors for the regression line in Figure 54 are:

$R^2 = 97.9\%$
P constant $= 0.038$
P DW% $= 0.001$

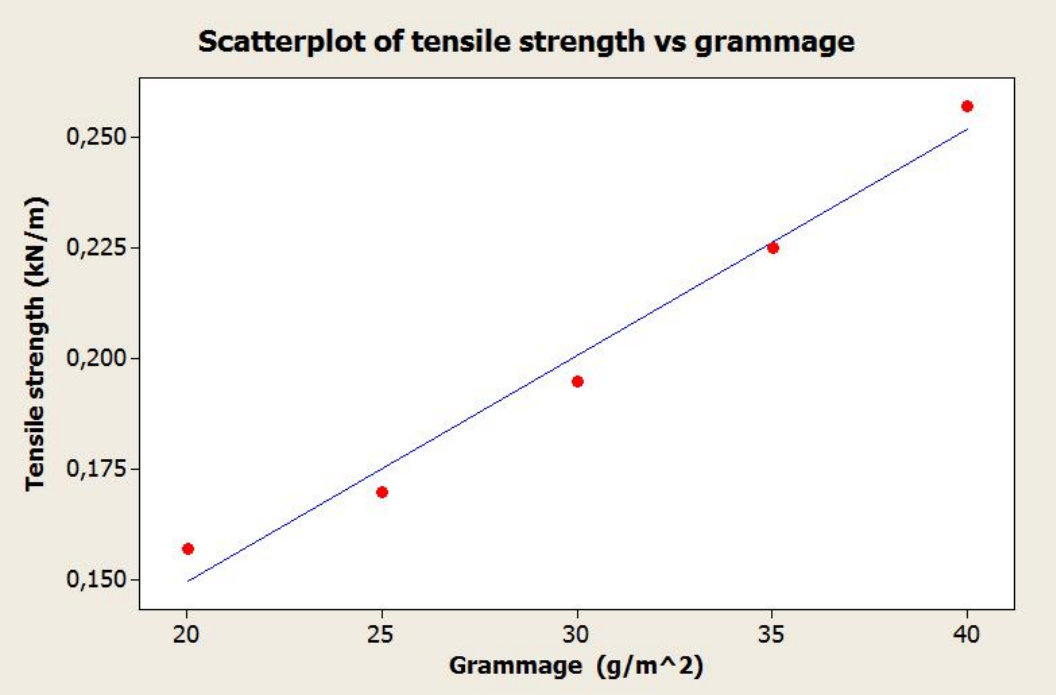

Figure 54: Linear regresssion plot for how the tensile strength is affected by the grammage of the cellulose filters.

The regression line in Figure 55 has predictors:

$R^2 = 98.0\%$
P constant = 0.013
P DW% = 0.001

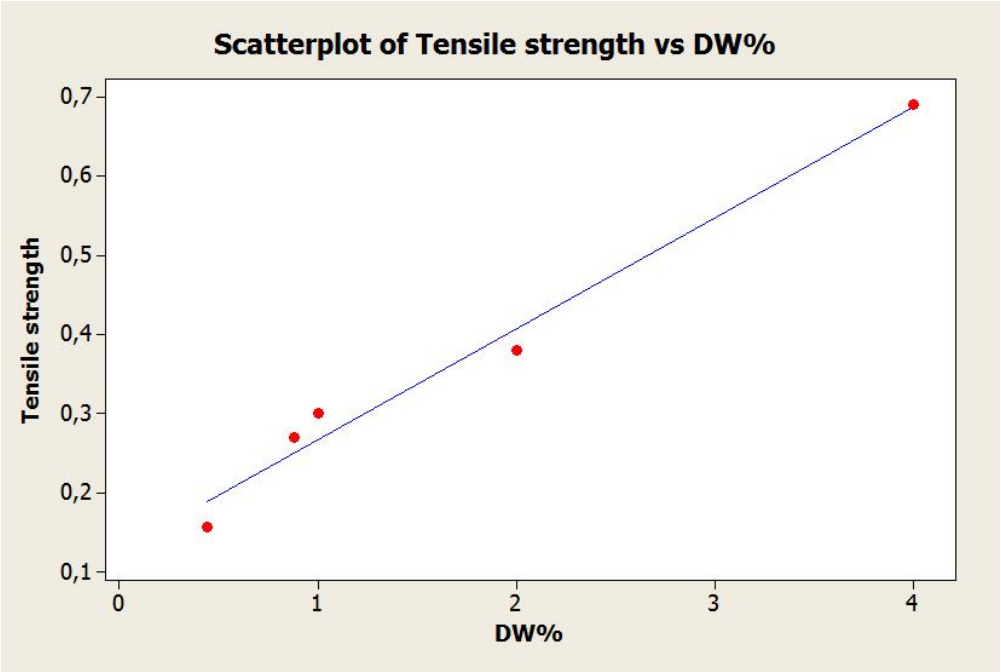

Figure 55: Linear regresssion plot for how the tensile strength is affected by the dry weight content of cellulose before freeze drying.

4.3.3 BET surface area

The total surface area was assessed for three types of filters, all with equal grammage of 20 g/m^2, but varying dry weight content of 0.44%, 0.88% and 2.00%, respectively. 2 samples were run of the filter with DW% of 0.44, one for 0.88% and a total of 3 samples with DW% of 2.00. All BET- and adsorption/desorption plots can be found in Appendix A.2, only the resulting BET surface area values are presented here, see Table 4.

Dry weight content	**Total surface area** (m^2/g)
0.44 # 1	3.2811
0.44 # 2	3.7641
0.88	3.9567
2.00 # 1	4.1762
2.00 # 2	4.7442
2.00 # 3	5.1003

Table 4: BET surface area of the 6 filters tested.

5 Discussion

5.1 Templating

The basic idea behind these experiments was that a perfect monolayer of Ugelstad polystyrene beads could be used as a hydrophobic template where the hydrophilic cellulose nanofibrils were to fill the cavities between the spheres. See Figure 56 for a visualization of the goal template and Figure 57 for the imagined NFC filter with pore size controlled by the sphere diameter.

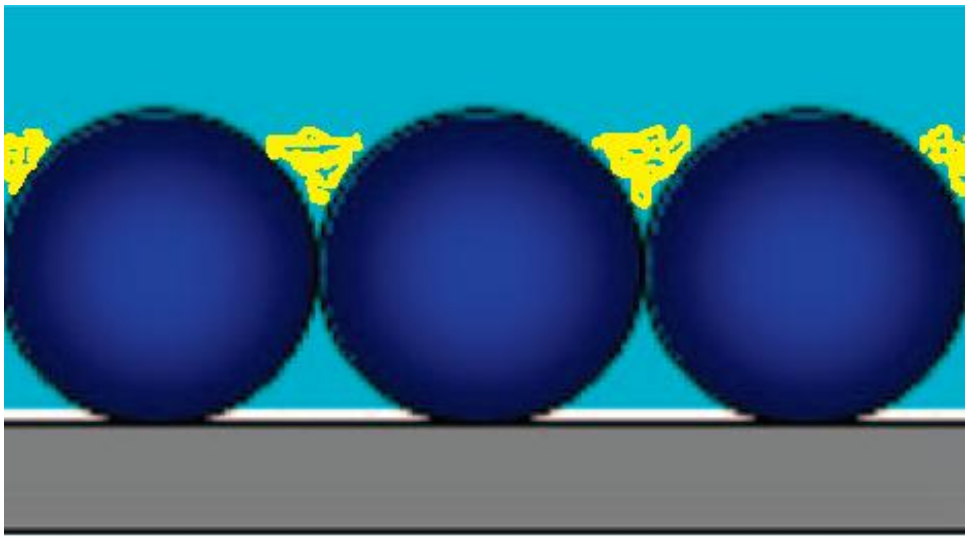

Figure 56: Hydrophobic template of Ugelstad beads where nanocellulose from a dilute suspension of NFC has precipitated in between of the hydrophobic spheres.

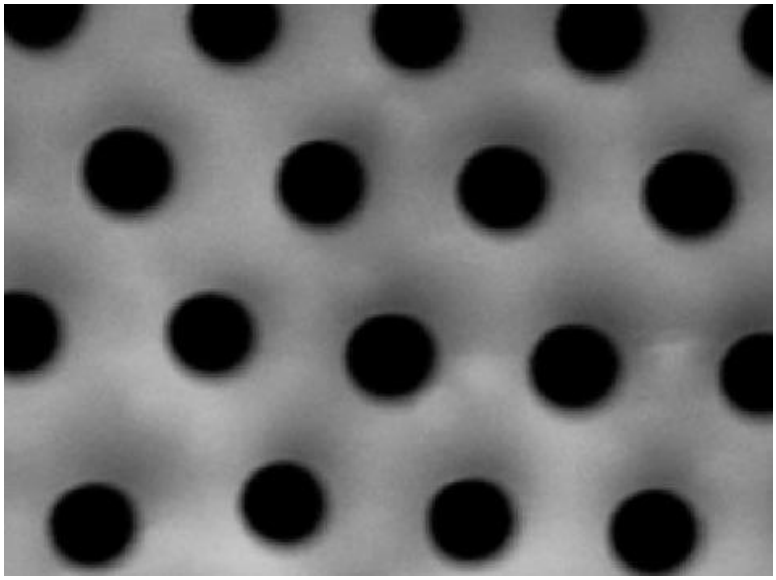

Figure 57: NFC filter with porosity determined by the size of the hydrophobic beads. As the thickness of the NFC film would be in the μm-range, it should be sandwiched in between two supporting layers. Illustration borrowed from [14].

The main hindrance for monolayer formation was an agglomeration of the Ugelstad beads as larger lumps of beads were seen in the optical microscope. Agglomeration is generally avoided by adding e.g. capping agents that attain a net charge of the same sign at a given pH. The bead surface charges will then hinder agglomeration by electrostatic repulsion of the beads.

If a perfect monolayer had been obtained, the combined bead-layer and petri dish were to be heated slightly so that the beads would stick both to each other and to the underlying petri dish to form *one connecting template*. After experimenting with varying oven temperatures and residence times, it was concluded that necessary temperature for slight melting was not reached before the polystyrene petri dish buckled and curled up. Polystyrene has a melting point of 240°C, while the petri dish buckled already after 10 minutes at 90°C. Due to the unsatisfying results (see Figure 27 on page 70), focus was set on controlling the porosity and permeance of cellulose filters by varying the NFC solvent and freeze drying of NFC mass.

It should be mentioned that the idea was conceived before theory on air filtration mechanisms was fully studied. The majority of air particulates are captured by *depth filtration*, see Section 2.2.4. A thin '2-dimensional' air filter design of the type presented in Figure 57 would therefore not be an ideal air filter for capturing sub-μm particles.

5.2 Filters prepared by solvent evaporation

Ethanol and isopropanol were chosen based on their 100% solubility in water and since their polarity index is lower than for water[19]. Solvents with a lower polarity index will exert a reduced capillary pull on neighboring cellulose fibrils during evaporation, and should therefore result in a filter with a higher degree of porosity and permeance, see Section 2.3.2 on page 28.

The difference in permeance was negligible between filters prepared from 3 pass in 100% water, 50% ethanol and 50% isopropanol, consult Figure 38 on page 84. Filters prepared from 3 pass in 100% ethanol had an average permeance that was almost 4 times higher than the rest, with an average of 0.3748 $\frac{\mu m}{Pa \cdot s}$.

The polarity index of pure water, ethanol and isopropanol is 9, 5.2 and 3.9, respectively. It is therefore logical to assume that the permeance of the 100% isopropanol filters would be slightly higher than those prepared with 100% ethanol, if the filters had not been stuck to the petri dish. The surface morphology of filters from 3 pass in 100% ethanol and 100% isopropanol was similar, compare Figure 36 and 37 on page 81 and 82. The filters from 50%

isopropanol and 50% ethanol had also similar permeance values between 0.090 and 0.098 $\frac{\mu m}{Pa \cdot s}$. Anyhow, the resulting permeance of filters from 3 pass in 100% isopropanol would unlikely be satisfactory for the goal applications. The type of solvent had a lower effect on the resulting permeance than expected, as a large change in solvent polarity (e.g. from pure water to 50% ethanol or isopropanol) resulted in a minor change in permeance.

Nothing may be concluded on any of the filters' porosity as the methods used for filter thickness evaluation gave highly different results, see Table 3 on page 83 for the diverging values. For example, the porosity of the filters from 3 pass in pure water was either 2.88% or 57.54%, depending on whether the standard instrument or SEM cross section view of filters cast in epoxy was employed. The last method where this filters' cross section was viewed in a S(T)EM gave a porosity value of 95.64%, which is highly unlikely. A fourth and better method for determining the average thickness of cellulose filters should therefore be established if the calculated porosity values are to be reliable.

The average surface pore size of the filters prepared by solvent evaporation of 3 pass was typically below a few μms.

Due to small apparent pore size and low permeance, their filtration efficiency should be high, also against lung damaging dust with size range 0.7μm - 7μm. Unfortunately, the required pressure difference to obtain a reasonable through-put of air would be correspondingly high, consult Section 2.2.3. The surface pores of filters prepared from TEMPO-pretreated wood mass could not be visualized with the S(T)EM, as the surface cracked up during focusing of the electron beam. Such dense films may serve better as e.g. osmotic membranes than as air filters, if they are surface modified to become hydrophobic[49].

5.3 Filters prepared by freeze drying

In general, the NFC filters prepared by solvent evaporation did not yield sufficiently high permeance values. It was not possible to breathe through any of them, which is a minimum requirement if they are to be used in respirators. A new preparation method was therefore developed, where cellulose suspensions were subjected to *freeze drying*. Only mechanically treated wood mass was used in this filter preparation step.

The first set of filters were frozen with liquid nitrogen which boils at -196°C. All filters cracked, both when immersed in the pan of liquid nitrogen and when transferred to the vacuum drier. See Figure 40 on page 85 for an example of the filters obtained by this procedure.

One explanation of the cracking may be an uneven distribution of temperature in the freezing suspensions. As the lower and lateral parts of the cellulose suspension were in $\sim$ direct contact with the nitrogen, amorphous ice could be formed here, while ice crystals had time to develop in the upper parts of the suspension. Areas that allow ice crystal formation will expand, while areas with amorphous ice will not, see "Ice crystal formation" in Section 2.3.3. Hence, tensile stress generates in the frozen cellulose suspension, which leads to cracking.

Another explanation of the filters' cracking might be the difference in thermal expansion coefficient of ice and polystyrene, which the plastic petri dishes are made of. As the low temperature induces a contraction in the polystyrene, the opposite occurs in the freezing water. This will create a compressive stress in the frozen cellulose mass, that might form a slightly compressed film that cracks when the petri dish expands when trans-

ferred to the vacuum drier. Several experiments were performed in which a petri dish containing cellulose suspension was completely immersed in liquid nitrogen by putting a weight on top of the lid. Still, the suspensions cracked during the vacuum drying step.

For simplicity, 'filters prepared by freeze drying' out this section refers *only* to those frozen in a deep freezer.

The permeance values of the filters prepared by freeze drying were in the range 1000 - 3500 $\frac{\mu m}{Pa \cdot s}$, which made it possible to breathe through them. Even if they were weaker than filters prepared by solvent evaporation, all the freeze dried filters had an average tensile strength that exceeded the recommended minimum of 0.032 $\frac{kN}{m}$. They felt quite strong when handled and they could easily be bent. This is promising, as pleating the filter material increases the effective filter area which reduce the pressure drop for a given flow rate cf. Section 2.2.3.

The effect of filter grammage and DW% on the resulting permeance and tensile strength was evaluated by Minitab. The regression line of grammage vs permeance is presented in Figure 50 on page 95. An R^2 value of 96.2% and P-values below 0.005 strongly suggest that the per-

meance decreases linearly as a function of filter grammage. An increase in the dry weight content of cellulose in the filters before freeze drying tended to reduce the air permeance, but with more uncertainty due to the higher predictor values. See the regression line in Figure 51 on page 96.

Figure 52 and 53 on page 98 show that both an increase in the grammage and the DW% increases the average tensile strength of the filters. This was also supported by the regression lines which both had R^2 values of $\sim 98\%$ and P-values below 0.04. It is not surprising that more and denser material increases the strength of the filter, as the number of fibril bonds increase both when increasing the filter grammage and the dry weight content.

The correlation between permeance vs filter grammage combined with cellulose mass height before freeze drying was not statistically significant. The regression equation for the latter relation had an R^2 of only 80.5% which describes a poor plot fit. It should be noted that a larger number of test filters would in general contribute to a larger certainty in the conclusions made.

As for the filters prepared by solvent evaporation, the different methods used to assess the thickness of the freeze dried filters resulted in a large span in values with a concomitant variation in the filter porosity. The standard instrument from Lorentzen & Wetter AB compressed the filters during testing, and the measured value decreased continuously as the probe sank into the soft and porous filters. S(T)EM was obviously not the best choice for filter thickness evaluation as it was difficult to see where the actual filter cross section began and ended, so that the side wall of the tilted filters were erroneously assumed to be part of the filter thickness. An example of this issue is presented in Figure 58. The calculated porosities of the filters that were evaluated by cross-section S(T)EM were all above 90%, which is likely to be high above the true value. As the true filter thickness was difficult to determine, so was the porosity of the various filters. The best way of evaluating the filters was therefore to see how filter permeance and strength varied as a function of dry weight content and filter grammage. As the filter cross section had a layered structure, one can not speak of true pore sizes. The surface pore sizes of the filters gave merely an indication of the degree of porosity.

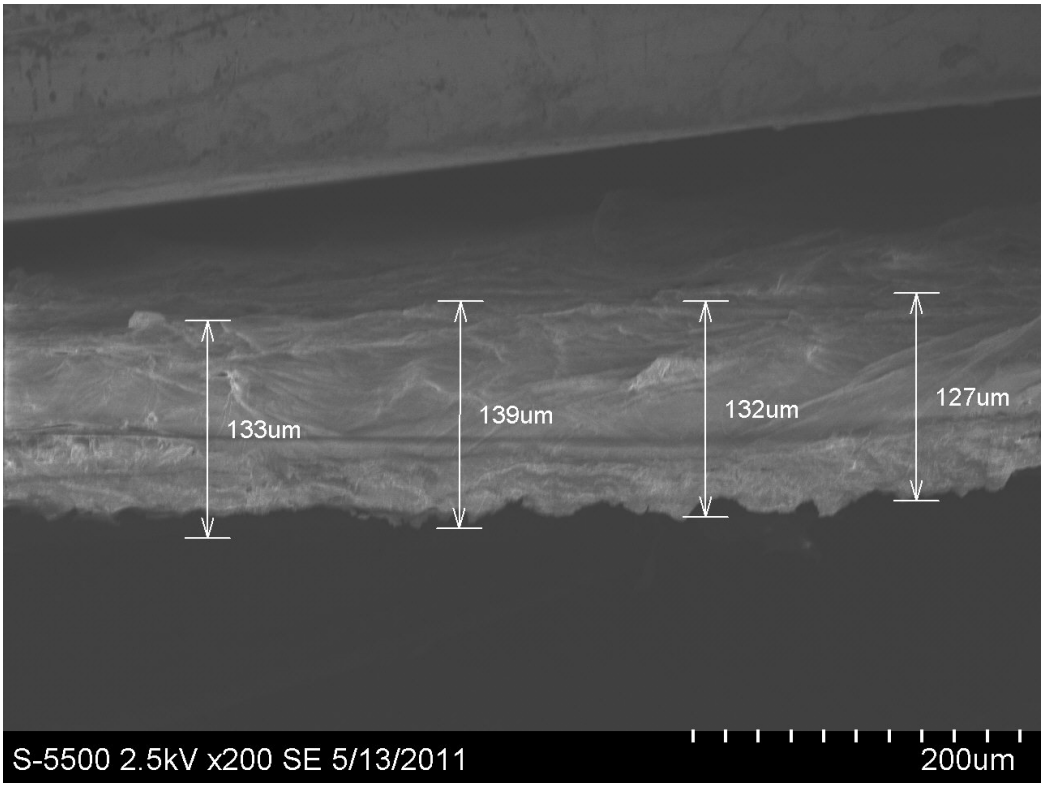

Figure 58: An example of a typical cross section image where it is difficult to determine the actual cross section without including the slope of the slanting filter. In this image: grammage of 20 g/m^2 combined with a dry weight content of 2%.

The BET surface area seemed to increase with increasing dry weight content, see Table 4 on page 101. This result is opposite of what is expected as it has been shown that fibrils bond strongly to each other during solvent evaporation. Agglomeration and bonding between fibrils was allowed to occur for the filters with DW% of 0.88 and 2.00. It was therefore expected that these filters had a

lower surface area compared to the filters with DW% of 0.44 where no evaporation took place before freeze drying. Performing a regression analysis on the data in Table 4 gave a R^2-value of 74.6%, which means that the fit is poor between data points and the resulting regression line. Hence, a larger number of filters with various DW% should be tested in order to find the link between DW% of a filter and its surface area. It should be noted that 3 - 5 $\frac{m^2}{g}$ is close to nothing compared to the maximum 133 $\frac{m^2}{g}$ which theoretically may be obtained for a cellulose mass that has not been subjected to TEMPO-pretreatment (average fibril diameter of 20 nm).

6 Conclusion

A wide variety of pure NFC filters has been prepared by either solvent evaporation or freeze drying of cellulose suspensions. All filters have been characterized with respect to permeance, tensile strength and surface morphology. The filters obtained from solvent evaporation were all too dense for air filtration purposes, where cellulose mass in 100% ethanol gave the highest average permeance value of 0.3748 $\frac{\mu m}{Pa \cdot s}$.

The most promising filters prepared by freeze drying had permeance values that were $\sim 10^4$ times higher compared to the most porous filters prepared by solvent evaporation. The permeance of freeze dried filters could be controlled by varying the filter grammage or dry weight content of the cellulose mass before freeze drying.

All filters, both prepared by solvent evaporation and freeze drying, had tensile strengths above the required for air filters used in commercial and residential filtration systems. Filters prepared by freeze drying of aqueous NFC suspension may then be an alternative to synthetic polymer materials which currently are used in air filters.

7 Further work

First of all, the fissures and grooves in the freeze dried filters should be avoided by hindering larger ice crystals to form during the freezing of the cellulose suspensions. Ongoing experiments focus on this, where the cellulose suspensions are subjected to periodic stirring during the freezing step. Employing supercritical drying of the cellulose suspensions instead of freeze drying will also avoid the formation of cracks in the filters.

The filters should be tested to establish their cut-off value, collection efficiency, flow rate and if electrostatic charges build up. The filter requirements will depend on their use as either a HEPA- or ULPA filter, or as respirators for humans. The pressure drop across the filter and the maximum pressure difference they are able to withstand is also of interest. Testing of NFC filters will be performed by post doc. Laura Alexandrescu during 2011.

'Composite' cellulose filters which combine TEMPO-pretreated wood mass with purely mechanically processed mass could be created to meet a range of filtration demands. Several cellulose filters with varying porosity can be prepared in a sandwich structure to form a gradient

density media. If a binder or support structures are necessary to increase the mechanical strength of the NFC filters, the reinforcement material should also be *biodegradable* (such as starch or flax), so that the filter as a whole remains an environmentally friendly alternative.

References

[1] K. Sutherland, *Filters and filtration handbook*. Elsevier Science Publishing Company, 5 ed., 04 2008.

[2] "*http* : *//www.inda.org/pubs/handbooks/*."

[3] D. B. Purchas and K. Sutherland, *Handbook of Filter Media*. Elsevier, 2002. ISBN 10: 1-85617-375-5 ISBN 13: 978-1-85617-375-9.

[4] C. Fellers and B. Norman, *Pappersteknik*. Avdelningen for pappersteknik Kungl. Tekniska Hogskolan Stockholm, 1996.

[5] M. Nilsson, A. Mihranyan, S. Valizadeh, and M. Strømme, "Mesopore structure of microcrystalline cellulose tablets characterized by nitrogen adsorption and sem: The influence on water-induced ionic conduction," *The Journal of Physical Chemistry B*, vol. 110, no. 32, pp. 15776–15781, 2006. PMID: 16898725.

[6] "*http* : *//healthguide.howstuffworks.com/*."

[7] "*https* : *//www.rkb.us/*."

[8] "*http* : *//www.nilu.no*."

[9] K. B. . Schnelle and C. A. . Brown, *Air Pollution Control Technology Handbook*. CRC Press, 2002.

[10] "*www.cdc.gov/niosh/docs*/2003 − 136/2003 − 136*b.html*."

[11] I. M. Hutten, *Handbook of Nonwoven Filter Media*. Elsevier science and technology, 2007.

[12] Wikipedia, "Kozenycarman equation wikipedia free encyclopedia," 2011. [Online; accessed 13-May-2011].

[13] "Filtration media comprising non-charged melt-blown fibers and electrically charged staple fibers. patent.."

[14] J. Cheng, Y. Zhang, P. Gopalakrishnakone, and N. Chen, "Use of the upside-down method to prepare porous polymer films with tunable surface pore sizes," *Langmuir*, vol. 25, no. 1, pp. 51–54, 2009.

[15] F. Guillemot, A. Brunet-Bruneau, E. Bourgeat-Lami, T. Gacoin, E. Barthel, and J.-P. Boilot, "Latex-templated silica films: Tailoring porosity to get a stable low-refractive index," *Chemistry of Materials*, vol. 22, no. 9, pp. 2822–2828, 2010.

[16] B. Kirby, *Micro- and Nanoscale Fluid Mechanics - Transport in Microfluidic Devices*. Cambridge University Press, 2010.

[17] A. W. Adamson and A. P. Gast, *Physical chemistry of surfaces*. Wiley & Sons, 1997.

[18] "http://hyperphysics.phy-astr.gsu.edu/hbase/surten.html."

[19] J. A. Byers, "Solvent polarity and miscibility."

[20] M. Henriksson, L. A. Berglund, P. Isaksson, T. Lindstrom, and T. Nishino, "Cellulose nanopaper structures of high toughness," *Biomacromolecules*, vol. 9, no. 6, pp. 1579–1585, 2008. PMID: 18498189.

[21] V. P. Khare, A. R. Greenberg, S. S. Kelley, H. Pilath, I. Juhn Roh, and J. Tyber, "Synthesis and characterization of dense and porous cellulose films," *Journal of Applied Polymer Science*, vol. 105, no. 3, pp. 1228–1236, 2007.

[22] Y. Zhang, H. Shao, C. Wu, and X. Hu, "Formation and characterization of cellulose membranes from n-methylmorpholine-n-oxide solution," *Macromolecular Bioscience*, vol. 1, no. 4, pp. 141–148, 2001.

[23] "http://inventors.about.com/library/inventors."

[24] Wikipedia, "Freeze-drying — wikipedia, the free encyclopedia," 2011. [Online; accessed 13-May-2011].

[25] H. Jin, Y. Nishiyama, M. Wada, and S. Kuga, "Nanofibrillar cellulose aerogels," *Colloids and Surfaces A: Physicochemical and Engineering Aspects*, vol. 240, no. 1-3, pp. 63 – 67, 2004.

[26] S. Hoepfner, L. Ratke, and B. Milow, "Synthesis and characterisation of nanofibrillar cellulose aerogels," *Cellulose*, vol. 15, pp. 121–129, 2008. 10.1007/s10570-007-9146-8.

[27] T. Nge, M. Nogi, H. Yano, and J. Sugiyama, "Microstructure and mechanical properties of bacterial cellulose/chitosan porous scaffold," *Cellulose*, vol. 17, pp. 349–363, 2010. 10.1007/s10570-009-9394-x.

[28] H. Schoof, J. Apel, I. Heschel, and G. Rau, "Control of pore structure and size in freeze-dried collagen sponges," *J Biomed Mater Res.*, vol. 58, pp. 352–357, 2001.

[29] N. Dagalakis, J. Flink, and P. Stasikelis, "Design of an artificial skin. part iii. control of pore structure," *Journal of Biomedical Materials Research*, vol. 14, pp. 511–528, 1980.

[30] O'Brien++, "Influence of freezing rate on pore structure in freeze-dried collagen-gag scaffolds," *Biomaterials*, vol. 25, pp. 1077–1086, 2004.

[31] O. Ishida, D. Kim, and S. Kuga, "Microfibrillar carbon from native cellulose," *Cellulose*, vol. 11, pp. 475–480, 2004.

[32] J. L. Stephenson, "Ice crystal formation in biological materials during rapid freezing," *Annals of the new york academy of sciences*, vol. 85, 2006.

[33] "www.myneurolab.com."

[34] "Heterogen katalyse, anders holmen, insitutt for kjemisk prosessteknologi, ntnu, 2008."

[35] B. Gawel, "Colloid chemistry and functional materials characterization techniques gas physisorption : Study of the porosity of materials characterization techniques gas physisorption : Study of the porosity of materials." Powerpoint Lecture.

[36] "Procedure of n2 adsorption analysis. developed by bartlomiej gawel and approved by iva kralova, ntnu. faculty of natural sciences and technology at the department of chemical engineering.."

[37] K. Birdi, *Surface and colloid chemistry : principles and applications*. CRC Press, 2010. 9781420095043.

[38] C. Eyholzer, *Dried Nanofibrillated Cellulose and its Bionanocomposite*. PhD thesis, Luleå University of Technology, February, 2011.

[39] P. Y. Bruice, *Essential organic chemistry*. Pearson International Edition, 2006.

[40] Wikipedia, "Cellulose — wikipedia, the free encyclopedia," 2011. [Online; accessed 1-June-2011].

[41] M. Manninen, "Nanofibrillated cellulose-water interactions," in *Presentation*.

[42] E. C. Homonoff, R. E. Evans, and C. D. Weaver, "Nanofibrillated cellulose fibers: Where size matters in opening new markets to nanofiber usage.," in *Presentation to 2008 TAPPI Nanotechnology Conference*, 2008.

[43] S. Ahola, *Properties and interfacial behaviour of cellulose nanofibrils*. PhD thesis, Helsinki University of Technology, 2008.

[44] A. F. T. et al, "Microfibrillated cellulose, a new cellulose product," *J. Appl. Polym. Sci.*, 1983.

[45] G. Chinga-Carrasco and K. Syverud, "Computer-assisted quantification of the multi-scale structure of films made of nanofibrillated cellulose," *Journal of Nanoparticle Research*, vol. 12, pp. 841–851, 2010. 10.1007/s11051-009-9710-2.

[46] C. A. Bishop, *Vacuum deposition onto webs, films, and foils*. William Andrew, 2006.

[47] G. Chinga-Carrasco, Y. Yu, and O. Diserud, "Quantitative electron microscopy of cellulose nanofibril structures from eucalyptus and pinus radiata kraft pulp fibres," *Microscopy and micro-analysis*, vol. Accepted for publication, not yet printed, 2011.

[48] M. Henriksson and L. A. Berglund, "Structure and properties of cellulose nanocomposite films containing melamine formaldehyde," *Journal of Applied Polymer Science*, vol. 106, pp. 2817–2824, 2007.

[49] G. Rodionova, M. Lenes, y. Eriksen, and y. Gregersen, "Surface chemical modification of microfibrillated cellulose: improvement of barrier properties for packaging applications," *Cellulose*, vol. 18, pp. 127–134, 2011. 10.1007/s10570-010-9474-y.

[50] G. Chinga-Carrasco, Y. Yu, and O. Diserud, "Quantitative electron microscopy of cellulose nanofibril

structures from eucalyptus and pinus radiata pulp fibres," *Microscopy and micro-analysis*, 2011.

[51] D. Eklund and T. Lindstrøm, *Paper chemistry*. DT paper science publications, 1991.

[52] I. Siró and D. Plackett, "Microfibrillated cellulose and new nanocomposite materials: a review," *Cellulose*, vol. 17, pp. 459–494, 2010. 10.1007/s10570-010-9405-y.

[53] T. Saito, Y. Nishiyama, J.-L. Putaux, M. Vignon, and A. Isogai, "Homogeneous suspensions of individualized microfibrils from tempo-catalyzed oxidation of native cellulose," *Biomacromolecules*, vol. 7, no. 6, pp. 1687–1691, 2006.

[54] T. Lindström and M. Ankerfors, *NanoCellulose Developments in Scandinavia*. 2009.

[55] A. Isogai, "Benefits and challenges of tempo-oxidized cellulose nanofibrils. (powerpoint)."

[56] Wikipedia, "Pinus radiata — wikipedia, the free encyclopedia," 2011. [Online; accessed 13-May-2011].

[57] Wikipedia, "Ethanol — wikipedia, the free encyclopedia," 2011. [Online; accessed 13-May-2011].

[58] Wikipedia, "Isopropyl alcohol — wikipedia, the free encyclopedia," 2011. [Online; accessed 27-May-2011].

[59] "Scandinavian pulp, paper and board, testing committee. scan-p 53:84," 1983.

[60] Walpole, Myers, Myers, and Ye, *Probability and statistics for engineers and scientists*. Pearson International Edition, 2007.

A Appendix

A.1 Raw data for all filters

	3p_H2O	3p_50_etOH	3p_100_etOH	3p_50_iso
Average thickness(SEM + epoxy) (µm)	15,43	18,87	23,93	21,46
Average thickness, S(T)EM (µm)	343,2	257,55	230,25	
Average thickness, standard instrument (µm)	35,29	39,57	63,69	37,07
SEM Volume(cm^3)	0,087557562	0,107077848	0,135790826	0,121774807
S(T)EM Volume (cm^3)	1,947488994	1,461467921	1,306554023	
Standard instr. Volume (cm^3)	0,200253166	0,224540033	0,361409015	0,210353779
weight(g)	0,12755	0,1254	0,1206	0,1261
Porosity, SEM thickness (%)	2,882935888	21,9259615	40,79128751	30,96546926
Porosity, S(T)EM thickness (%)	95,63369377	94,27972391	93,8464083	
Porosity, standard instrument thickness (%)	57,53708418	62,76833191	77,75373701	60,03558053
Average permeance (µm/Pa*s)	0,0839	0,09771	0,3748	0,09464
Average tension strength (kN/m)	2,10625	tear	1,0525	1,6933

Figure 59: Raw data 1

	T/3p_H2O	T/3p_50_iso	20_044	20__088
Average thickness(SEM + epoxy) (µm)	21,65	10,51	142,71	276,15
Average thickness, S(T)EM (µm)				
Average thickness, standard instrument (µm)	24,29	18,75	162,67	140,5
SEM Volume(cm^3)	0,122852962	0,059639013	0,809808142	1,567013653
S(T)EM Volume (cm^3)				
Standard instr. Volume (cm^3)	0,137833647	0,106396907	0,923071197	0,797267493
weight(g)	0,13505	0,1286	0,1205	0,1217
Porosity, SEM thickness (%)	26,71456062	-43,75377584	90,07995485	94,82242333
Porosity, S(T)EM thickness (%)				
Porosity, standard instrument thickness (%)	34,67971336	19,42121685	91,29716823	89,82357439
Average permeance (µm/Pa*s)	too brittle	too brittle	3350,9	1794,12
Average tension strength (kN/m)	2,92	too brittle	0,1567	0,27

Figure 60: Raw data 2

	30_033	35_044	40_044	40_059
Average thickness(SEM + epoxy) (µm)				
Average thickness, S(T)EM (µm)			638,82	
Average thickness, standard instrument (µm)				
SEM Volume(cm^3)				
S(T)EM Volume (cm^3)			3,624985196	
Standard instr. Volume (cm^3)				
weight(g)	0,1835	0,2132	0,2439	0,2414
Porosity, SEM thickness (%)				
Porosity, S(T)EM thickness (%)			95,51446444	
Porosity, standard instrument thickness (%)				
Average permeance (µm/Pa*s)	2626,67	2007,29	1817,47	1495,55
Average tension strength (kN/m)	0,1867	0,225	0,2567	0,3983

Figure 61: Raw data 3

A.2 BET analysis

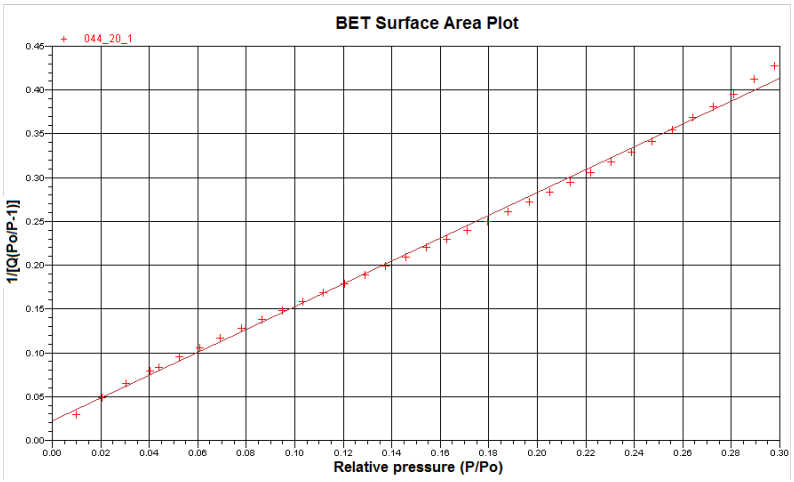

Figure 62: BET plot of freeze dried filter from 3 pass cellulose mass in water with grammage of 20 g/m^2 and dry weight content of 0.44%.

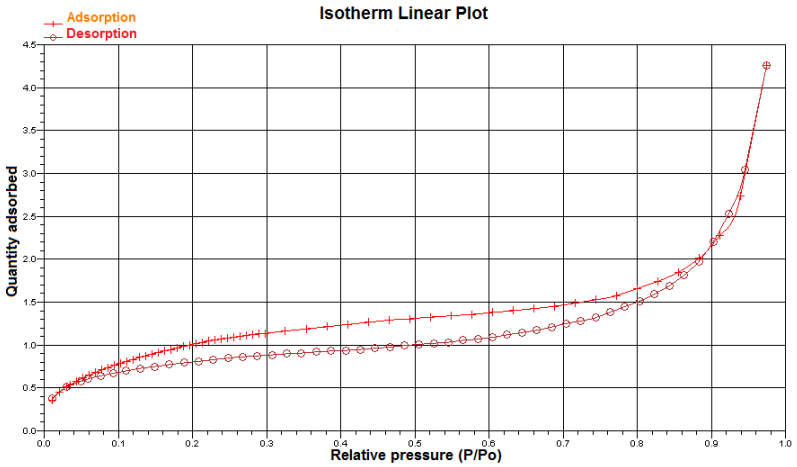

Figure 63: Isotherm adsorption/desorption plot for same filter as in Figure 62.

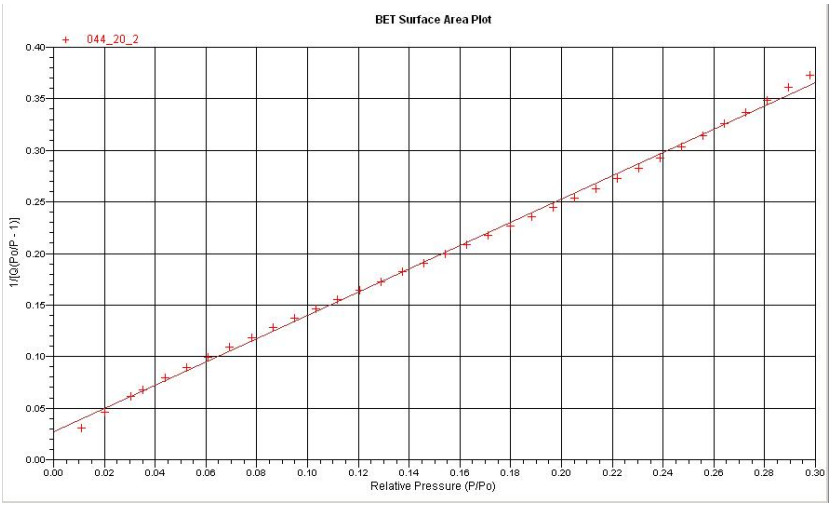

Figure 64: BET plot of freeze dried filter nr 2 from 3 pass cellulose mass in water with grammage of 20 g/m^2 and dry weight content of 0.44%.

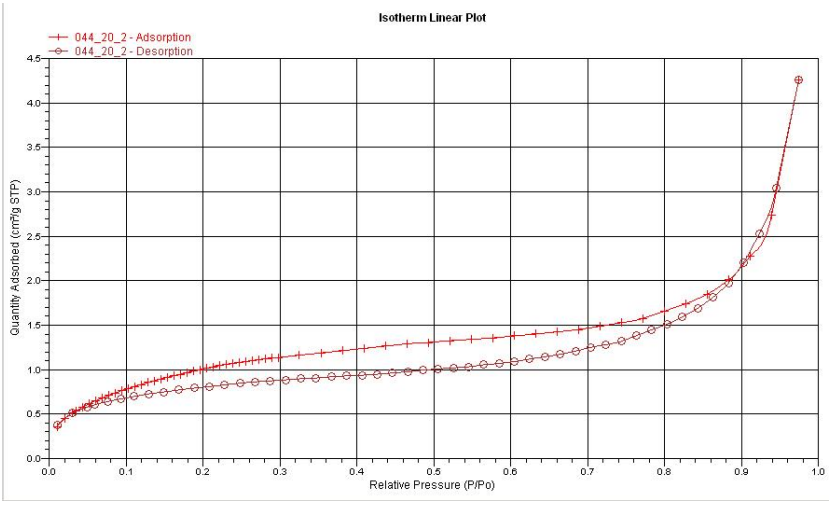

Figure 65: Isotherm adsorption/desorption plot for same filter as in Figure 64.

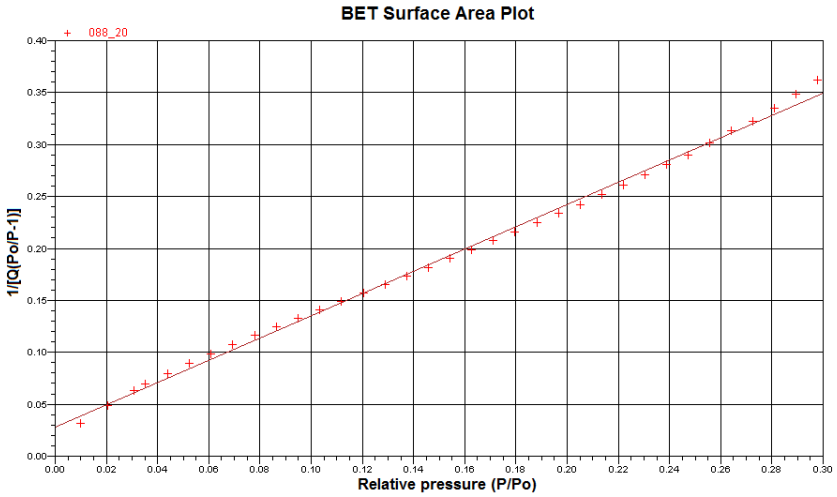

Figure 66: BET plot of freeze dried filter from 3 pass cellulose mass in water with grammage of 20 g/m^2 and dry weight content of 0.88%.

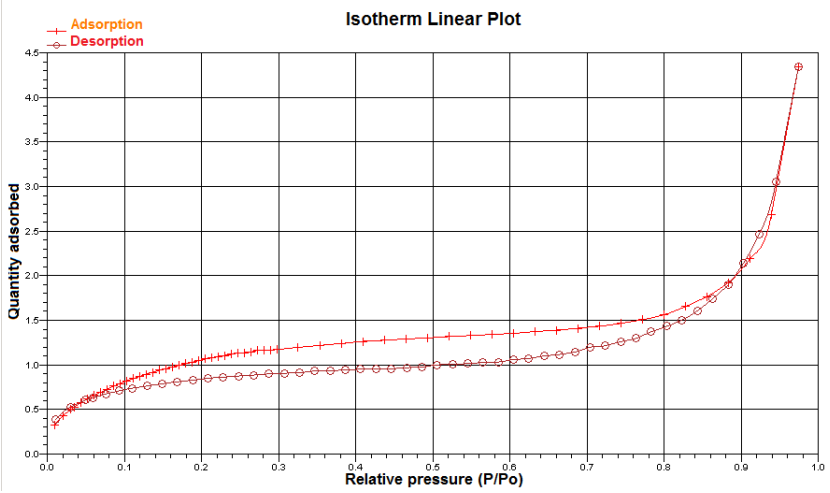

Figure 67: Isotherm adsorption/desorption plot for same filter as in Figure 66.

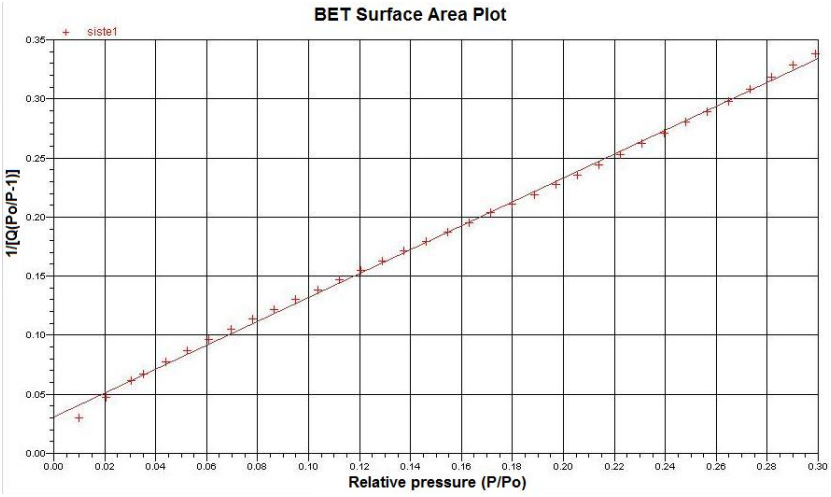

Figure 68: BET plot of freeze dried filter from 3 pass cellulose mass in water with grammage of 20 g/m^2 and dry weight content of 2.00%.

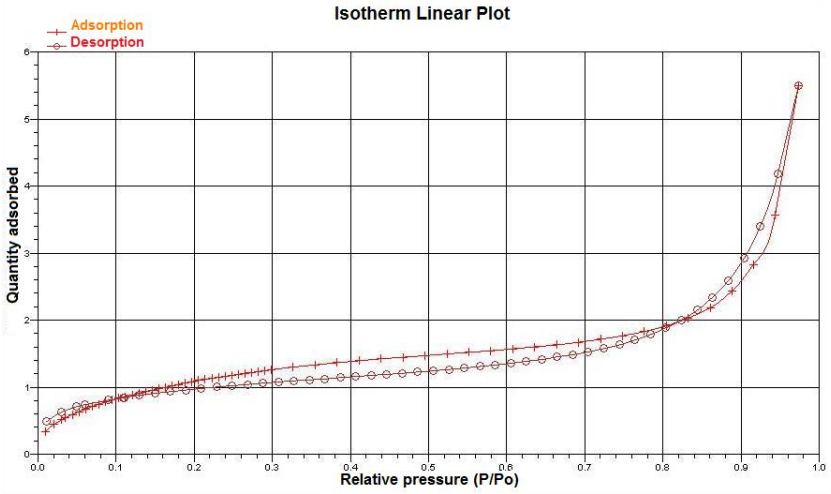

Figure 69: Isotherm adsorption/desorption plot for same filter as in Figure 68.

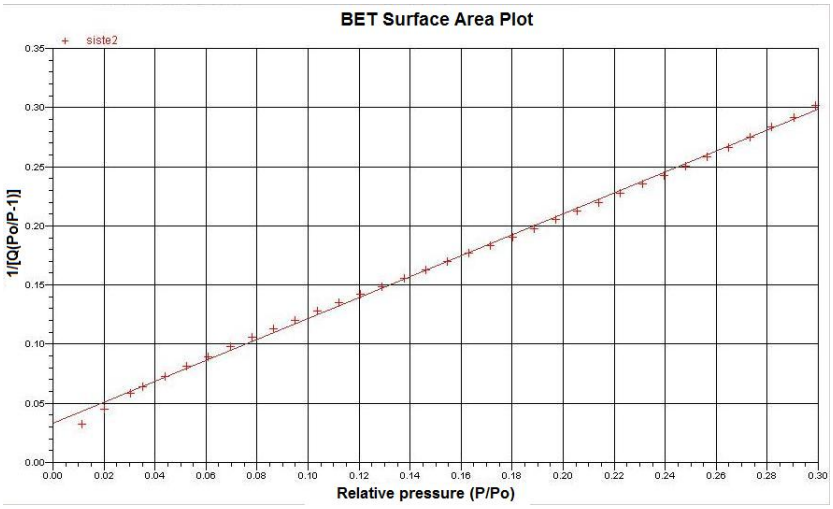

Figure 70: BET plot of freeze dried filter nr 2 from 3 pass cellulose mass in water with grammage of 20 g/m^2 and dry weight content of 2.00%.

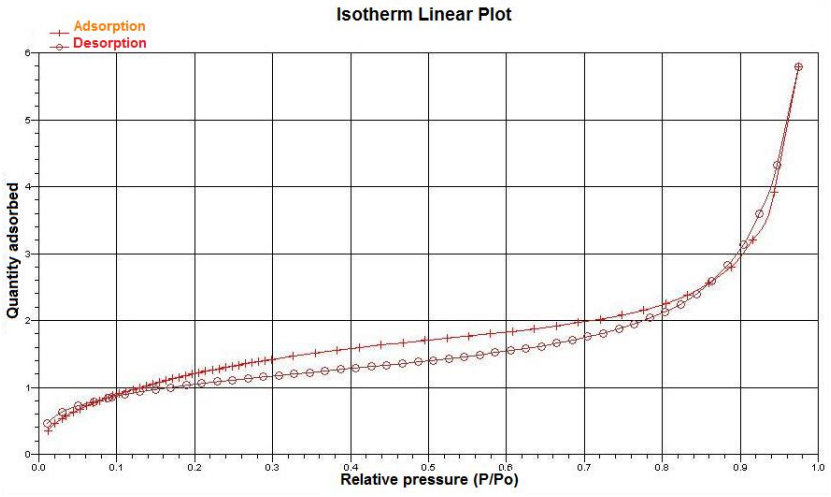

Figure 71: Isotherm adsorption/desorption plot for same filter as in Figure 70.

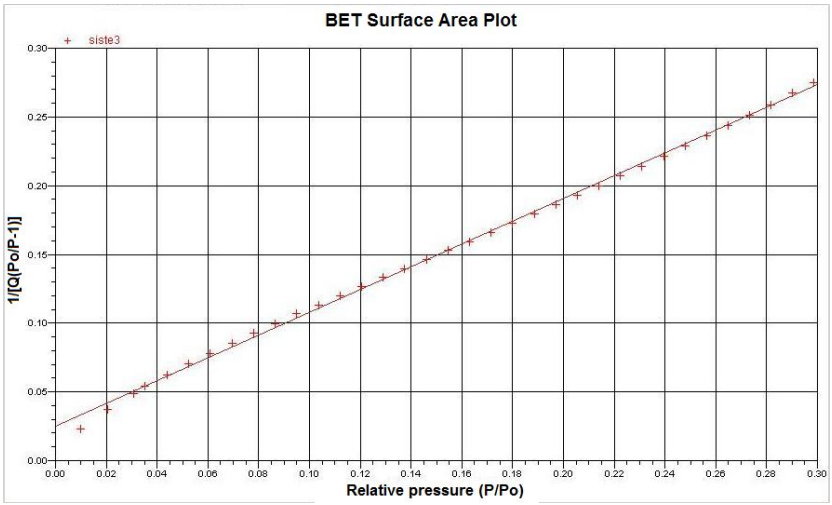

Figure 72: BET plot of freeze dried filter nr 3 from 3 pass cellulose mass in water with grammage of 20 g/m^2 and dry weight content of 2.00%.

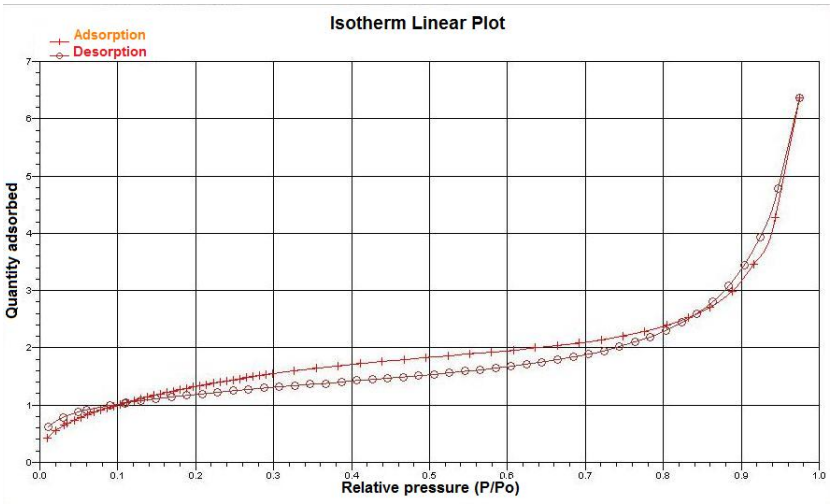

Figure 73: Isotherm adsorption/desorption plot for same filter as in Figure 72.

A.3 Solvent exchange

The amount of isopropanol/ethanol left after 5 rounds of centrifugation was calculated to be $\sim 0.09765\%$. An approximate volume of 80 ml was used in each bottle. After the first centrifugation in pure water, the pellet with NFC/water measured $\sim$ 20 ml. The supernatant water was carefully removed. $\sim$ 60 ml of ethanol (or isopropanol) was then added before stirring. Hence, 75% of the water was removed for every cycle of centrifugation and washing. After the 5th centrifugation, the supernatant solution containing $\sim 0.39\%$ water was removed and 60 ml pure ethanol added, so that the resulting water content of '100%' ethanol (or isopropanol) is below 1/1000. Since the ethanol used in the experiments was of 96% purity, this content is therefore what is ment by '100%' ethanol.

A.4 Regression line equations

The equation of the regression line in Figure 50 on page 95 can be presented as:

Permeance$[\frac{\mu m}{Pa \cdot s}]$ = 4633$[\frac{\mu m}{Pa \cdot s}]$ - 82.3 $[\frac{\mu m}{Pa \cdot s}]/[\frac{g}{m^2}]$ · (Filter grammage$[\frac{g}{m^2}]$)

For the combined effect of filter grammage and cellulose mass height on the filter permeance, the expression for the straight (3D) line was:

Permeance$[\frac{\mu m}{Pa \cdot s}]$ = 3094$[\frac{\mu m}{Pa \cdot s}]$ + 178 $[\frac{\mu m}{Pa \cdot s}]$/[m]·(Height of mass in petri dish[m])- 74,4$[\frac{\mu m}{Pa \cdot s}]/ [\frac{g}{m^2}]$·(Filter grammage$[\frac{g}{m^2}]$)

The equation for the regression line for the correlation between permeance and dry weight content is:
Permeance$[\frac{\mu m}{Pa \cdot s}]$ = 3531$[\frac{\mu m}{Pa \cdot s}]$ - 1586 $[\frac{\mu m}{Pa \cdot s}]$/[DW%] · (DW%)

The regression line in Figure 55 on page 100 has equation:

Tensile strength (kN/m) = 0,127(kN/m) + 0,14($\frac{kN}{m}$/%)· DW%

The equation for the regression line in Figure 54 is:

Tensile strength (kN/m) = 0,0478(kN/m) +
0,00510($\frac{kN}{m}$)/($\frac{g}{m^2}$)·Grammage ($\frac{g}{m^2}$)